

---

# Carrier-Envelope Phase Control for the Advancement of Attosecond Pulse Generation

Fabian Lücking

---



München 2014



---

# **Carrier-Envelope Phase Control for the Advancement of Attosecond Pulse Generation**

**Fabian Lücking**

---

Dissertation  
an der Fakultät für Experimentalphysik  
der Ludwig-Maximilians-Universität  
München

vorgelegt von  
Fabian Lücking  
aus Datteln, Deutschland

München, den 18. Juni 2014

Erstgutachter: Prof. Dr. Ferenc Krausz  
Zweitgutachter: PD Dr. Thomas Udem  
Tag der mündlichen Prüfung: 25. Juli 2014

---

## Zusammenfassung

Wenn die von einem Laser emittierten Lichtpulse so kurz werden, dass ihre Dauer nur noch wenige Schwingungszyklen des elektrischen Feldes umfasst, kommt der Phase zwischen Trägerwelle und Einhüllender (CEP) eine entscheidende Rolle zu. Ihre Regelung ist essentiell für jene Experimente, die die schnellsten Prozesse in der Natur auf der Zeitskala von Attosekunden ausloten. Mehr als zehn Jahre nach Beginn der Attosekunden-Ära ist die etablierte Methode der CEP-Regelung zum Hindernis für experimentelle Fortschritte geworden. Einerseits erfordern immer komplexere Experimente, dass das elektrische Feld der Pulse über viele Stunden konstant bleibt. Andererseits zeichnet sich eine Entwicklung der Pulsdauer zu immer kürzerer Dauer in Richtung eines einzigen Zyklus ab, was eine steigende Präzision der Regelung erfordert. Die gleichzeitige Erfüllung schon dieser beiden Anforderungen ist mit der konventionellen Methode nicht zu erreichen. Schlussendlich kann die niedrige Effizienz der zugrunde liegenden nichtlinearen Prozesse nur die Verwendung von Lasersystemen mit deutlich erhöhter Wiederholrate ausgeglichen werden. Um die Erzeugung von Attosekunden-Pulsen voranzutreiben, müssen neue Ansätze zur CEP-Regelung einer dreifachen Herausforderung gerecht werden, die dieser Dissertation ihren Rahmen gibt: Einerseits hohe Präzision und andererseits hohe Langzeittauglichkeit zur Verfügung zu stellen, und überdies neue Wege zur CEP-Regelung von derzeit in Entwicklung befindlichen Laserquellen mit hoher Durchschnittsleistung aufzuzeigen.

Diese Dissertation beschreibt die Anpassung einer alternativen Methode der CEP-Regelung auf Pulse mit einer Dauer von wenigen Zyklen. Die intrinsischen Beschränkungen der konventionellen Technik werden damit behoben. Der solchermaßen stabilisierte Oszillator bietet geringstes CEP-Rauschen über mehrere zehn Stunden Laufzeit ohne Phasensprünge. Zusätzlich wird eine Abwandlung der Methode beschreiben, die deren Anwendbarkeit für Verstärkersysteme erweitert.

Die CEP-Regelung in Systemarchitekturen für hohe Durchschnittsleistungen wird an zwei Lasersystemen untersucht, die exemplarisch für potentielle Attosekunden-Quellen mit Megahertz-Wiederholrate stehen. Es wird gezeigt, dass ein Scheibenlaser in Kombination mit zeitlicher Pulskompression genutzt werden kann, um Pulse in der Größenordnung von 10 fs zu erzeugen. Erste Experimente zu deren CEP-Stabilisierung ebnen den Weg für den ersten CEP-stabilen Scheibenlaser. Der zweite Ansatz betrifft die CEP-Regelung eines Oszillator-Verstärker-Systems. Das CEP-Rauschverhalten verschiedener Faserverstärker wird untersucht. Es wird gezeigt, dass die Überhöhung des Pulszugs in einem passiven Resonator auch von einer groben Stabilisierung der CEP-Änderungsrate deutlich profitiert.

Um Pulse von wenigen Zyklen Dauer auf eine Energie von Millijoule und darüber hinaus zu bringen, wird Verstärkung und zeitliche Kompression auf absehbare Zeit unverzichtbar bleiben. Unabhängig von der hierzu gewählten Technologie ist es von entscheidender Bedeutung, den Einfluss dieser Prozesse auf die CEP gering zu halten. Die Verwendung eines mit der alternativen CEP-Regelung ausgestatteten Oszillators zur zeitlich gestreckten Verstärkung wird beschrieben, was in hochenergetischen Pulsen mit über 24 Stunden konstanter Wellenform

resultiert. Alsdann wird ein neuartiger CEP-Aktuator beschrieben, der in Kombination mit einer schnellen Messmethode die CEP-Korrektur eines jeden Pulses bei einer Bandbreite von mehreren Kilohertz leistet. Das Resultat ist ein Pulszug auf Millijoule-Niveau, dessen CEP-Rauschen mit dem eines Nanjoule-Oszillators vergleichbar ist. Abschließend wird ein Experiment vorgestellt, mit dem der Einfluss von Hohlleiter-Kompression auf die CEP untersucht wird. Die Ergebnisse werfen neues Licht auf den Ursprung zusätzlichen Rauschens in solchen Aufbauten, und zeigen Wege zu dessen Vermeidung auf.

---

## Abstract

When the optical pulses emitted by a laser become so short in time that they encompass only a few cycles of the carrier wave, the phase between carrier and envelope becomes a crucial parameter. The ability to control this carrier-envelope phase (CEP) is elemental to experiments probing the fastest processes in the microcosm, occurring on the time-scale of attoseconds. More than a decade into the attosecond era, the limitations of the established CEP stabilisation technique have begun to curtail experimental progress. First, increasingly complex experiments require many hours of uninterrupted operation at the same waveform. Second, the pulses used in experiments are approaching the single-cycle boundary, calling for ever-decreasing CEP noise. With the conventional stabilisation technique, already these two requirements cannot be fulfilled simultaneously. Ultimately, the low efficiency of the underlying nonlinear processes can only be compensated by driver lasers at a higher repetition rate than available at present. In order to advance attosecond pulse generation, novel approaches to CEP control thus face a threefold challenge that outlines this thesis: To simultaneously provide low CEP noise and long-term operation to present-day few-cycle lasers and amplifiers, and to investigate CEP control capability in high average power sources that are currently under development.

This thesis describes the adaptation of cavity-external CEP stabilisation for use with few-cycle pulses. The intrinsic limitations of the conventional feed-back technique are lifted. A laser oscillator is demonstrated to maintain record-low CEP noise for tens of hours of operation free from phase discontinuities. In addition, a modification of the technique is presented that further enhances the applicability to amplified systems.

Two routes are investigated to achieve CEP control in system architectures that represent potential megahertz repetition rate driver sources. In combination with temporal pulse compression, a thin-disk laser is shown to yield few-cycle pulses. Experiments are presented that provide the groundwork towards the first CEP-stabilised thin-disk oscillator. The second approach targets the seed oscillator of a fibre chirped-pulse amplifier. The CEP noise properties of different amplification regimes are examined. Intensity enhancement of the output pulses in a passive resonator is shown to benefit greatly even from a coarse lock of the CEP slip rate.

For few-cycle pulse energy to reach the millijoule level and above, amplification and temporal compression will remain indispensable in the foreseeable future. Maintaining CEP stability across such stages is crucial, irrespective of the technology employed. Cavity-external CEP control is demonstrated to enable more than 24 hours of constant-CEP operation in chirped-pulse amplifiers. Furthermore, a novel actuator is introduced that, in conjunction with a fast means of measuring the CEP, is able to provide phase correction of the amplified waveform up to several kilohertz bandwidth. The result is a train of millijoule-level pulses with residual CEP noise comparable to that of state-of-the-art nanojoule oscillators. Eventually, an experiment is presented to examine the influence of different types of hollow-core fibre-based temporal compression on the CEP. The findings shed new light on the origin of adverse effects introduced by this technique, and point out ways towards effective compensation.

## Relevant publications

### Journal articles

A. Anderson, F. Lücking, T. Prikoszovits, M. Hofer, Z. Cheng, C. Neacsu, M. Scharrer, S. Rammler, P. Russell, G. Tempea, and A. Assion. *Multi-mJ carrier envelope phase stabilized few-cycle pulses generated by a tabletop laser system*. Appl. Phys. B **103**, pp. 531–536 (2011). F.L. helped with the experiments and edited the manuscript.

F. Lücking, A. Assion, A. Apolonski, F. Krausz, and G. Steinmeyer. *Long-term carrier-envelope-phase-stable few-cycle pulses by use of the feed-forward method*. Opt. Lett. **37** (11), pp. 2076–2078 (2012). F.L. performed all experiments, analysed the data, and wrote the manuscript.

B. Borchers, F. Lücking, and G. Steinmeyer. *Acoustic frequency combs for carrier-envelope phase stabilization*. Opt. Lett. **39** (3), pp. 544–547 (2014). F.L. performed all experiments together with B. B., separately analysed the data, and co-wrote the manuscript. The article states an equal contribution of B. B. and F.L.

F. Lücking, A. Trabattoni, S. Anumula, G. Sansone, F. Calegari, M. Nisoli, T. Oksenhendler, and G. Tempea. *In situ measurement of nonlinear carrier-envelope phase changes in hollow fiber compression*. Opt. Lett. **39** (8), pp. 2302–2305 (2014). F.L. performed all experiments involving the f-to-2f interferometers, analysed the data, and wrote most of the manuscript.

F. Lücking, V. Crozatier, N. Forget, A. Assion, and F. Krausz. *Approaching the limits of carrier-envelope phase stability in a millijoule-class amplifier*. Opt. Lett. **39** (13), pp. 3884–3887 (2014). F.L. conceived and performed the experiment together with V.C., analysed the data, and wrote the manuscript.

O. Pronin, M. Seidel, F. Lücking, J. Brons, V. Pervak, A. Apolonski, T. Udem, and F. Krausz. *Next-generation source of waveform-controlled light* (2014). Manuscript in preparation. F.L. conceived the experiment together with O. P., performed preparatory measurements, and co-wrote the manuscript.

### Conference contributions (Talks)

A. Anderson, F. Lücking, T. Prikoszovitz, M. Hofer, Z. Cheng, T. Le, C. C. Neacsu, G. Tempea, and A. Assion. *Tabletop generation of carrier envelope phase stabilized multi-mJ few-cycle pulses*. In *CLEO:2011 - Laser Applications to Photonic Applications*, p. CWG6. Optical Society of America (2011).

F. Lücking, A. Assion, A. Apolonski, and F. Krausz. *Long-term CEP-stable few-cycle pulses using the feed-forward method in an all-monolithic setup (Post-deadline)*. In *CLEO/Europe and EQEC*

---

2011 Conference Digest, p. PDB.2. Optical Society of America (2011).

F. Lücking, A. Assion, A. Apolonskiy, F. Krausz, and G. Steinmeyer. *Long-term CEP-stable few-cycle pulses using the feed-forward method*. In *8th International Conference on Ultrafast Optics, Monterey, California, USA* (2011).

F. Lücking, O. Pronin, J. Brons, A. Assion, A. Apolonski, and F. Krausz. *Reliable carrier-envelope phase control for current and future attosecond experiments (Invited)*. In *Conference on Lasers and Electro-Optics 2012*, p. CW1D.3. Optical Society of America (2012).

M. Seidel, O. Pronin, J. Brons, E. Fedulova, F. Lücking, I. Angelov, V. Pervak, A. Apolonski, and F. Krausz. *Approaching the few-cycle pulse regime with thin-disk oscillators*. In *Advanced Solid-State Lasers Congress*, p. ATu4A.7. Optical Society of America (2013).

O. Pronin, M. Seidel, J. Brons, F. Lücking, V. Pervak, A. Apolonski, T. Udem, and F. Krausz. *Carrier-envelope phase stabilized thin-disk oscillator*. In *Advanced Solid-State Lasers Congress*, p. AF3A.5. Optical Society of America (2013).

F. Lücking, V. Crozatier, and A. Assion. *Arbitrary carrier-envelope phase control in a 10 kHz, mJ-class amplifier*. In *Conference on Lasers and Electro-Optics 2014*, p. STh3E.2. Optical Society of America (2014).

F. Lücking, A. Trabattoni, S. Anumula, G. Sansone, F. Calegari, M. Nisoli, T. Oksenhendler, and G. Tempea. *Direct measurement of nonlinear carrier-envelope phase changes in hollow fiber compression*. In *Conference on Lasers and Electro-Optics 2014*, p. SW1E.2. Optical Society of America (2014).

#### Conference contributions (Posters)

F. Lücking, A. Apolonskiy, A. Assion, and F. Krausz. *24-hour constant waveform operation of a Ti:sapphire amplifier*. In *9th International Conference on Ultrafast Optics, Davos, Switzerland* (2013).

F. Lücking, V. Crozatier, and A. Assion. *High-speed carrier-envelope phase control in a 10 kHz, mJ-class amplifier*. In *Ultrafast Phenomena 2014*, p. 09.Wed.P3.52. Optical Society of America (2014).

F. Lücking, A. Trabattoni, S. Anumula, G. Sansone, F. Calegari, M. Nisoli, T. Oksenhendler, and G. Tempea. *In-situ measurement of intensity-dependent carrier-envelope phase changes in hollow fiber compression*. In *Ultrafast Phenomena 2014*, p. 08.Tue.P2.52. Optical Society of America (2014).

Book chapter

G. Steinmeyer, B. Borchers, and F. Lücking. *Carrier-envelope phase stabilization*. In K. Yamanouchi and K. Midorikawa (editors), *Progress in Ultrafast Intense Laser Science*, volume 104 of *Springer Series in Chemical Physics*, pp. 89–110. Springer Berlin Heidelberg (2013).

# Contents

1	Introduction	1
1.1	Motivation and outline	3
1.2	The carrier-envelope phase	5
1.3	Measuring the CEP and its changes	8
1.3.1	Oscillators	8
1.3.2	Amplifiers	9
1.4	Conventional CEP stabilisation	11
1.4.1	Working principle	12
1.4.2	Shortcomings	12
2	Cavity-External CEP Control for Few-Cycle Pulses	15
2.1	Working principle	15
2.2	Necessary modifications	19
2.2.1	AOFS considerations	19
2.2.2	Correction of spatial and angular chirp	20
2.3	Solutions for long-term operation	21
2.3.1	Stable interferometers	21
2.3.2	Minimizing auxiliary phase drift	25
2.3.3	Preventing oscillator CEO frequency drift	25
2.4	Precise stabilisation over extended time	27
2.4.1	Laser oscillator	28
2.4.2	Stabilisation module	28
2.4.3	RF signal chain	29
2.4.4	Phase noise characterisation	31
2.4.5	Long-term operation	33
2.5	Pulsed-mode operation	35
2.5.1	Working principle	35
2.5.2	Measurement set-up	37
2.5.3	Results	38
2.5.4	Outlook	41
2.6	Summary	42

3	Towards CEP Stability of High Repetition Rate XUV Driver Lasers	43
3.1	Concepts	44
3.1.1	Intracavity HHG in oscillators	45
3.1.2	Average power scaling	46
3.1.3	Enhancement in passive resonators	46
3.2	CEP-stable few-cycle pulses from a thin-disk oscillator	47
3.2.1	Spectral broadening and temporal pulse compression	47
3.2.2	CEO frequency detection and cavity-external stabilisation	50
3.2.3	Further developments	52
3.3	Cavity-enhanced fibre amplifier seeded by an Yb:KYW oscillator	52
3.3.1	Oscillator CEO detection and stabilisation	53
3.3.2	CEP noise induced in fibre amplification	55
3.3.3	Effect of CEO lock on enhancement cavity	56
3.4	Summary and outlook	58
4	CEP Stability and Robustness for High Energy Pulses	59
4.1	Multi-pass amplifier system layout	60
4.2	Day-long operation of CEP-stable amplifiers	62
4.2.1	High energy system	62
4.2.2	High repetition rate system	64
4.3	Millijoule-level pulses at the limits of CEP stability	66
4.3.1	Sources of CEP noise in amplifiers	66
4.3.2	Spectrogram-based fast measurement of the CEP	68
4.3.3	The acoustic grating phase as a CEP shifter	71
4.3.4	High-speed CEP correction	72
4.3.5	Outlook	75
4.4	Hollow-fibre compression and its impact on the CEP	76
4.4.1	In-situ single-shot interferometric measurement technique	77
4.4.2	Experimental layout	78
4.4.3	Characterisation	80
4.4.4	CEP noise in pressure gradient and static pressure geometry	81
4.4.5	XUV generation with different loop configurations	84
4.5	Summary	87
5	Conclusion	89
	Appendix	90
A	Noise Analysis in the Frequency Domain	91
B	Numerical Analysis and Data Archiving	93

Contents	ix
List of Acronyms	97
List of Figures	99
Bibliography	101
Acknowledgements	117



# Chapter 1

## Introduction

*“There is plenty of room at the bottom”* – in his iconic speech, held in December 1959 before the American Physical Society in Pasadena, Richard Feynman envisaged the numerous possibilities that would arise from exploring and controlling matter on the single-atom scale [Fey60]. A few months later and less than a hundred kilometres away, Theodore Maiman succeeded in building the first laser [Mai60]. Whereas electron microscopy opened a window into the smallest spatial dimensions, the laser today has become our looking glass to explore also the smallest *temporal* scale of nature. The invention of mode-locking [Har64] was the starting point for the continuous development of lasers towards the emission of light pulses on the femtosecond time-scale. These so-called ultrafast lasers have become invaluable tools to examine the properties of matter, allowing processes as fast as chemical reactions to be observed [Zew88].

Today, laser oscillators emitting in the near infrared (IR) provide pulses that last about 5 fs, encompassing only a few cycles of the carrier wave. The electric field of such pulses is thus no longer adequately described by merely knowing its cycle-averaged intensity envelope. Instead, its actual shape depends on the phase between the carrier wave and its (conceptual) envelope – the carrier-envelope phase (CEP). Control of this parameter had long remained elusive, which becomes understandable when considering the minuscule temporal dimensions involved. As one light cycle of about 3 fs corresponds to a phase of  $2\pi$ , keeping the CEP constant to within  $\pi/10$  (300 mrad) translates to achieving a precision of 150 as in the timing between the pulse envelope and the carrier wave – a value far beyond the picosecond time resolution of modern electronics. The breakthrough idea was supplied by the field of time-keeping or, more precisely, precision metrology, with the realisation that the spectral properties of the entire laser output are determined by two easily measurable radio frequencies. This provided a direct link between radio and light frequencies which unlocked unprecedented levels of precision in optical metrology [Hän06]. The connection between the frequency comb properties and the pulse-to-pulse phase evolution had been realised early on [Eck78], and when means to influence the CEP [Xu96] were combined with an absolute frequency measurement [Tel99], CEP control had come within reach. Yet even today, it remains among the most difficult parameters to control in any laser system.

CEP control became the enabling technology for attosecond science, even though it remained unreliable and offered limited stability. The exploration of the time-scale governing the changes

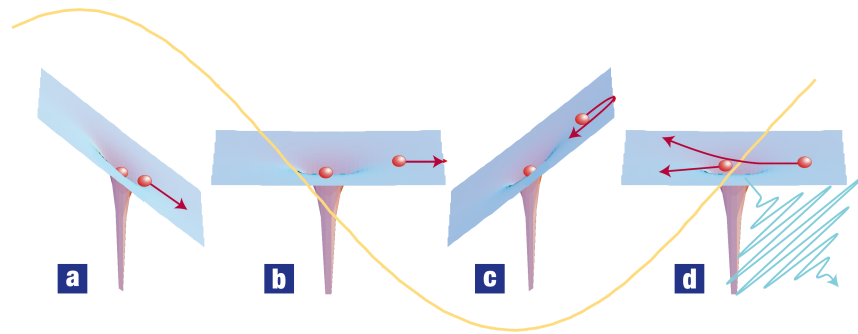


**Figure 1.1:** The three-step model of HHG, taking place once per half-cycle of the IR laser field, shown in yellow. **a)** Tunnel ionisation. **b),c)** Acceleration of the electron in the oscillating laser field. **d)** Re-collision of electron and ion, resulting in an XUV pulse. Image from [Cor07].

of an electron distribution in an atomic or molecular system calls for pulses of sub-femtosecond duration. As no laser medium offers sufficiently wide-band gain, such short pulses can only be produced by nonlinear interactions. The process underlying the birth of an attosecond light pulse is called high-order harmonic generation (HHG). In semi-classical terms, it can be described as a three-step process as depicted in Figure 1.1 [Cor93]. A neutral rare gas atom is subjected to a laser field strong enough for one of its valence electrons to tunnel-ionise. For this process to become sufficiently probable, a field strength on the order of  $1 \text{ V/\AA}$  is necessary, corresponding to an intensity of  $10^{13}$ - $10^{14} \text{ W/cm}^2$ . The liberated electron then propagates under the influence of the electric field of the laser, being accelerated away from the parent ion until the laser field reverses direction as the next half-cycle begins. Finally, in the event of a re-collision, the energy imparted on the electron by the IR laser field is then shed in the form of an attoseconds-long light pulse in the extreme ultraviolet (XUV) spectral range. The maximum energy converted in this way depends on the atomic ionisation potential and the driving laser intensity and wavelength, and can reach several 100 eV. The process produces two harmonic pulses for every cycle of the laser field, resulting in a burst of several XUV pulses for a long driver pulse. However, only the most intense half-cycle produces a harmonic pulse with the maximum energy. By filtering out the lower-energy XUV emission, an isolated pulse lasting only a few tens of attoseconds can be obtained [Hen01]. In order to optimise the HHG process towards the production of such isolated attosecond pulses (IAP), the interaction of atom and light must be confined to as few driver cycles as possible. As the IR driver pulses approach few-cycle duration, it is the CEP that determines the electric field strength of successive half-cycles. Due to the highly nonlinear nature of HHG, small changes of the CEP on the  $\pi/10$ -level have dramatic effects on the spectral and temporal shape of the XUV emission [Boh98, Nis03].

Among the milestone achievements of attosecond science, enabled by CEP control, are the direct measurement of the electric field of a laser pulse [Gou04], the time-resolved study of ionisation [Uib07] and photoemission processes [Sch10], and sub-femtosecond switching of electrical currents in solids [Sch13]. CEP control itself, however, has seen little innovation over the years. As of today, the established technique and its shortcomings have begun to be a limiting factor

to experimentalists. Suffering from intermittent phase discontinuities on the time-scale of hours, conventional CEP control is ill-suited for long-term measurements, which are required by an increasing number of applications. This is aggravated further when trying to improve the control precision, the second parameter demanded by present and future experiments. Finally, its applicability to novel laser sources apart from Ti:sapphire is largely unexplored.

## 1.1 Motivation and outline

Today, more than a decade into the “attosecond era”, the basic techniques for the generation and measurement of XUV pulses have been established. The role of attosecond pulses undergoes a transition from objects of study to tools in their own right. XUV-pump, XUV-probe measurements are one example, prospected to probe charge transfer in large biomolecules [Cor07]. First applications in adjacent fields are being considered, such as the use of HHG or IAP as seed sources for free electron lasers [Lam08]. All of these applications require a dependable source of XUV radiation with high yield.

For the advancement of attosecond pulse generation, CEP control must overcome a threefold challenge. The first aspect is a consequence of the trend towards ever shorter driver pulses, which allow for a more efficient transfer of energy to the cut-off region. Shorter pulses raise the dependence of the electric field shape on the CEP, calling for a control mechanism with lower residual noise. The second aspect is long-term robustness, i. e., the ability to maintain a constant CEP over tens of hours without discontinuities. The reason for this requirement is that HHG relies on highly nonlinear interaction, and is consequently plagued by low efficiency. Energy conversion hardly exceeds  $10^{-4}$  for XUV bursts and  $10^{-6}$  for IAPs [FF10], such that few-cycle IR pulses with millijoule energy are required for an acceptable yield. The current level of technology allows for such pulses to be produced at a repetition rate of a few tens of kilohertz at best, leading to very long integration times. CEP jumps, as are common in the established technique, render such a measurement useless. Experiments thus become a tedious task if, e. g., one XUV streaking spectrogram – which takes about an hour – is replaced by several tens in order to obtain meaningful statistics [Sch10]. Fortunately, diode-pumped solid state (DPSS) lasers have advanced enough to present an alternative option to present-day IR driver lasers. Average power scaling has been demonstrated up to the kilowatt range with sub-picosecond pulses. Such sources represent the proverbial silver bullet, enabling a hundredfold increase in repetition rate, and hence XUV photon flux. However, suitable means of CEP control at this power level are still lacking, the investigation of which represents the third aspect.

The aim of this thesis is to point out avenues along which these challenges may be met. Throughout each of the main Chapters 2 to 4, the guiding motifs are CEP noise performance, long-term robustness, and the prospective applicability of the techniques to power-scalable lasers. The structure of the main part is displayed in Figure 1.2, its three chapters ordered roughly by the regimes of pulse energy concerned.

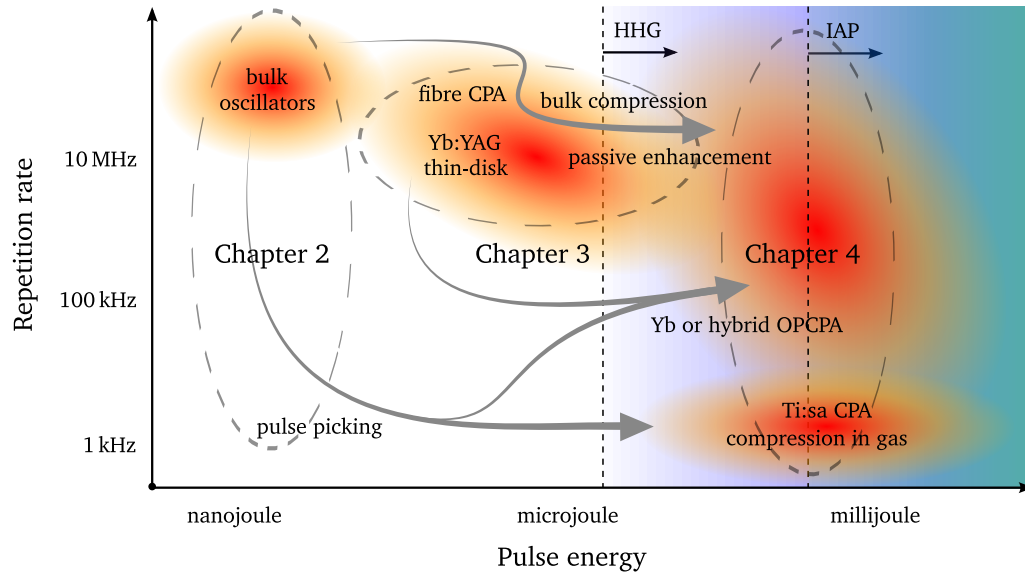


**Figure 1.2:** Schematic overview of the energy and repetition rate regimes treated in this work. The red areas coarsely denote the parameters that the mentioned technologies give access to, either presently or in the foreseeable future. The dashed areas mark the parameter ranges relevant to the respective chapters. The arrows represent possible paths of increasing intensity, i. e., amplification, compression, or enhancement.

- **Chapter 1** continues with an overview of the basic concepts and techniques that play a role in the course of this work. The principle and shortcomings of conventional feed-back CEP stabilisation is introduced.
- **Chapter 2** describes the adaptation of a cavity-external CEP control approach for use with few-cycle pulses. After solving the issues connected with the so-called “feed-forward” technique, both short-term stability and long-term robustness are characterised. A modification of the technique is presented that further enhances the applicability to amplifier systems.
- **Chapter 3** gives an overview of the concepts underlying power-scalable geometries for IR attosecond driver lasers. The output of an ultrafast thin-disk laser is shown to be feasible for few-cycle pulse generation, and CEP stabilisation is attempted in cavity-external configuration. A hybrid bulk and fibre system is presented next, intended for intensity enhancement in a passive cavity. The results shed light on the CEP properties of high-power fibre amplification and enhancement cavities alike.
- **Chapter 4** directs the attention towards the preservation of CEP properties through amplification and compression processes at the millijoule energy level. The challenges encountered are similar for all technologies employed to obtain such energetic pulses. The technique introduced in Chapter 2 is applied to an amplifier seed source in 24-hour operation. CEP noise induced in amplification is investigated and shown to be markedly

distinct from that in oscillators. Its correction in a fast stabilisation loop is presented. The last section deals with the impact of high-energy pulse compression on the CEP. The results are confirmed in a beam-line generating isolated attosecond pulses.

- **Chapter 5** summarises the thesis. The achieved results are reviewed along with their expected impact on current and future attosecond experiments.

## 1.2 The carrier-envelope phase

The output of a laser oscillator is limited to the longitudinal modes of its optical cavity, given by the frequencies

$$f_m = \frac{mc}{2L}, \quad m \in \mathbb{N}, \quad (1.1)$$

where  $c$  denotes the speed of light and  $L$  the optical path length of the cavity. Disregarding higher spatial modes and assuming sufficient gain in the amplifying medium, only the one mode experiencing the highest gain starts to oscillate. This regime is called continuous wave (CW) lasing. The superposition of two sine waves of different frequencies results in an amplitude modulation, also called beating. The modulation frequency of the envelope corresponds to the frequency difference of the two interfering waves. When a multitude of such waves with equidistant frequencies interfere, the result is an amplitude-modulated signal whose carrier frequency is the mean frequency of the contributing waves weighted by their relative amplitude. The width of the constructive interference, in turn, decreases with the number of interfering waves. The technique of mode-locking can be employed to produce this situation in a laser oscillator, with the contributing waves being the longitudinal modes of the cavity [Har64]. Such oscillators are at the core of every laser source treated in this work.

The output of a mode-locked laser is a comb of equidistant lines, spaced by the cavity free spectral range  $c/2L$ , in this context called the repetition rate  $f_{\text{rep}}$  (Figure 1.3). In the time domain, this corresponds to a train of pulses whose duration is inversely proportional to the spectral bandwidth  $\Delta f$  and hence the number of phase-locked oscillating modes,  $m$ :

$$\tau \approx \frac{1}{\Delta f} = \frac{1}{mf_{\text{rep}}} \quad (1.2)$$

Their temporal separation is given by the cavity round-trip time,  $t_{\text{rt}} = 1/f_{\text{rep}}$ . Modern laser oscillators based on a broadband gain medium like titanium-doped sapphire (Ti:sa) and Kerr lens mode-locking (KLM, [Spe91]) can emit spectra that span up to an octave of frequencies in the IR region (central wavelength  $\lambda_c = 800$  nm, center frequency  $f_c = c/\lambda_c = 375$  THz,  $\Delta f \approx 200$  THz) [Mor99]. This corresponds to a pulse duration of less than 5 fs, or two cycles of the carrier wave ( $\tau_{\text{cyc}} = 1/f_c = 2.67$  fs). Depending on the way mode-locking is achieved, the average output power can be almost equal in CW and pulsed operation. In the above example, it is on the order of 1 W at a repetition rate of roughly 100 MHz. With the energy of

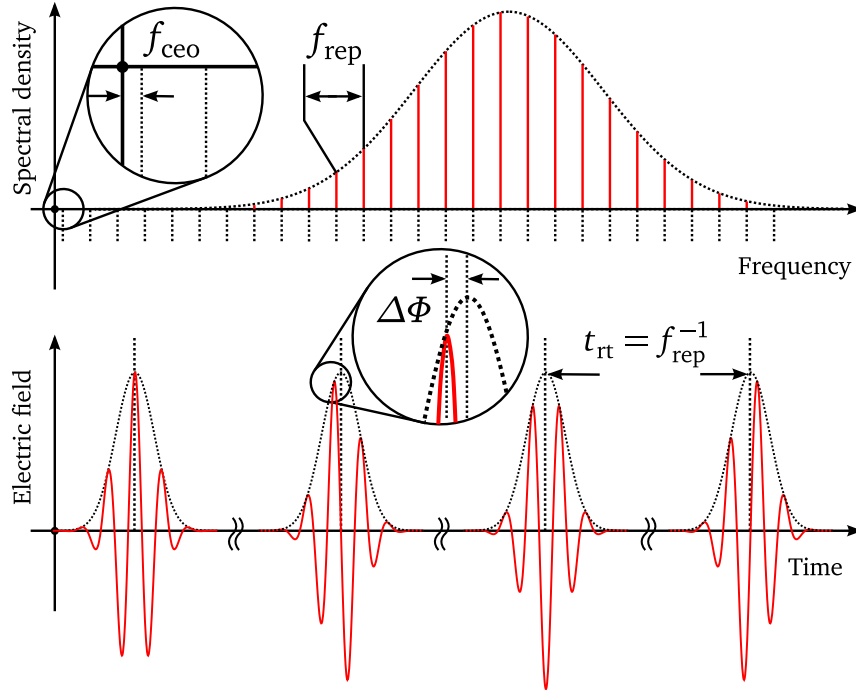


**Figure 1.3:** Frequency and time domain representation of the output of a mode-locked laser. The frequency comb of longitudinal modes corresponds to a train of short pulses spaced by the cavity round-trip time  $t_{\text{rt}} = 1/f_{\text{rep}}$ . The offset of the comb,  $f_{\text{ceo}}$ , is connected to the pulse-to-pulse phase slip  $\Delta\Phi = 2\pi(f_{\text{ceo}}/f_{\text{rep}})$ . Here,  $f_{\text{ceo}} = f_{\text{rep}}/4$ , such that every fourth pulse is identical.

one resonator round-trip ( $1\text{ W} \cdot 10\text{ ns} = 10\text{ nJ}$ ) confined to a pulse lasting mere femtoseconds, extreme peak power is achieved for brief moments in time (2 MW in the above case). The resulting intra-cavity intensity is high enough to induce a range of nonlinear phenomena. Most importantly in this case, the index of refraction of a material,  $n$ , becomes a function of the intensity  $I$ . Expanded to the first order,

$$n = n(I) = n_0 + n_2 I, \quad (1.3)$$

with  $n_2$  being the nonlinear coefficient of the refractive index. This effect has several consequences of spatial (self-focusing) and temporal nature (self-phase modulation, SPM) [Sie86, Ch. 10]. The latter imparts an intensity-dependent phase shift  $\Delta\Phi_{\text{nl}}$  on the pulse. In a mode-locked laser, this is one of two effects that induce a difference between the phase velocity  $v_{\text{ph}} = \omega/k$  experienced by the carrier and the group velocity  $v_g = d\omega/dk$  at which the pulse envelope propagates. Here,  $k = 2\pi/\lambda$  denotes the wavenumber and  $\omega = f/2\pi$  the angular frequency. The other effect is dispersion, i. e., the wavelength dependence of the refractive index:

$$\Delta\Phi_{\text{disp}} = L_{\text{disp}} \frac{\omega^2}{c} \frac{dn(\omega)}{d\omega} = 2\pi L_{\text{disp}} \frac{dn(\lambda)}{d\lambda}, \quad (1.4)$$

where  $L_{\text{disp}}$  is the length of the dispersive medium. The pulse in a mode-locked laser oscillator thus experiences a round-trip phase shift between carrier and envelope of

$$\Delta\Phi = \Delta\Phi_{\text{disp}} + \Delta\Phi_{\text{nl}}, \quad (1.5)$$

denoting the pulse-to-pulse change of the carrier-envelope phase (CEP). As one round-trip takes the time  $t_{\text{rt}}$  and phase changes are distinguishable only within  $[0, 2\pi]$ , let

$$\frac{1}{2\pi} \left( \frac{\Delta\Phi}{t_{\text{rt}}} \bmod 2\pi \right) = \frac{1}{2\pi} \left( \frac{\partial\Phi}{\partial t} \bmod 2\pi \right) \equiv f_{\text{ceo}}, \quad (1.6)$$

the carrier-envelope offset (CEO) frequency [Hel03]. In order to obtain an expression for the electric field of the output pulse train, we convolute the field of a single pulse with a Dirac delta function:

$$E_{\text{train}}(t) = A(t) \exp(i2\pi(f_c t + f_{\text{ceo}} t)) \otimes \sum_{m=-\infty}^{+\infty} \delta(t - mt_{\text{rt}}), \quad (1.7)$$

where  $A(t)$  denotes the pulse envelope and  $f_c = c/\lambda_c$  the central frequency of the comb. A Fourier transform yields the frequency domain expression

$$\tilde{E}_{\text{train}}(f) = \tilde{A}(f - f_c) \cdot \sum_{m=-\infty}^{+\infty} \delta(f - (mf_{\text{rep}} + f_{\text{ceo}})). \quad (1.8)$$

As can be seen from the argument of the delta function, the phase shifts induced by dispersion and nonlinearity cause all lines in the mode-locked laser frequency comb to be shifted by a frequency  $f_{\text{ceo}} \in [0, f_{\text{rep}}]$ . The frequency of every mode thus can be written in the form

$$f_m = mf_{\text{rep}} + f_{\text{ceo}}. \quad (1.9)$$

That implies that determining the precise frequency of light on the order of hundreds of terahertz reduces to measuring two frequencies in the easily accessible radio-frequency (RF) domain. Equation 1.6 links the CEO frequency to the pulse-to-pulse CEP slip by

$$\Delta\Phi = 2\pi \cdot \frac{f_{\text{ceo}}}{f_{\text{rep}}}. \quad (1.10)$$

Setting the offset to the  $N$ -th fraction of the repetition rate thus results in every  $N$ -th pulse having identical CEP. A zero-offset comb therefore corresponds to a train of constant-CEP pulses.

The notion of the mode-locked laser lines being offset from the longitudinal modes of the resonator appeared already in an early theoretical work on active mode-locking [McD67]. The relation between the offset and the pulse-to-pulse phase slip was first established in [Eck78], but means of both measurement and control were out of reach at that time. When this became

feasible towards the end of the 1990s, control of the CEO frequency and the CEP paved the way for precision metrology and attosecond science, respectively.

### 1.3 Measuring the CEP and its changes

The first successful measurement of CEP changes was achieved by comparing successive pulses in cross-correlation [Xu96]. The technique delivered experimental evidence on the influence of both dispersion and nonlinear phase shifts inside the oscillator cavity. Complex and technically demanding, the experiment was not suitable for actual stabilisation of the CEP.

#### 1.3.1 Oscillators

The breakthrough came with the technique of self-referencing [Tel99], which is preferably described in the frequency-domain picture of the mode-locked laser output as sketched in Figure 1.4. Equation 1.9 yields the frequency of any line in the spectrum. Subjecting a line from the low-frequency part of the comb  $f_m$  to sum-frequency generation (SFG) leads to new lines at

$$2f_m = 2mf_{\text{rep}} + 2f_{\text{ceo}}. \quad (1.11)$$

If the fundamental comb spans an entire octave, it contains lines close to this newly-generated component with an index  $n = 2m$  such that

$$f_n = 2mf_{\text{rep}} + f_{\text{ceo}}. \quad (1.12)$$

The two combs differ by the CEO frequency. Their superposition on a detector therefore leads to an amplitude modulation at  $f_{\text{ceo}}$  that can be measured in time. The CEO frequency thus becomes accessible as an RF signal that can be analysed and used for stabilisation. Note that the CEP of

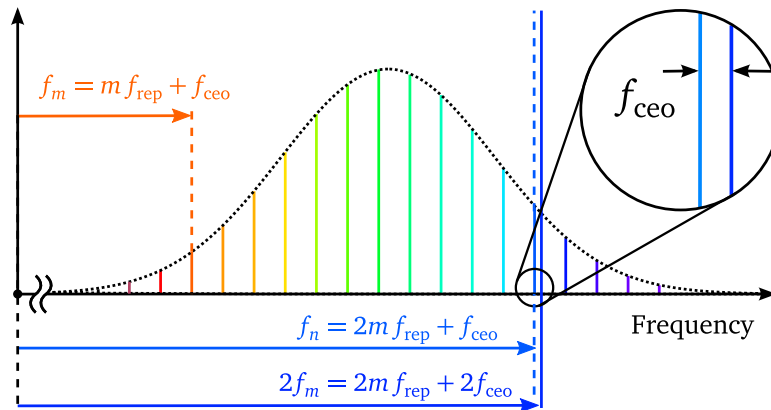
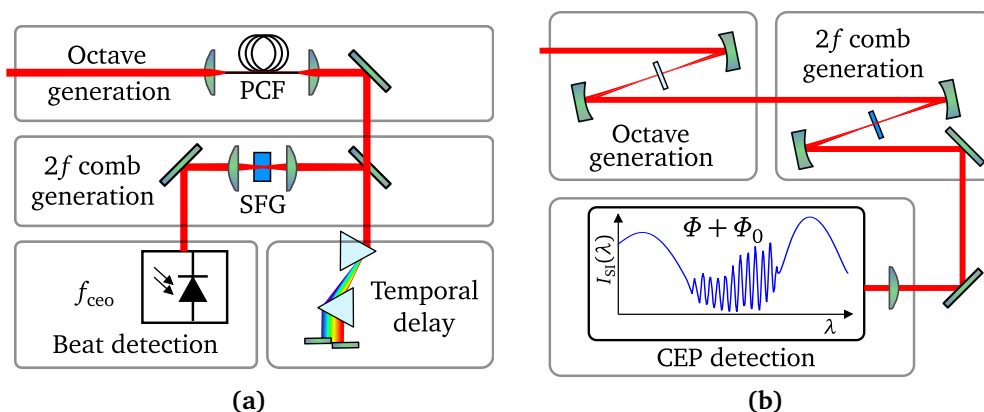


Figure 1.4: Schematic representation of the self-referencing technique.

a single pulse cannot be determined this way, as  $f_{\text{ceo}}$  only determines its rate of change. The corresponding device is called an f-to-2f interferometer. Numerous implementations have been demonstrated, one of which is shown in Figure 1.5a. The basic constituents remain unchanged, though. If the oscillator input bandwidth is not octave spanning, a device is introduced to extend it. If the required additional bandwidth is small compared to that already obtained from the oscillator, SPM in bulk materials or single-mode fibres is sufficient to achieve this [Apo00]. The most common method today is supercontinuum generation in a photonic crystal fibre (PCF) [Gen07], which significantly relaxes the requirements in terms of input energy and bandwidth. In any case, a temporal delay stage is required to compensate the group delay between the high and low frequency regions of the comb. The  $2f$  comb is generated in a nonlinear frequency conversion stage, and the interference signal is received in the RF spectrum by a photodiode. The advantages and drawbacks of different interferometer types will be discussed in detail in Section 2.3.1.

### 1.3.2 Amplifiers

The average power of amplified ultrafast sources is limited by both the available pump sources and thermal considerations. The repetition rate of amplifiers aimed at high pulse energy is therefore reduced correspondingly. With repetition rate significantly less than 1 MHz, the RF heterodyning technique described before cannot be applied due to excess  $1/f$  noise. Instead, self-referencing can also be applied to yield a modulation in the frequency domain, giving access to the CEP of a single pulse (except for an unknown offset) [Kak01]. Stripping Equation 1.7 of



**Figure 1.5:** Layout of f-to-2f interferometers. **a)** Oscillator CEO frequency detection. The depicted implementation is of quasi-common path type [Gre09]. A prism pair is used to spatially separate the high- and low-frequency spectral regions and introduce a temporal delay. **b)** Single-shot CEP detection of amplified pulses. The basic building blocks are the same as in the time-domain self-referencing technique, apart from the delay line. Instead of employing a PCF, broadening of the input spectrum is usually achieved in a bulk medium, e. g., sapphire.

the delta comb, we obtain expressions for the electric field of a single pulse in the time and frequency domain:

$$E(t) = A(t) \cos(\omega_c t + \Phi), \quad \tilde{E}(\omega) = \tilde{A}(\omega) \exp(i\Phi) \quad (1.13)$$

Its second harmonic carries twice the CEP. The SFG process leads to a phase lag of  $\pi/2$ , and the dispersion of the crystal causes a temporal delay  $\tau$  which results in a phase shift of  $\exp(i\omega\tau)$ :

$$\tilde{E}_{2\omega}(\omega) = \tilde{A}_{2\omega}(\omega) \exp\left(i\left(2\Phi + \frac{\pi}{2} + \omega\tau\right)\right). \quad (1.14)$$

Superposition of the two fields then yields a spectral interference pattern

$$I_{\text{SI}}(\omega) = |\tilde{E}(\omega) + \tilde{E}_{2\omega}(\omega)|^2 \quad (1.15)$$

$$\propto |\tilde{E}(\omega)|^2 + |\tilde{E}_{2\omega}(\omega)|^2 + 2\tilde{E}(\omega)\tilde{E}_{2\omega}(\omega) \cdot \cos(\omega\tau + \Phi + \pi/2) \quad (1.16)$$

The spectral interference thus contains an oscillation with a period determined by the delay between the fundamental and the SFG comb. The phase of this oscillation, in turn, is proportional to the CEP. After measuring the interference pattern with a spectrometer, numerical demodulation can be used to extract the phase [Tak82]. As both nonlinearity and material dispersion cause unknown phase shifts not included in the above deduction, the CEP of the input pulse can only be determined to an offset  $\Phi_0$  that depends on both the input pulse energy and the ambient conditions. Note that spectral self-referencing, too, requires octave bandwidth.

An f-to-2f interferometer relying on spectral interference does not require a delay line, obviating the need for spatial separation of the  $f$  and  $2f$  components. This allows for a collinear geometry as shown in Figure 1.5b. Furthermore, as the available pulse energy is considerably higher, white-light generation (WLG) can be used to obtain the necessary spectral bandwidth [Bro99]. On the other hand, the acquisition of an entire spectrum is time-consuming, and the data must be processed to obtain a value of the CEP. Single-shot CEP detection is therefore limited to sources with a repetition rate in the kilohertz range and below.

For pulse energies at the microjoule level and beyond, the CEP can also be detected by other means. These exploit phenomena that are directly dependent on the electric field of the laser pulse. The most well-known of these is the so-called phase-meter [Pau03], based on the directional momentum asymmetry of electrons generated in above-threshold ionisation. Due to its relative complexity and stringent requirement in terms of pulse duration, it has not yet found common use. Recently, a similar effect has been observed in a solid [PC14]. The set-up complexity would be significantly reduced this way, but the approach still suffers from low signal-to-noise ratio.

## 1.4 Conventional CEP stabilisation

CEP stabilisation of IR driver lasers for attosecond experiments is usually achieved in a two-stage process. The first step is the stabilisation of the seed oscillator CEO frequency to an  $N$ -th fraction of its repetition rate. When the pulse train is reduced in repetition rate by pulse picking, the division factor is chosen a multiple of  $N$ , such that the amplified pulses have identical CEP. In the second step, when a sufficiently high pulse energy is available, the CEP of single pulses can be measured and corrected. Optical parametric amplification (OPA) also offers a means to CEP stabilisation through frequency mixing [Bal02] which is independent of the oscillator. Although it in principle provides perfect long-term stability, it strongly couples the phase stability to intensity noise and drift. In addition, the technique suffers from low conversion efficiency (typically on the order of a few percent), making it both expensive and prone to adding noise. Therefore, it is usually applied to amplifier-level pulses. Furthermore, its use is limited in practice to the wavelength range above  $1.5\ \mu\text{m}$ . The efficiency of an additional SFG conversion step to the near IR scales with the inverse bandwidth, and would make an additional amplification step unavoidable.

The remainder of the introduction deals with seed oscillator stabilisation by means of feed-back. The alternative cavity-external technique based on frequency shifting is the subject of Chapter 2, whereas the CEP correction in amplifiers is treated in Chapter 4.

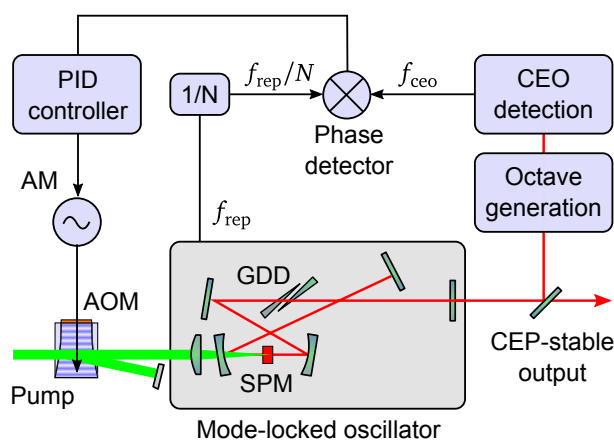


**Figure 1.6:** Block diagram of PLL-based stabilisation of the CEP frequency in an oscillator. The measured IL value is compared with the reference in a phase detector. The phase difference is passed through a PID. The servo acts on the pump intensity, changes of which lead to changes in pulse energy. These couple to the CEP via SPM. The resonator dispersion serves as a slow actuator. AM: Amplitude modulation input. GDD: Intracavity group delay dispersion.

### 1.4.1 Working principle

Self-referencing as described in Section 1.3.1 provides the oscillator CEO frequency as an RF signal.  $f_{\text{ceo}}$  can be influenced either by dispersion or by the nonlinear phase shift induced by SPM (Equation 1.6). For oscillators with intracavity prisms, tilting of the end mirror [Ude99, Jon00] provides a means of quickly altering the dispersion, but present-day broadband oscillators rely exclusively on dielectric mirrors for dispersion management. In this case, the insertion of intracavity glass wedges can be used for slow control. Nonlinear phase shifts provide a faster means of actuation. The most widespread means of CEO frequency control through SPM is to modulate the pump intensity [Pop01]. The altered gain then changes the energy of the pulse circulating in the cavity and the CEP shift it experiences per round-trip.

Stabilisation to a reference RF signal – commonly  $f_{\text{ceo}}/4$  – is then achieved by closing a phase-lock loop (PLL) [Gar79]. As depicted in Figure 1.6, the phase comparison between the current CEO frequency and the reference signal is used as the error signal. It passes proportional-integral-derivative (PID) loop filter, and the resulting servo output is fed back to the actuator.

Frequency analysis of the in-loop (IL) error signal can provide information on the quality of the stabilisation performance. However, note that all noise that emerges in the detection, such as from the fibre coupling and the interferometer delay line, is masked in the IL signal. A more realistic measure is obtained in an out-of-loop (OOL) comparison, i. e., with a second interferometer that is not part of the feed-back loop.

### 1.4.2 Shortcomings

The PLL technique requires non-zero frequencies for phase comparison. Therefore,  $f_{\text{ceo}} = 0$ , a pulse train with constant CEP, cannot be achieved this way. This is of little relevance to experiments performed with amplified pulses at reduced repetition rate, but does impose a limitation on the high-repetition rate sources described in Chapter 3. Furthermore, recent experiments have shown the feasibility of exploring certain attosecond processes with nanojoule-level pulses. These include the CEP-dependent emission of electrons from nanoscale metal tips [Krü11] and plasmon-assisted HHG in microstructures [Par11]. Modifications exist to provide a constant CEP even in with the conventional feed-back technique, either through frequency-shifting one of the two interfering combs in the  $f$ -to- $2f$  interferometer [Rau09] or by directly locking the  $f$ -to- $2f$  output to a DC level without phase comparison [Lee05]. The first approach comes at the cost of large non-shared paths in the interferometer, which results in considerable phase drift over time and high sensitivity to external perturbations. The latter suffers from the ambiguity of signal loss and good stabilisation, as well as from  $1/f$  noise reducing CEO stability.

The most important shortcoming of conventional CEP stabilisation, however, is the inherent property of feed-back loops to trade lock stability against robustness [Moo14]. The loop gain

maps the actuator range to the expected phase error. If the loop gain is chosen such as to accommodate even the largest phase excursions that might occur in the laboratory environment, the CEP stabilisation performance is too low to be of use for few-cycle experiments. A high loop gain results in high stability, but a perturbation that exceeds the available range likely results in a loss-of-lock event. Even if the lock is re-established and the CEO frequency is stabilised again, the resulting value of the CEP is effectively random. With a second stabilisation loop after the amplifier, the CEP can in principle be restored to its former value. However, as these commonly control the CEP through changes of dispersion in the beam path after the oscillator, this can result in a different pulse envelope, an effect that becomes more pronounced with shorter output pulses.

None of this would be a severe limitation with experiments taking on the order of an hour. In fact, state-of-the-art commercial feed-back stabilisation systems can be expected to provide up to a few hours of constant-CEP operation, depending on the environment. However, advanced experiments exploring sub-femtosecond processes often require several hours of integration. During this time, the driving laser source must simultaneously provide low CEP noise and high robustness against external perturbations. Even neighbouring fields of attosecond science would profit greatly from increased long-term CEP stability. In femtochemistry, for instance, cold-target recoil ion momentum spectroscopy is used to study the CEP-dependent outcome of chemical reactions [Kli13]. As such experiments literally require days of uninterrupted measurement, one resorts to the so-called phase-tagging technique [Wit09]. As a result, the data acquired with random CEP can still be used to establish a relation between the phase and the reaction outcome. Long-term robust CEP control would therefore open up the added possibility of actively controlling rather than just observing chemical reactions.

An alternative CEP control technique, based on shifting the frequency of the comb lines external to the oscillator, was projected to circumvent both the bandwidth limitation and the stability-versus-robustness dilemma. This motivated the adaptation of the technique to few-cycle pulses, as described in Chapter 2.



## Chapter 2

# Cavity-External CEP Control for Few-Cycle Pulses

Mode-locked laser oscillators with titanium-doped sapphire (Ti:sa) as the active medium have been the tool of choice for the generation of femtosecond pulses for more than two decades. Lasers based on rare-earth doped media that provide pulses lasting longer than 100 fs are slowly becoming commercially available, but at present there is hardly an alternative when shorter pulses are needed. Virtually all experiments involving CEP-stable pulses have therefore relied on a Ti:sa oscillator in some way. Representing the workhorse of attosecond science, these lasers were the first in which the limitations of conventional CEP control have become relevant. Recent experiments have called for a simultaneous increase in short-term stability and long-term uninterrupted operation, which cannot be achieved with established methods as described in Section 1.4. The topic of this chapter is the adaptation of a recently-demonstrated alternative CEP stabilisation method, known as the feed-forward technique, for use with state-of-the-art few-cycle Ti:sa oscillators. The idea behind it, based on cavity-external frequency shifting, is introduced in Section 2.1. Prior work has concentrated solely on the frequency domain characteristics and short-term measurements. Section 2.2 thus deals with the necessary changes to make the novel technique suitable for the use in time-domain applications. Additional difficulties arise when aiming to maintain CEP stability over long periods of time. Section 2.3 deals with possible solutions. Their experimental implementation is the subject of Section 2.4, along with the results gathered with the prototype. A modification of the technique is introduced in Section 2.5 which further enhances the applicability to seeding amplifiers with  $< 100$  kHz repetition rate.

### 2.1 Working principle

When the “direct frequency comb synthesis” technique [Kok10] was introduced in 2010, its building blocks had long been known in the ultrafast science community (e. g., see [Hal84, Jon01]). In hindsight, the novelty consisted in seeing both the frequency- and time-domain pictures at the same time, and then combining existing methods from both sides. The underlying notion is that stabilising the pulse-to-pulse phase slip of an ultrashort pulse train is equivalent to cancelling all fluctuations in the carrier-envelope offset frequency carried by each line in

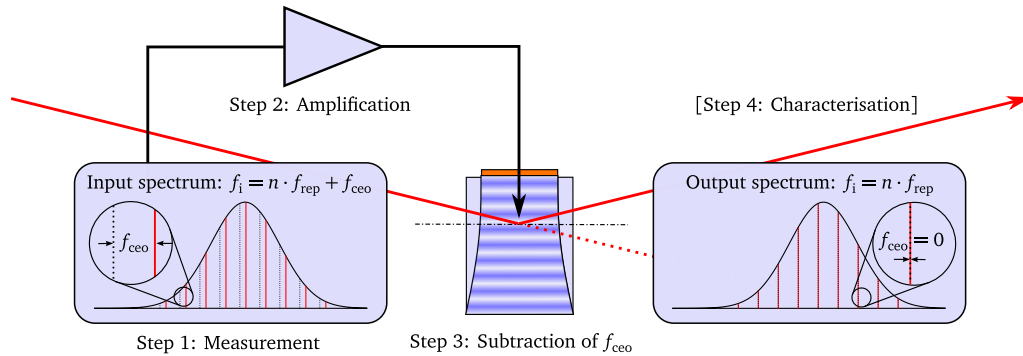


**Figure 2.1:** Cavity-external CEP stabilisation. The input frequency comb offset  $f_{ceo}$  is measured, amplified, and eventually subtracted from the light frequency of every single comb line. A zero-offset comb is produced only in the -1<sup>st</sup> diffraction order of an AOFS by momentum transfer from the optical to the acoustic waves. The CEO phase stability needs to be characterised in a separate interferometer, as the in-loop signal remains unaffected.

its spectrum. The task of producing a zero-offset frequency comb, which is equivalent to a train of pulses with identical CEP (Section 1.2), reduces to subtracting the time-dependent CEO frequency from each line in the spectrum. By definition, the CEO frequency cannot be larger than the laser repetition rate. As the lasers commonly used in ultrafast instrumentation have a repetition rate of about 100 MHz, the desired frequency shift is very small compared to the optical frequency of each line (about 350-400 THz for a Ti:sapphire laser). One possible way to achieve such a change in the frequency of the light is by an acousto-optic frequency shifter (AOFS). In these devices, a transducer driven by a radio frequency (RF) signal launches a travelling longitudinal sound wave into a bulk crystal. The induced density modulation acts like a grating to an incoming beam of light, giving rise to diffraction primarily in low ( $< 2$ ) orders. In contrast to a static grating, the travelling wave Doppler-shifts the frequency of the light up or down, depending on whether the light is deflected towards or away from the propagation direction of the acoustic wave. This can also be understood in terms of momentum conservation in the photon-phonon interaction [Rei97, p. 329]. This process also conserves the phase, effectively meaning that the transient grating in the AOFS adds its phase to that of the light.

The cavity-external CEP stabilisation technique thus involves three steps, as depicted in Figure 2.1.

1. *Measurement of the CEO frequency.* Independent from the actual laser source to be stabilised (hence the name “cavity-external”), the CEO frequency of the pulse train is measured. This can be done by any of the interferometric methods introduced in Section 1.3.1.
2. *Amplification of the signal.* Because the signal obtained in the detection is many orders of magnitude less powerful than what is required by an AOFS device, several stages of amplification and filtering are necessary.

3. *Subtracting the CEO frequency.* The drive frequency of the AOFS is subtracted from all lines of the spectrum. When using the sum of the CEO frequency and a fixed-frequency RF signal to drive the AOFS, the results in an output comb with its offset determined by the latter. In particular, adding an integer multiple of the laser repetition rate to the CEO frequency also produces a zero-offset comb.

As opposed to the situation in the conventional PLL-based CEP stabilisation scheme, this technique involves neither a comparison to some fixed reference nor an error signal that would indicate the difference between the current and desired value. The error is known intrinsically by measurement of the CEO frequency, and is “fed forward” for direct correction. This is possible because there is a simple and determined outcome of the interaction of photon and phonon in the AOFS, namely that the frequency of every diffracted photon is shifted by the frequency of the phonon. The measurement of the comb offset, which can happen before the AOFS, is not influenced by the stabilization. Strictly speaking, for the method to be truly “forward”, the correction must be applied to the very pulse used in the measurement. Although this can in principle be fulfilled with a very long delay line for the optical pulse, such effort would both impractical and unnecessary.<sup>1</sup> Since the pulse-to-pulse CEP evolution in a mode-locked laser is continuous (in the sense that the CEO frequency is well-defined, as opposed to a random CEP from shot to shot), the error induced by the time lag between measurement and correction can easily be quantified. In the terms of control theory, one can define an (quasi-)loop bandwidth, i. e., the highest frequency at which a spectral component of CEP noise can still be compensated. This is given roughly by a quarter of the inverse time delay between the measurement of the offset and its correction in the frequency shifter. At this frequency, the time lag translates to a phase lag of  $\pi/2$ .

As the electronic signal processing is limited to RF amplification, mixing and filtering, this time delay is dominated by the time it takes the acoustic wave to propagate from the transducer to the interaction region with the light. This delay varies with the AOFS device, but maximum diffraction efficiency is usually achieved after the acoustic wave has propagated a distance somewhat larger than the desired acoustic aperture. For the class of devices in question here, this distance amounts to about 1 mm. Travelling at the speed of sound in a crystalline medium (on the order of 5000 m/s) for a distance of about 1 mm, the acoustic wave limits the correction bandwidth to 1.25 MHz. Note that this is about one order of magnitude higher than the bandwidth demonstrated with a conventional stabilization loop, and well in excess of the relaxation oscillation frequency of common Ti:sapphire lasers (see Section 1.4).

The FF technique was shown to provide a stabilised CEO frequency with record-low phase error (45 mrad RMS, 0.2 Hz–2.5 MHz), and in contrast to any feed-back scheme, this does not come

---

<sup>1</sup> This, along with the term being undeniably catchy, is presumably the reason that the term “feed-forward” was coined in spite of being inaccurate. In this work, the term “cavity-external” is used instead, but in order to prevent confusion with other acronyms for the carrier-envelope phase (CEP), or enhancement cavities (EC), the abbreviation “FF” was chosen.

at the cost of reduced robustness. For as long as the oscillator remains mode-locked and a CEO signal is provided, the output CEO frequency remains stabilised. Deviations in CEP may still occur through changes of the acoustic phase stemming from changes in drive frequency, but they are limited to slow, continuous drift. A loss-of-lock event in a PLL, in comparison, results in a random CEP once the lock is re-acquired.

Another advantage lies in the fact that the stabilised CEO frequency of the output pulse train  $f_{\text{out}}$  can be chosen quite freely. Designating the free-running offset  $f_{\text{ceo}}(t)$ , the AOFS drive frequency  $f_{\text{drv}}$ , and  $f_{\text{ext}} = f_{\text{rep}} - f_{\text{out}}$  the mirror frequency of  $f_{\text{out}}$ , the following equation must be fulfilled:

$$f_{\text{ext}} + f_{\text{ceo}}(t) = f_{\text{drv}} \quad (2.1)$$

$$\Leftrightarrow f_{\text{out}} = f_{\text{rep}} + f_{\text{ceo}}(t) - f_{\text{drv}}. \quad (2.2)$$

The non-stabilised offset serves as the free parameter and can be coarsely set by tuning the intra-cavity dispersion. Setting  $f_{\text{out}} = 0$  (or  $= f_{\text{rep}}$ , which is equivalent), i. e., achieving a train of pulses with identical CEP, is in fact the most simple case. Using conventional stabilisation, this preferable situation is hard to achieve, and the solution is prone to adding noise (see Section 1.4).

These features make the FF technique highly desirable in the context of experiments probing ultrafast processes in the time domain, but several changes are necessary to make them accessible. The starting point of the developments described in this chapter was the proof-of-principle experiment conducted by Koke *et. al.* [Kok10]. They employed an oscillator supplying 10-fs pulses that were frequency-broadened in a PCF to obtain a spectral coverage of more than one octave. This took place before the actual CEO frequency detection and stabilisation, meaning that the entire experiment was run on temporally distorted pulses with a duration on the order of picoseconds. The interferometers used in the experiments were quasi-common path  $f$ -to- $2f$  type devices, providing a low-noise detection of  $f_{\text{ceo}}$ , but also high sensitivity to changes of ambient conditions [Gre09]. Furthermore, both interferometers were placed after the AOFS, with the in-loop (IL) device being fed by the non-diffracted part of the beam. As will become clear in Section 2.3, this configuration is of limited practical use. The Bragg diffraction in the AOFS causes a spatial chirp in the output beam. Initially, this had been exploited in the interferometer used for out-of-loop (OOL) characterisation to spatially separate the  $f$  and  $2f$  components in order to adjust the temporal delay. When adapting the system to stabilise few-cycle pulses, such chirp needs to be compensated. The focus of the early experiment was placed on precision as opposed to long-term robustness, clearly illustrated by the strongly increased CEP error on longer measurement times (570 mrad within 35 min as opposed to 45 mrad within 5 s). The group has since provided a more in-depth analysis of the noise [Kok11] as well as results achieved with a combination of feed-back and cavity-external schemes [Bor11], retaining their focus on frequency-domain problems.

In contrast, the work described here concentrates on time-domain applications. The aim is

to harness the favourable properties of the FF technique for use in attosecond science, both directly in the form of an oscillator pulse train as well as in seeding amplifiers at reduced repetition rate. To this end, effort is directed at three aspects: Choosing a low-dispersion, high-efficiency AOFS enabling re-compression of the output to few-cycle pulses, cancelling spatial and angular chirp to the extent possible, and ensuring that the stabilisation scheme can provide high phase stability over prolonged periods of time. These questions had been analysed independently by Sebastian Koke, drawing similar conclusions [Kok12, p. 60ff]. However, to the best of the author's knowledge, the solution suggested there were not put into practice.

## 2.2 Necessary modifications

### 2.2.1 AOFS considerations

In order to serve as a replacement for conventional CEP stabilisation, a system based on the FF technique needs to provide comparable output power, calling for highly efficient diffraction in the AOFS. Realistically, this means a value of  $> 75\%$ . Most acousto-optic devices optimised for this parameter employ tellurium dioxide ( $\text{TeO}_2$ ) as the diffracting medium. However, this material is highly dispersive [Web03], forbidding its use with pulses of even moderately broad spectra. Crystal quartz provides an alternative, but requires a comparably high RF drive power to obtain an acceptable diffraction efficiency, making the RF amplification stage more expensive. Another constraint is the ratio of drive frequency to the length of the acousto-optic medium, with lower path length resulting in a higher drive frequency (and lower diffraction efficiency). Furthermore, considering the large amount of amplification necessary, the input CEO frequency should be easily separable from zero, its mirror frequency, and the repetition rate, in order to facilitate low- or band-pass filtering. For an oscillator of 70-80 MHz repetition rate, this suggests a range of about 5-25 MHz for  $f_{\text{ceo}}(t)$ . Because a crystal quartz AOFS of sufficiently short length reaches the desired diffraction efficiency only upwards of about 70 MHz, directly using the amplified offset is not an option (Equation 2.1). Rather, it needs to be summed with the repetition rate or a fixed RF source for zero-offset operation and characterisation, respectively. Finally, a crystal quartz AOFS device with a length of 20 mm was chosen. It provides a total diffraction efficiency of more than 80 % when driven with 12 W of RF power. Water cooling was necessary to prevent heat build-up. The material group delay dispersion (GDD) of approximately  $650 \text{ fs}^2$  can be compensated by 16-20 reflections off a dispersive mirror (DM) pair, making the use of a complex prism compressor unnecessary.

### 2.2.2 Correction of spatial and angular chirp

As the AOFS is based on Bragg diffraction, the output angle of the diffracted light is dependent on both the optical and the acoustic wavelengths in the phase-matched case,

$$\tan \Theta = \frac{\lambda_0}{2n_0\Lambda} = \frac{\lambda_0 f_{\text{drv}}}{2n_0 v_{\text{ac}}}, \quad (2.3)$$

where  $\lambda_0$  denotes the wavelength of the light,  $\Lambda$  the acoustic wavelength,  $n_0$  the index of refraction of the acousto-optic material, and  $v_{\text{ac}}$  the speed of sound in the medium [Rei97, p. 330]. The values in this case ( $\lambda_0 = 800$  nm,  $v_{\text{ac}} = 5720$  m/s,  $n_0 = 1.54$ ) result in an angle in the milliradian range, where the relation can be assumed to be linear. The AOFS thus imparts a linear angular chirp on the output beam. When the device is placed at the waist of a focused beam (as is commonly done due to the limited aperture of the acoustic grating), this angular chirp transforms to a linear spatial chirp at the point of re-collimation. This opens several possibilities for correction. First, the angular chirp can be corrected to some extent by placing an element with the inverse angular dependence right after the phase shifter. Close to ideal correction could be achieved by an identical device in opposite configuration, or a double pass through the same shifter. This would come at a high cost in efficiency and complexity, as additional steps would have to be taken for frequency division of the driver signal and for proper re-compression of the pulses. A simpler approach is the placement of a prism close to the AOFS, oriented such that the angular chirp is roughly compensated as shown in Figure 2.2a. The calculated spatial chirp properties after such an arrangement are displayed in Figure 2.2b,

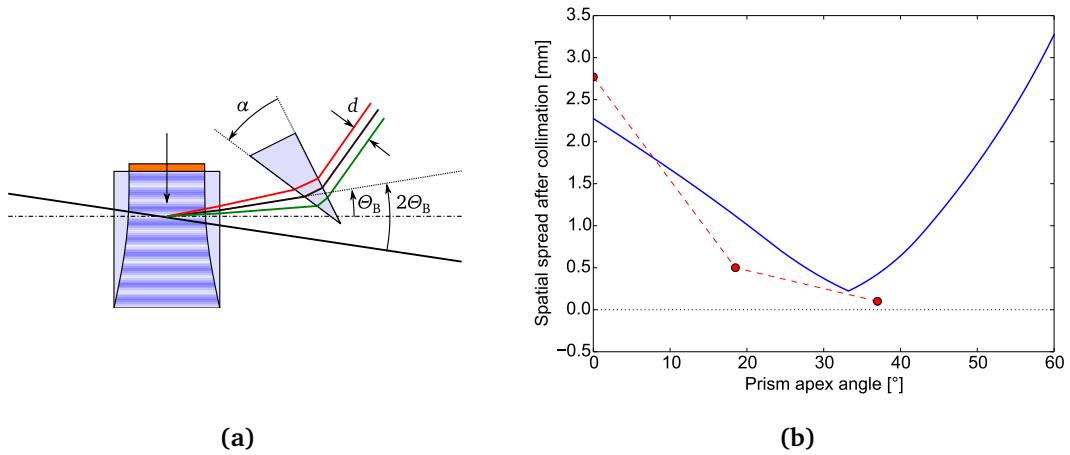


**Figure 2.2:** Compensation of the angular chirp induced by the AOFS Bragg grating. **a)** Schematic drawing of prism positioning.  $\alpha$ : apex angle.  $\Theta_B$ : Bragg angle.  $d$ : spatial spread. **b)** Output beam spatial chirp properties after AOFS and BK7 prism, assuming a spectral span of 635-955 nm and collimation after 50 cm. *Blue solid trace*: Calculated spatial spread  $d$ . *Red dotted trace*: Measured spatial spread, distance approximately 1 m after collimation.

assuming the values of the AOFS described in Section 2.2.1, an input spectrum spanning from 635 to 955 nm, and a focal length of 50 cm. The data plotted assume a BK7 prism placed at the respective angle of minimum deviation. With the optimal apex angle of  $33.6^\circ$ , the output angle spread of the spectral edges is reduced from 4.55 mrad to about  $450 \mu\text{rad}$ , or  $1.41 \mu\text{rad}/\text{nm}$ . This translates to a spatial spread between the spectral edges of  $225 \mu\text{m}$  after re-collimation. As the AOFS is placed in the focal plane, the angular chirp should vanish completely. Measurements of the output spatial spread were performed for apex angles of  $18.5$  and  $37^\circ$ , as well as without a prism (red data points in Figure 2.2b), yielding at least qualitative agreement to the calculated values. The residual angular spread after collimation was measured to  $0.88$  and  $0.16 \mu\text{rad}/\text{nm}$  for the two prisms, showing that this value approaches zero for an optimized apex angle as well. A third (thus far untested) alternative for compensation of the angular chirp is a static transmission grating with a period equal to that in the AOFS device. Unfortunately, gratings with such low line density (on the order of 15 lines/mm) are not commercially available. A sample might, however, be fabricated either by femtosecond direct writing in glass.

## 2.3 Solutions for long-term operation

As mentioned above, the first demonstration of the FF technique yielded record-setting stability of the CEO frequency on the time-scale of seconds, but suffered from slow phase drift occurring within minutes to hours. This drift can be caused by a multitude of sources both in measurement and correction of the phase. In the first case, the most important source of error is interferometer drift. This is an issue in any kind of CEP stabilisation, although it is temptingly easy to overlook in feed-back type systems (see Section 1.4), where performance data are often inferred from an in-loop device. For the characterisation of the FF scheme performance, two devices are needed, which aggravates the problem. In the latter case, the CEP error arises from the fact that external factors also affect the relative phase of optical and acoustic waves. Last but not least, it has to be ensured that the driving frequency stays within the range required by the AOFS. If the favourable performance of FF CEP stabilisation is to be transferred to the time-scale on which experiments are run in present-day laboratories, these issues have to be taken care of.

### 2.3.1 Stable interferometers

The self-referencing measurement process described in Section 1.3 is sensitive to the optical phase of both interfering parts of the frequency comb. Consequently, any phase changes arising in the interferometer will transfer to the RF phase of the measured CEO frequency  $f_{\text{ceo}}(t)$ . Interferometers of the f-to-2f type employed for CEO frequency detection need to introduce a temporal delay between the two components before the frequency conversion stage in order to obtain temporal overlap and interference at the detector. Therefore, spatially separated propagation of the two is inevitable, making such interferometers vulnerable to several forms of external noise. The dominant sources of noise are mechanical vibration and changes in ambient

conditions. The former, most pronounced at frequencies above 10 Hz, can be mitigated to some extent by keeping the non-shared paths small by interferometer layout [Gre09], separation by polarisation [Tsa10], or using dispersive mirrors [Müc05, Cre08]. Changes in temperature, air pressure or humidity will still have an impact on the phase.

Even in the case of a perfectly drift-free interferometer, phase errors may arise from the means of obtaining a sufficiently broad spectrum. Unless one resorts to the comparison of higher harmonics of the frequency comb [Hit14], spectral coverage of at least one optical octave is needed. Only very few laser oscillators fulfil this requirement directly from the resonator [Rau09]. Most commonly, a fraction of the oscillator output is broadened via supercontinuum generation in a photonic crystal fibre (PCF). With a core size of about  $2\ \mu\text{m}$ , these fibres are very alignment-sensitive, and due to the highly nonlinear nature of the broadening process, changes in coupling efficiency result in strong changes to the optical phase of the comb lines.

An attractive alternative is the so-called monolithic interferometer relying on difference frequency generation [Fuj05]. This type of device combines the generation of an octave-spanning spectrum with the frequency conversion step in a single crystal. The input pulses are focused into a periodically poled lithium niobate (PPLN) crystal. Simultaneously, the spectrum is broadened by SPM, and quasi-phase-matched four wave mixing takes place. As in the f-to-2f, the frequency conversion takes place among the spectral edges. In this case, additional components are generated at the long-wavelength edge by DFG between lines on the high and low frequency edges of the comb. As both pump and idler frequencies carry the CEO frequency, the resulting comb has an offset of zero. At the overlap of the fundamental and the newly-generated comb, an RF beat signal at  $f_{\text{ceo}}$  can be detected by a photodiode. Because the generation of spectral content at the very edges of the spectrum and the frequency mixing are narrowly confined in

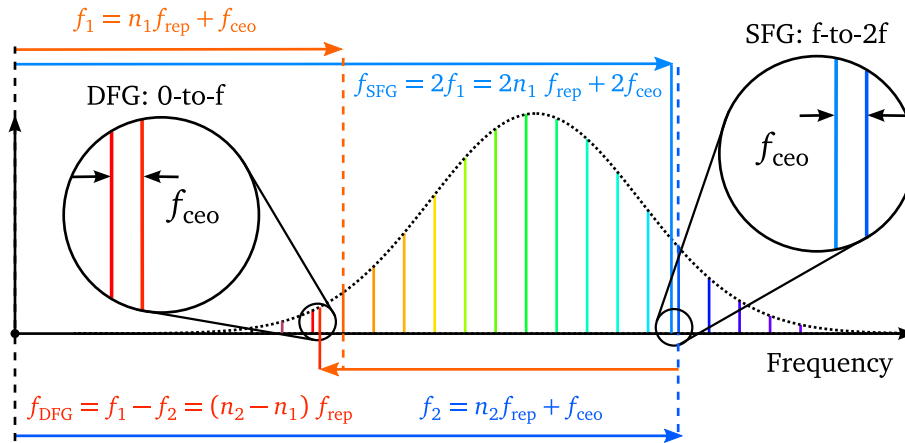


**Figure 2.3:** The self-referencing scheme in the SFG (f-to-2f) and DFG (0-to-f) variations. The comb offset  $f_{\text{ceo}}$  is always observed as a frequency beating between adjacent lines of two combs. One comb is the fundamental, the other has been produced from the fundamental by a form of nonlinear frequency conversion.

space and time, no delay needs to be introduced. The DFG interferometer requires the input pulses to have both a comparatively high energy ( $> 3$  nJ as opposed to 0.1-1 nJ when employing a PCF for broadening) and a fairly broad spectrum to start from ( $> 200$  nm at -10 dB). However, being almost immune to external noise and drift and practically alignment-free, it is the only available option for uninterrupted CEP-stable operation over hours to days. Furthermore, in order to measure the performance of the system with as little phase drift as possible, also the second interferometer used for OOL characterisation needs to be of this type. Taking into account the aforementioned requirements with respect to bandwidth and intensity, such a measurement represents a benchmark in its own right.

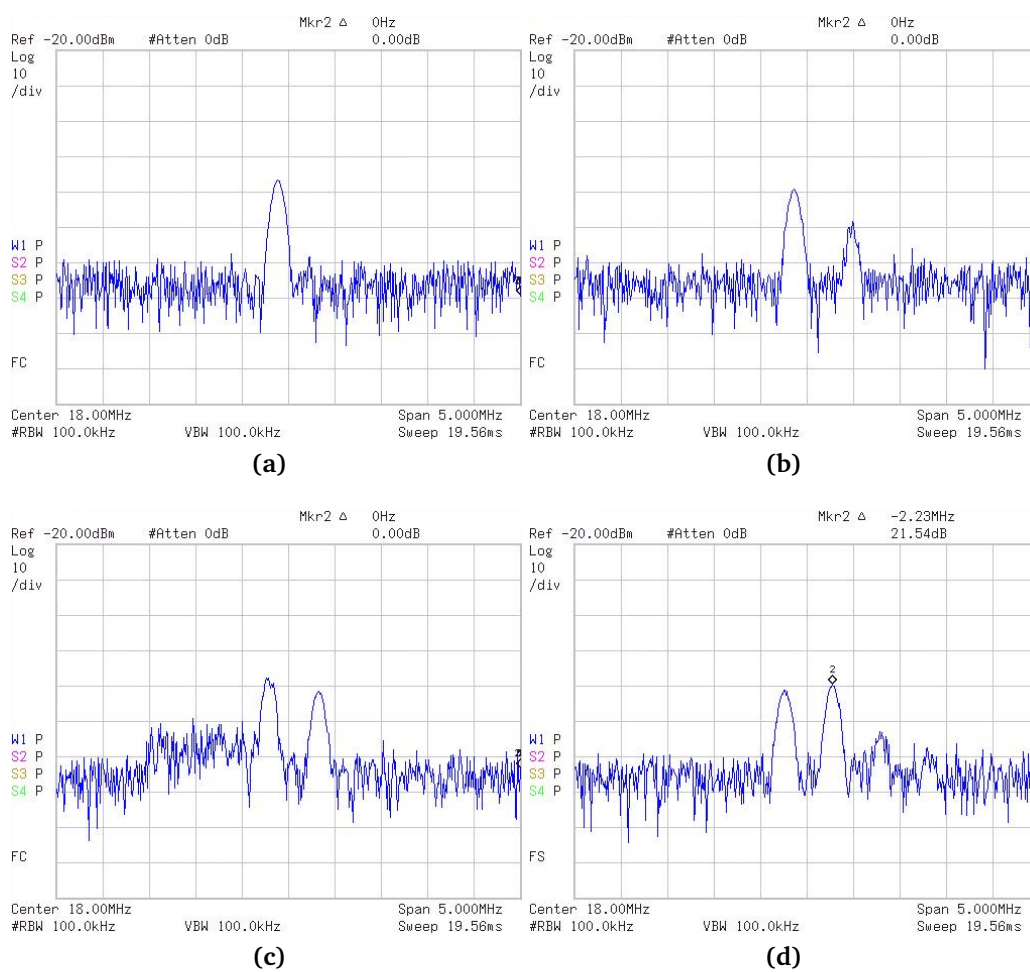


**Figure 2.4:** RF spectrum of the CEO beat signal, measured by a DFG-type interferometer placed in the non-diffracted beam after the AOFS. a) AOFS off. b) AOFS on, diffracted power 30 mW. c) diffracted power 67 mW. d) diffracted power 100 mW. The frequency axis scale is 500 kHz per division for all plots.

In a first experiment, the layout given in [Kok10] was replicated, but employing the AOFS described in Section 2.2.1 and a DM compressor. The in-loop CEO detection, still situated behind the shifter, was replaced by a monolithic DFG interferometer. A dispersive mirror-based Ti:sa oscillator (rainbow, Femtolasers) provided 300 mW average power in  $< 7$  fs pulses at a repetition rate of 76 MHz. A CEO signal of 25 dB signal-to-noise ratio (SNR) was measured with the AOFS switched off (Figure 2.4a). The offset signal ( $\sim 18$  MHz) was mixed with an RF source at 67 MHz to reach the AOFS drive frequency at 85 MHz. Gradually increasing the RF power sent to the AOFS, an additional peak appeared in the RF spectrum of the CEO signal (Figure 2.4b). The diffracted optical power was approximately 30 mW at this point. Further increasing the RF power to an output power of 67 and 100 mW, the additional peak became more pronounced, then even a third appeared (Figure 2.4c and d, respectively). Lowering the RF power, the peaks disappeared again. All the while, the diffraction efficiency into the first order was considerable lower than when driving the AOFS with a fixed RF source, where 75-80% are readily achieved.

The rise of equidistant side-bands to the original CEO beat was caused by the onset of amplitude modulation to the power in the interferometer. The modulation frequency is given by the frequency spacing. Inadvertently, an oscillating loop was built due to the strong coupling of CEO signal strength to input power found in the DFG-type interferometer, shifting power between the diffraction orders. This problem was not encountered in the earlier experiment because the PCF broadening stage was situated before the AOFS. However, it could have become an issue even with fibre-based f-to-2f devices when trying to increase the diffraction efficiency. Although the occurrence of self-oscillation makes this configuration unsuitable for reliable operation, it at least allows a reasonable estimation of the correction bandwidth that can be expected of the stabilisation system. The frequency spacing of the side-bands is the inverse delay introduced by the signal chain. The path consists of the CEO measurement, RF mixing and amplification, generation, and propagation of the density wave to the interaction region with the light. The shorter this path, the higher the frequency of the oscillating loop as the delay decreases. This was verified experimentally, resulting in an rising line spacing with decreasing distance of the light to the transducer. The effective CEP stabilisation bandwidth could thus be determined to 500-750 kHz.

Mitigation of the self-oscillation problem requires that the IL interferometer be placed before the AOFS. In order to obtain re-compressible pulses with a good beam profile, the signal intended for the CEO detection must be split off the oscillator output. It serves only to detect the CEO signal of the oscillator, as the PPLN crystal is both highly dispersive and usually introduces wavefront errors due to the hard focus and strong SPM. A significant part of the oscillator output power is lost this way, although it can still be used for non-CEP-critical applications. Running cavity-external stabilisation in this fashion places high demands on the oscillator, as approximately 600 mW are needed to produce a CEP-stabilised, compressed output beam of 200 mW. Alternatively, the entire output can be sent through the DFG interferometer when beam profile and compressibility are of lesser concern. This is almost always the case when the laser is used to seed a multi-pass amplifier, where temporal stretching of the input pulses

is required in any case. This application will be described in detail in Chapter 4. The optical power requirements in this case are considerably relaxed, with an upper limit of 300 mW being set by the PPLN crystal.

### 2.3.2 Minimizing auxiliary phase drift

In addition to shifting the frequency of the optical wave by that of the acoustic wave, the AOFS also adds the relative phase of the acoustic wave to the incoming light to the beam being diffracted. Leaving aside the intended corrections based on the measurement in the IL interferometer, this relative phase can be changed in three ways. First, a phase error can arise in the RF signal chain. Analogous to dispersion in optics, most RF components exhibit a frequency dependence in their transmission delay. For single-frequency RF waves, frequency changes thus result in phase changes. These phase changes are mostly negligible for the small frequency changes involved, but in the case of higher-order band-pass filters, they can become significant. There are other important reasons that changes in drive frequency should be kept small, which are presented in the following section. Still, it is possible that the large long-term phase error reported in [Kok10] was caused by this effect. Second, the finite travelling time of the acoustic wave to the interaction region translates any frequency change to a phase change, increasing with the distance between the transducer and the traversing light. In addition to the stabilisation bandwidth being inversely dependent on the travelling time, this effect provides another incentive to keep the distance as small as possible. Lastly, taking the beam position as the origin of a coordinate system, transverse movement of the AOFS or the beam itself are indistinguishable from changes in the acoustic phase. Therefore, even mechanical movement of components can cause CEP drift, making a robust mechanical design imperative.

Koke *et. al.* have suggested to use an RF phase shifter to correct for these issues, e. g., in the form of a compensation network [Kok12, p. 65]. For the purpose of long-term stabilisation, this has turned out to be unnecessary, as will be shown in this chapter. They also envision the application of such a device as a CEP actuator independent of the stabilisation system. The experimental realisation of the idea is described in Section 4.3.

### 2.3.3 Preventing oscillator CEO frequency drift

Using the output of a photodiode to drive an AOFS requires considerable amplification. In the case of the FF technique presented here, about 90-100 dB gain are necessary over the entire RF signal chain. To preserve (or even enhance) the SNR, frequency filtering and narrow-band amplification are essential. This is most critical in the final amplification stage, which provides the largest gain per stage. Whereas low-pass filtering is sufficient before mixing the free-running offset with the auxiliary RF signal, the sum frequency of the two needs to be band-pass filtered narrowly. As was mentioned in Section 1.3, in a non-stabilised oscillator, slow changes of the CEO frequency are largely dependent on the ambient conditions. These usually act through

changes of the intra-cavity dispersion or the beam pointing of the pump laser. In a controlled environment, especially for systems with a hermetically sealed cavity, the range of such changes can be as low as a few megahertz ( $<0.1 \cdot f_{\text{rep}}$ ) per day (e. g., see Figure 2.17 in the last section of this chapter). In many laboratories, however, this magnitude of drift is reached within hours, particularly with alignment-sensitive ultra-broadband oscillators generating pulses with  $< 7$  fs.

In order to ensure long-term CEP stabilisation with the FF technique, one therefore has to implement a slow control that keeps the quasi-free running oscillator CEO frequency within the limits set by the narrowest band-pass filter. Such a control needs to be neither fast nor precise, and is best implemented in a simple feed-back configuration. The most important step is the reliable derivation of an error signal. In order to avoid the complexity and other drawbacks of phase-locking the CEO frequency itself, some form of frequency-to-voltage conversion and subsequent comparison with a voltage reference is preferable. A simple implementation of the so-called tracking filter provides a solution [Gar79]. Here, a PLL is used to lock a voltage-controlled oscillator (VCO) to the CEO frequency, and the control voltage of the VCO provides a DC level proportional to the input frequency (see Figure 2.5). Note that this circuit is (for practical considerations) immune to the drawbacks mentioned in Section 1.4 because the loop encompasses RF signals only. Its bandwidth is determined by electronics exclusively, rather than by the complex interaction of electronic, optical, and acoustic effects. Alternatively, one could also make use of the fact the spatial separation of the diffraction orders is linearly dependent on the acoustic drive frequency (Equation 2.3). A precise differential position measurement would thus provide direct access to changes in drive frequency. Utilizing four-quadrant photodiodes, micrometer spatial resolution can be reached, corresponding to a frequency precision of a few tens of kilohertz, which would be sufficient.

Aiming for the correction of changes in the laser CEO frequency occurring on the time-scale of seconds, the actuator should not be significantly faster to avoid adding noise. Furthermore, it should be capable of making continuous (as opposed to stepwise) adjustments. Thin intra-cavity glass wedges are commonly employed for dispersion control in few-cycle laser oscillators, and

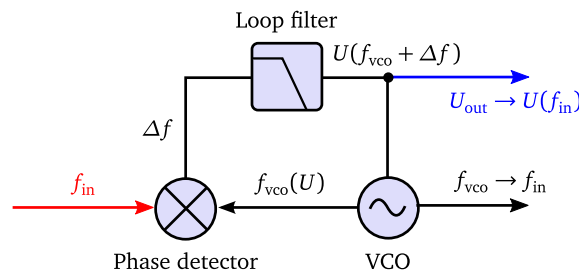


**Figure 2.5:** Block diagram of a tracking filter. A voltage-controlled oscillator is phase-locked to the incoming signal  $f_{\text{in}}$ . The frequency/phase difference between the oscillator output  $f_{\text{vco}}$  and  $f_{\text{in}}$  passes a loop filter and is fed back to the control voltage input of the VCO. In the steady state,  $f_{\text{vco}} \rightarrow f_{\text{in}}$ , and  $U_{\text{out}}$  is proportional to  $f_{\text{in}}$ .

have been used to control the pulse-to-pulse phase slip since the early days of CEP stabilisation [Xu96]. However, they are often mounted on linear translation stages motorised by piezoelectric ratchet drives which induce considerable vibration when in action. Direct piezoelectric actuation, in turn, provides too little range. Influencing the CEO frequency by pump power changes and mirror tilt are no option due to their by-effects on output power and spectral distribution, in addition to beam pointing in the latter case. A further method towards slow and continuous change of the CEO frequency is to control the Ti:sa crystal temperature [Yun09]. Mounting a heater element on the crystal holder of the oscillator available for the experiments described in the following (rainbow UHP, Femtolasers), a coupling constant of temperature to CEO frequency change of 1.2 MHz/K was determined.

In a simple digital control loop with a cycle time on the order of 1 s, the VCO control voltage can be sampled, processed in a slow proportional-integral (PI) loop, and fed back to the heater element to keep the CEO frequency within the desired limits. Of course, the temperature of the crystal should stay within a few Kelvin in order to avoid detrimental effects on the rest of the laser cavity. Should the range be insufficient, movement of the glass wedges can be implemented in addition.

Note that this “slow loop” does not constitute a frequency (let alone CEP) stabilisation in the usual sense, as can be seen from the following estimate. Measured with an RF spectrum analyser, the free-running CEO signal of a broadband Ti:sa oscillator shows a width of about 10 kHz when integrated for 1 ms, not limited by the resolution bandwidth. Assuming the best case, i. e., a mean offset of zero, this corresponds to a CEP slip from one pulse to the next of

$$\Delta\Phi = 2\pi \cdot \frac{f_{\text{ceo}}}{f_{\text{rep}}} = 2\pi \cdot \frac{10 \text{ kHz}}{100 \text{ MHz}} = 2\pi \cdot 10^{-4}. \quad (2.4)$$

Within  $10^4$  shots, or 100  $\mu\text{s}$ , the CEP of the output pulses changes by  $2\pi$ . A loop acting on the time-scale of seconds therefore simply serves to ensure reliable operation of the FF technique over long stretches of time.

## 2.4 Precise stabilisation over extended time

Taking into account the considerations described in the preceding sections, an FF stabilisation system was designed to fit the needs of ultrafast science experiments. Initially a breadboard-based prototype with external electronics, it has matured into an add-on module with a rack-mounted control box intended for use with a line of commercial Ti:sa oscillators (rainbow, Femtolasers). It was commercialized by the company under the name *CEP4* in 2012, but most of the measurements presented here were achieved with prototypes at the LMU in Munich from 2010 to 2011. The essence of these experiments was published in [Lüc12a].

### 2.4.1 Laser oscillator

The pulse train to be CEO-stabilised was provided by a commercial Ti:sapphire oscillator (rainbow, Femtolasers). It was pumped at a wavelength of 532 nm with up to 7 W of continuous wave (CW) power from a frequency-doubled diode-pumped solid-state (DPSS) ring laser (Verdi V-10, Coherent) placed within the oscillator housing. The Kerr-lens mode-locked (KLM) laser relied on dispersive mirrors for dispersion management and a pair of fused silica wedges for fine tuning [Sti94]. It delivered  $< 7$  fs pulses (FWHM) at a repetition rate of 76 MHz and an average power of 575 mW. The output spanned from 630 to 950 nm at the -10 dB level, the central wavelength amounted to 795 nm. To allow for temperature control, the crystal mount was fitted with a TO-220 package transistor. A small part of the output power was directed onto a photodiode mounted inside the laser housing to generate a repetition rate signal.

### 2.4.2 Stabilisation module

All optical components needed for stabilisation of the CEO frequency were mounted inside a modular enclosure attached to the laser housing. The footprint of the module was approximately  $35 \times 30 \text{ cm}^2$ . Its baseplate and the AOFS holder were water-cooled and connected in series to the cooling supply of the oscillator. Thus, temperature-related influence on the stabilisation performance was reduced. With a beam height of 12.7 mm above the baseplate, the set-up had low susceptibility to low-frequency mechanical vibrations. The input power into the module was distributed into two branches by a broadband beam splitter. About 250 mW were directed to

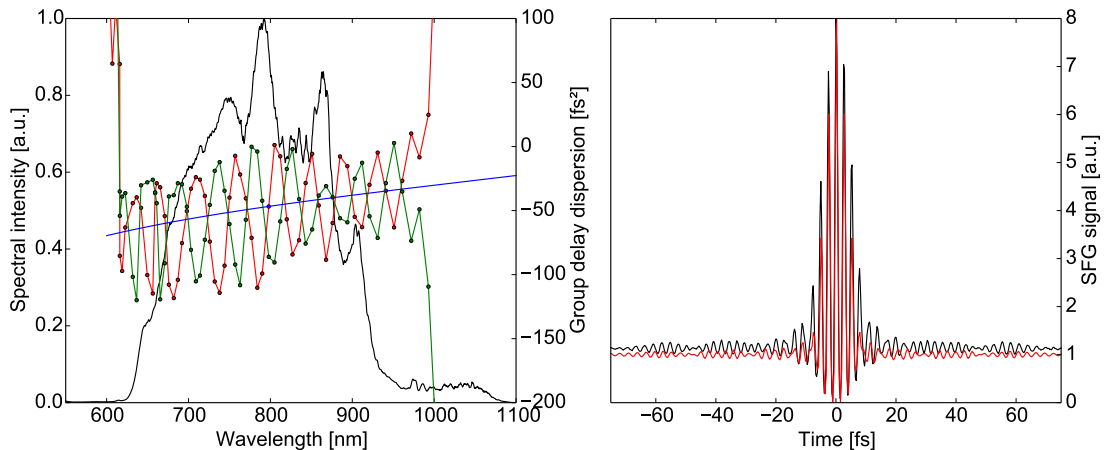


**Figure 2.6:** Spectral and temporal properties of the CEP-stabilised output pulse train. *Left panel:* Output spectrum (black trace). Complementary mirror pair target (blue) and measured GDD curves (red/green traces). *Right panel:* FRAC of the CEP-stabilised output pulses (black trace) and of the Fourier-limited pulse (red trace). Under assumption of a  $\text{sech}^2$  pulse shape, the traces indicate pulse durations of 6.5 and 4.7 fs FWHM, respectively.

the measurement section, containing a 0-to-f type interferometer as described in Section 2.3.1. It consisted of a 3 mm long PPLN crystal optimised for DFG (600 nm, 1200 nm  $\rightarrow$  1200 nm) placed between Ag-coated mirrors with 50 mm radius of curvature (ROC). The interference between the fundamental and the DFG-generated comb was band-pass filtered and detected by a fast InGaAs photodiode (FPD-510-V, Menlo Systems), providing the free-running CEO frequency  $f_{\text{ceo}}$  with a SNR of  $>35$  dB (100 kHz resolution bandwidth, RBW).

In the stabilisation branch, the remaining light was focused by a silver mirror of 1 m ROC into a crystal quartz AOFS of 20 mm length (custom model, Gooch & Housego, see Section 2.2.1), placed at the waist of the beam. When driven at optimum power at the nominal frequency of 85 MHz, the diffraction efficiency into the  $-1^{\text{st}}$  order amounted to  $> 80\%$  with some roll-off towards the spectral edges. Correspondingly, the output spectral bandwidth at the 10 dB-point was reduced to about 290 nm (640-930 nm).

A BK7 wedge was placed directly after the shifter in order to compensate the angular dispersion caused by the Bragg diffraction in the frequency-shifted beam (Figure 2.2b). The diverging beam was collimated by another Ag mirror of 1 m ROC and finally passed a DM pair. Figure 2.6 shows the spectral and temporal output profile measured after the stabilisation module. The mirror compressor was tailored to the dispersion of the two major dispersive elements, i. e., AOFS and compensation wedge. The red and green traces in Figure 2.6 show the GDD curves of the two mirrors. The dispersion was fine-tuned by translating the compensation wedge behind the shifter. After 11 reflections off each mirror, a pulse duration close to the oscillator output was determined by fringe-resolved autocorrelation (FRAC). The CEP-stabilised output power was 220 mW, which is sufficient for most usual oscillator applications. This value corresponds to an efficiency of 67 % with respect to the power entering the stabilisation branch. Apart from the diffraction losses in the AOFS of approximately 20 %, this was caused by 13 reflections off Ag mirrors, made necessary by the compactness of the unit.

### 2.4.3 RF signal chain

The purpose of the RF subsystem was to generate a driver signal to the AOFS at frequency  $f_{\text{drv}}$  that results in a CEO-stabilised diffracted beam, and to ensure that the input CEO frequency stays within the limits set by the system. It was divided into three sections, respectively dealing with the amplification of  $f_{\text{ceo}}$  and mixing with the mirror frequency of the desired output offset  $f_{\text{ext}} = f_{\text{rep}} - f_{\text{out}}$  to obtain  $f_{\text{drv}}$ , power amplification, and coarse stabilisation of the input CEO by feed-back to the crystal temperature. A schematic overview is given in Figure 2.7.

The pre-amplifier section provided a certain flexibility with respect to the input offset. Recalling Equation 2.1, the AOFS drive frequency is the sum of  $f_{\text{ceo}}$  and  $f_{\text{ext}}$ . Due to the necessary band-pass filtering, it must remain constant to within approximately 1 MHz (Section 2.1). Most experiments require an offset of zero (and thus  $f_{\text{ext}} = f_{\text{rep}}$ ), corresponding to a train of pulses with identical CEP (Section 1.2). For precision metrology, but also for the frequency-resolved

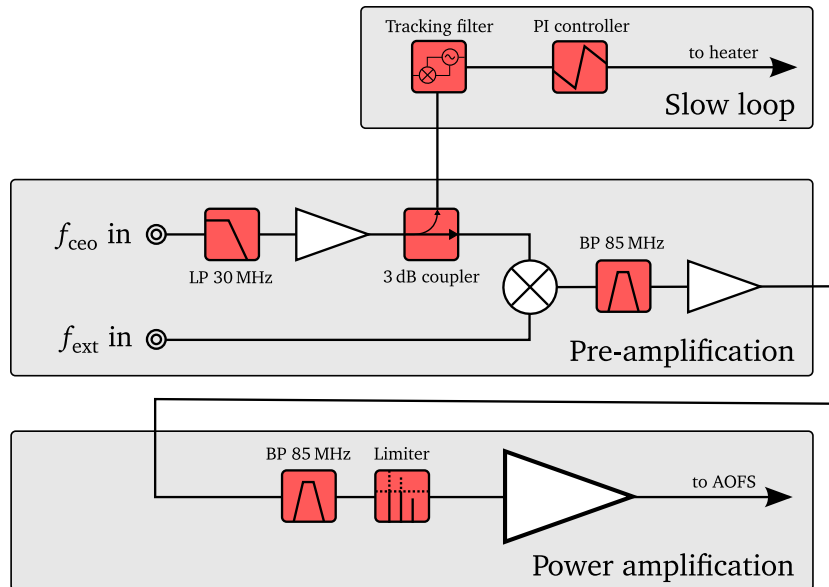


**Figure 2.7:** Block diagram of the RF signal chain used in the cavity-external CEP stabilisation. BP: band-pass filter. LP: low-pass filter.

characterisation of the residual noise described in the following section, the output offset needs to be non-zero, i. e., stabilised to a fixed frequency provided by an RF reference. This required the oscillator to run with a different CEO offset. Low-pass filters with a cut-off at approximately half the repetition rate (3 dB-cut-off at 30 MHz) were thus chosen to grant maximum flexibility. After two iterations of amplification and filtering, the signal from the photodiode had reached a power level sufficient for the reference input to a mixer (approx. 0 dBm). At this point, the signal was tapped by a directional coupler for both user monitoring and input to the slow feed-back stage.

After the mixer, the sum frequency of the two inputs was selected by a 3 MHz-wide band-pass filter, centred at the AOFS drive frequency of 85 MHz, and amplified again. A limiter set to -10 dBm protected the following final amplification stage and provided a stable power level. A second tap enabled the user to monitor the drive frequency. The final stage then provided 50 dB gain to reach the desired drive power level of approximately 40 dBm (10 W).

The frequency-to-voltage conversion as described in Section 2.3.3 took place in the third part of the RF system. The output voltage of the tracking filter was digitized by a microcontroller running a simple PI control loop with a user-set reference value. While the loop was open, the transistor mounted on the gain medium in the oscillator dissipated a constant current in the middle of its linear range. When the loop was closed, the dissipated power was varied by changing the gate voltage. Interlocks were in place to prevent overheating of the crystal and to detect mode-locking failure.

## 2.4.4 Phase noise characterisation

In the FF scheme, an independent OOL measurement is always necessary for a characterisation of the stability. No information on performance can be gained from the IL signals, because those remain unaffected by the stabilisation. Then again, derivation of the stabilisation performance from the IL interferometer data, which can only be done in feed-back based systems, leads to a considerable underestimation of the residual phase errors. Inside the loop, any noise induced by the interferometer will be cancelled perfectly up to the correction bandwidth. In the set-up presented here, the CEO-stabilised pulse train provided sufficiently high energy and short pulse duration to allow a second measurement in a monolithic DFG-type interferometer. This was essential for precise stabilisation and characterisation, in particular on long time-scales, as this type of interferometer is least prone to drifts. The interferometer was identical to the one used to detect the IL offset, and provided a 30 dB beat signal at the frequency  $f_{\text{ool}}$ .

A diagram of the measurement scheme is shown in Figure 2.8. To enable a heterodyne measurement of the residual phase noise of the CEO frequency, the system was set to shift the comb offset to a fixed frequency  $f_{\text{ext}}$  supplied by an RF generator. The signal from the OOL interferometer was band-pass filtered and amplified to a suitable power level. This signal at  $f_{\text{ool}}$  was mixed down with the reference signal at  $f_{\text{ext}}$ . The result was a DC voltage proportional to the sine of the phase between the OOL signal and the reference, granting access to the residual phase noise between the target RF and the actual stabilised output. Note that the phase noise of the CEO frequency is equivalent to the CEP noise of the pulse train for  $(f_{\text{ext}} \bmod f_{\text{rep}}) \rightarrow 0$ . Voltage-to-phase calibration was obtained by replacing the OOL signal by a second RF source

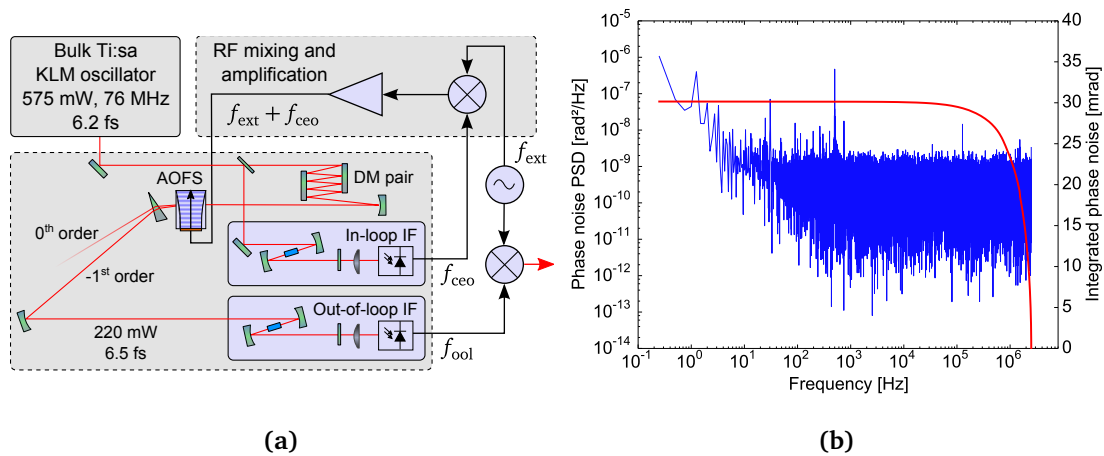


**Figure 2.8:** Frequency-resolved characterisation of cavity-external CEP stabilisation for few-cycle pulses. **a)** Experiment layout. See Figure 2.7 for a detailed view of the RF section. IF: interferometer. DM: dispersive mirror. **b)** Fourier transform of 4 s residual phase noise time series (0.5 mHz–5 kHz). *Blue curve:* phase noise PSD. *Red curve:* IPN.

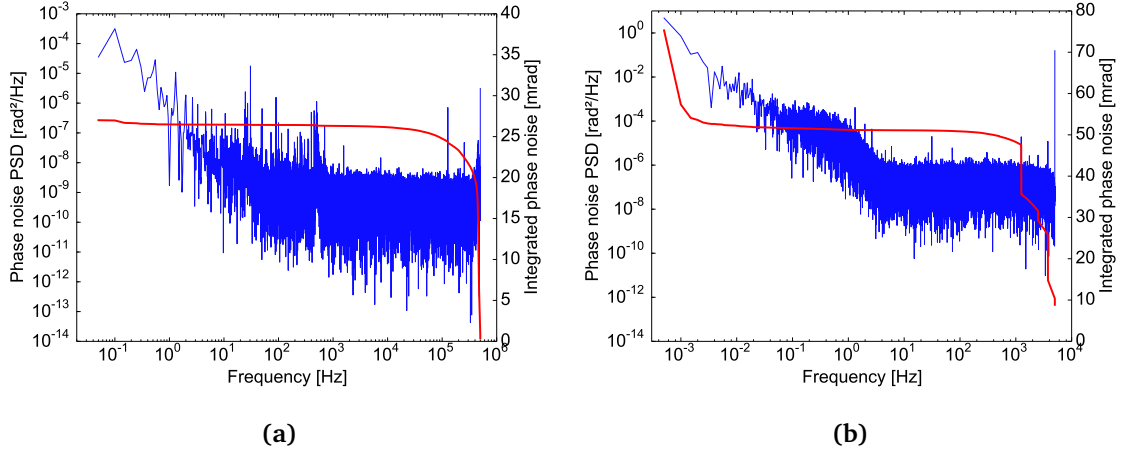


**Figure 2.9:** Fourier transform of phase noise time series measured in an OOL 0-to- $f$  interferometer for different measurement times and sampling rates. *Blue curve:* phase noise PSD. *Red curve:* IPN. **a)** 20 s time series, 50 mHz–500 kHz. **b)** 2000 s time series, 0.5 mHz–5 kHz.

of the same power level as the signal at  $f_{\text{ool}}$ , but fixed at a slightly different frequency. The resulting linear phase evolution between the two signals yielded a sine wave whose maxima indicate  $\pm \frac{\pi}{2}$  phase difference. For frequency-resolved analysis, the mixer output signal was low-pass filtered at the Nyquist frequency to prevent aliasing and was recorded with a digital sampling oscilloscope at the maximum available memory size of 20 million samples (MSa). Details on the numerical processing involved are given in Appendix B.

For short-term performance characterisation,  $f_{\text{ext}}$  was set to approximately 60 MHz, and the oscillator CEO frequency to about 25 MHz. At the time of this experiment, the system had not yet been equipped with a slow loop, so the oscillator remained entirely free-running for the measurements presented in the following. The mixer output was sampled at 5 MHz for 4 seconds. Correspondingly, the residual noise could be determined from 0.25 Hz to 2.5 MHz. A detailed explanation of terms and methods used for the characterisation of noise in this work is given in Appendix A. Figure 2.8b shows the Fourier analysis of the phase deviation measured in the OOL interferometer. The noise power spectral density (PSD, blue trace) shows narrow-band contributions characteristic of the noise sources mentioned in Section 1.3. Integration over the PSD yields the integrated phase noise (IPN, red trace). It shows no step-like features, meaning that none of the spikes in the PSD contributes significantly to the total phase error. Within 4 seconds, the statistical CEO phase error amounts to less than 30 mrad RMS. This value compares favourably to that measured in the proof-of-principle experiment (5 s, 0.2 Hz–2.5 MHz, 45 mrad) [Kok10]. With one period of the driving field lasting 2.7 fs, stabilisation to zero offset would result in a timing jitter of less than 13 as between carrier and envelope. In fact, this value represents an upper limit to the actual phase error since detection shot noise masks the underlying noise signature.

The exact contribution of detection shot noise to this figure cannot be directly measured, but based on the linearity and level of the PSD above 1 kHz, it can be safely assumed that the actual phase error is considerably lower. Even without accounting for this overestimation, the stabilisation performance achieved here is among the highest ever reported, surpassed only by a sophisticated combination of intra-cavity feed-back and cavity-external frequency shifting [Bor11].

When sampling at 1 MHz, the accessible frequency components of the residual noise (50 mHz to 500 kHz) encompass the entire range in which CEP noise can be expected to occur, from the typical frequency of relaxation oscillations over the acoustic band down to air currents. As can be seen from the smooth IPN trace in Figure 2.9a, detection shot noise [Bor14a] is the dominant contribution to an overall phase error of 30 mrad even with a five-fold increase of the acquisition time. However, problems arise when looking at a significantly longer measurement time. Figure 2.9b shows the results of a 2000 s phase noise time series sampled at 5 kHz. Notable steps occur in the IPN trace above 1 kHz, marking the influence of acoustic noise in the laboratory. These contribute about 25 mrad to the total IPN of 78 mrad, keeping the residual phase noise level comparable to that of the short-term measurements. More significant for long-term performance, however, is the  $1/f$ -like rise of the phase noise PSD and the corresponding rise in IPN on the time scale of minutes. This behaviour was caused by changes in the free-running oscillator CEO frequency. As was discussed in Section 2.3.3, the time delay between transducer and the interaction region translates frequency changes to phase changes that are imprinted on the diffracted light. The effect was enhanced by the narrow-band filtering employed. Steep pass-band edges in RF filters resulted in strong phase oscillations at the cut-off frequencies, leading to an unwanted phase modulation if the AOFS driver frequency drifted more than a few megahertz. The straightforward way of mitigating these problems is the addition of a mechanism that keeps the CEO frequency roughly constant.

#### 2.4.5 Long-term operation

Motivated by the  $1/f$ -like noise caused mostly by the changes of the free-running oscillator CEO frequency, a slow feed-back loop was developed as described in Section 2.3.3. With all other parameters unchanged, the performance of the system on longer time-scales was investigated with the slow loop activated. As early attempts indicated that the phase drift would exceed the range of  $\pm \frac{\pi}{2}$  accessible to the analogue mixer, a different phase detection was necessary. Here, the phase error between the RF reference and the OOL signal is measured via the phase detection circuit of a high-frequency lock-in amplifier (SRS844, Stanford Research Systems). The phase was sampled at 1 Hz and recorded with a PC-based data acquisition system.

The data from one of these long-term recordings are shown in Figure 2.10. Within 28 hours, the phase between OOL measurement and reference drifts by roughly  $3\pi$ . These large excursions were caused by flaws in the slow loop system, mostly related to the frequency-to-voltage conversion. Attempts were made towards a geometrical implementation based on the angular

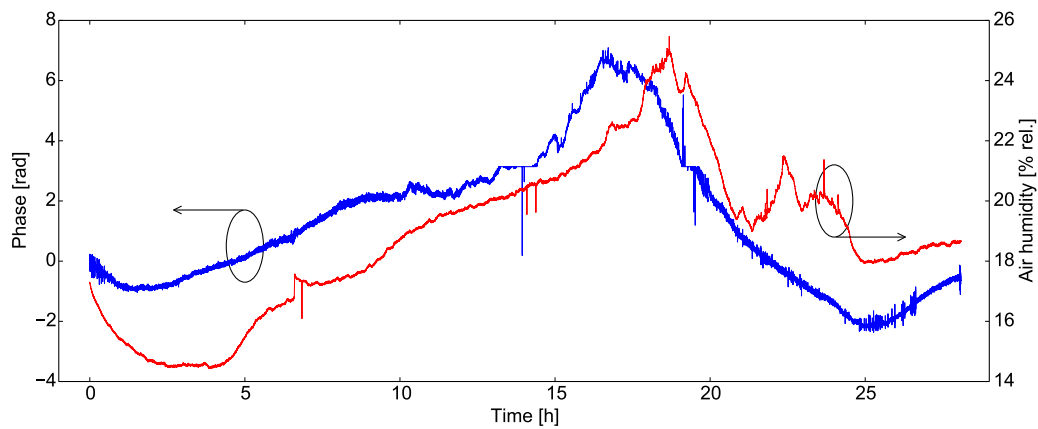


**Figure 2.10:** OOL phase recorded over more than one full working day with an early implementation of the slow feed-back loop. Artefacts around phase  $\pi$  are due to the wrap-around of the phase detection. *Blue curve:* measured phase. *Red curve:* relative humidity of environment air.

separation of the zeroth and first diffraction orders. However, it was found that the beam profile in the zeroth order changes significantly as the diffraction efficiency increases. Consequently, the four-quadrant diodes used for the detection showed a position reading that depended not only on the AOFS drive frequency, but also on the resulting diffraction efficiency, making such a loop prone to oscillation as well as slow drift. The approach was therefore abandoned in favour of the tracking filter solution described above.

Several problems were encountered with the RF circuitry at first. In particular, it was sensitive

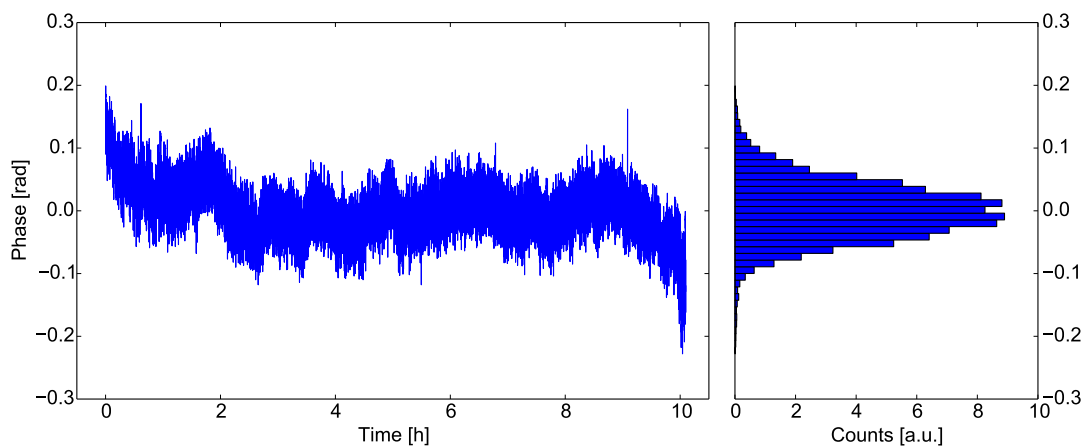


**Figure 2.11:** OOL measurement with functional slow feed-back correction of the oscillator CEO frequency. *Left panel:* measured phase. *Right panel:* histogram of phase values. Within 10 hours, the phase error amounts to less than 50 mrad RMS.

to changes in ambient conditions, e. g., temperature and air humidity. Figure 2.10 shows a parallel log of the latter and the OOL phase to illustrate the problem. Note that, regardless of the drift, a fixed phase relation is maintained at all times. Moreover, the drift of the absolute phase has negligible impact on the short-term performance, as the phase error of shorter segments rarely exceeds 150 mrad within any given 1-hour period of the measurement. This is in contrast to the situation in feed-back stabilisation, where a PLL loss-of-lock event would result in a random absolute phase after the lock is achieved again. The only comparable result known to the author is described in [Kim10], where a modified feed-back approach was employed to achieve a 56-hour CEP lock. However, the extended lock robustness came at the cost of short-term stability, and no figure is given of the magnitude of the OOL drift. When the free-running CEO frequency detection issues in the FF system had been resolved, the slow drift disappeared. The overall phase error could be reduced to 50 mrad RMS over a runtime of 10 hours (Figure 2.11).

## 2.5 Pulsed-mode operation

The frequency drift issues encountered with early implementations of the FF technique inspired the search for alternative solutions beyond the slow feed-back presented in the previous section. The modification presented in this section was suggested by Borchers *et. al.* [Bor13]. It exploits the fact that, in most amplification schemes used in ultrafast experiments, only a very small fraction of the pulses need to be CEP-stabilised, namely those that are picked for amplification. With seed oscillators possessing a repetition rate on the order of 100 MHz and amplifiers rather on the kilohertz level, the repetition rate difference opens up a new degree of freedom in the derivation of the AOFS drive signal.

The results in this section were achieved in close collaboration with Bastian Borchers, of Günter Steinmeyer's group at the Max Born Institute, Berlin. The essential findings have become the subject of a joint publication [Bor14b].

### 2.5.1 Working principle

For a pulse train of repetition rate  $f_{\text{rep}}$  and offset  $f_{\text{ceo}}$ , applying a cavity-external AOFS with driving frequency

$$f_{\text{drv},i} = n_i f_{\text{rep}} + f_{\text{ceo}}, \quad n_i \in \mathbb{Z}, \quad (2.5)$$

results in a zero-offset comb in the  $-1^{\text{st}}$  diffraction order. When the repetition rate is divided by a natural number  $m$ , resulting in the amplifier repetition rate

$$f_{\text{amp}} = \frac{1}{m} f_{\text{rep}}, \quad m \in \mathbb{N}, \quad (2.6)$$

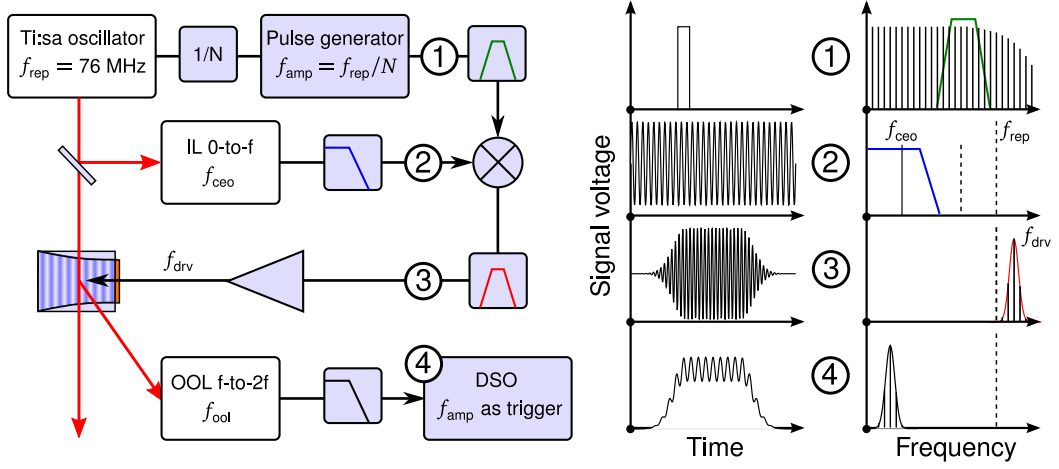


**Figure 2.12:** Signal synthesis and CEP characterisation scheme for pulsed-mode FF stabilisation. *Left panel:* experimental layout and signal synthesis. *Right panel:* schematic representation of signals in the time and frequency domain. The numbers denote the corresponding position in the synthesis and measurement scheme on the left panel.

this remains valid for every  $m$ -th pulse of the pulse train. Because the diffraction in the AOFS is subject to the superposition principle, this holds true even when the AOFS is driven by multiple frequencies  $f_{\text{drv},i}$  at the same time:

$$f_{\text{drv},i} = n_i f_{\text{amp}} + f_{\text{ceo}}, \quad m \in \mathbb{N}, n_i \in \mathbb{Z}. \quad (2.7)$$

Such an electronic frequency comb can readily be produced with a bandwidth of several tens of megahertz, corresponding to a short wave packet in the time domain. Simply put, the AOFS is driven by a broad frequency comb that is spaced with a fraction of the original repetition rate and which carries the CEO frequency as an offset. For common femtosecond amplifiers,  $f_{\text{amp}}$  is in the kilohertz range. In this case, the line spacing of the driving frequency comb is very small compared to the MHz-wide pass band of the filters in the RF amplification stages. Therefore, even for large excursions of  $f_{\text{ceo}}$ , a suitable driver signal is always ensured in the AOFS, provided that the RF comb is sufficiently broad. This scheme thus produces a pulse train with constant CEP at the amplifier repetition rate even in the presence of a drifting  $f_{\text{ceo}}$ . In practice, mirror frequency formation limits the acceptable drift to less than half the oscillator repetition rate. Yet, this restriction already allows for days or even weeks of CEP-stable amplifier operation for certain oscillators, as will be shown later.

In addition to being largely immune to CEO frequency drift in the free-running seed oscillator, pulsed-mode cavity-external CEP stabilisation provides several advantages compared to the original technique. First, as the mean frequency of the AOFS driver signal barely changes with  $f_{\text{ceo}}$ , neither does the position of the output beam. This potentially enhances the energy stability in a subsequent amplifier, and in the case of a system equipped with a grating stretcher, also CEP stability [Kak04]. With a duty cycle of only a few percent, the average RF power

dissipated in the AOFS is reduced drastically, alleviating cooling requirements and potentially enabling the use of cheaper RF components rated for lower average power.

### 2.5.2 Measurement set-up

The optical part of the pulsed-mode FF CEP stabilisation system is identical to that presented in Section 2.4. For the experiments in this section, a commercial implementation was used (rainbow CEP4, Femtolasers), comprising a DFG-type monolithic detection of the CEO frequency and an AOFS suitably compensated for spatio-temporal chirp. The signal synthesis scheme is shown in Figure 2.12. Compared to the original one (Figure 2.7), it includes an additional step to generate an RF frequency comb spaced by the reduced repetition rate, replacing the oscillator repetition rate in the original scheme.  $f_{\text{rep}}$  is divided down to obtain an amplifier repetition rate signal  $f_{\text{amp}}$ , which in turn is used to trigger a pulse generator (DG535, Stanford Research Systems). The latter is set to produce few-nanosecond pulses with steep rising and falling edges, corresponding to a kHz-spaced, zero-offset comb spanning beyond 100 MHz. In order to avoid mirror frequency formation, this signal is band-pass filtered before being mixed with the oscillator CEO frequency  $f_{\text{ceo}}$ . The frequency multiplication results in an approximately 20 MHz-wide RF frequency comb with line spacing  $f_{\text{amp}}$  and offset  $f_{\text{ceo}} \bmod f_{\text{amp}}$ . For efficient diffraction in the AOFS, the acoustic pulse length  $l_{\text{ac}}$  in the crystal should not be shorter than the beam diameter  $d$ ,

$$l_{\text{ac}} = \nu t_{\text{ac}} \approx 0.5 \frac{\nu}{\Delta f_{\text{ac}}} \geq d, \quad (2.8)$$

with  $t_{\text{ac}}$  the duration of the acoustic pulse and  $\Delta f_{\text{ac}}$  its bandwidth. For an optical beam of 1 mm diameter and the AOFS used before, the signal bandwidth should be limited to approximately 3 MHz. In order to facilitate the characterisation of the output phase stability, a surface acoustic wave filter of 300 kHz bandwidth centred at 85 MHz was chosen, placed prior to the final amplification stage. Due to the narrow filter bandwidth, the AOFS was driven by 4  $\mu\text{s}$  long acoustic transients, diffracting a total of 300 oscillator pulses each. The phase evolution of these short pulse trains is measured in a fibre-based f-to-2f interferometer with a dichroic mirror delay line [Gre09]. The CEO beat signal from an avalanche photodiode is recorded by a digital sampling oscilloscope (DSO, RTO1014, Rohde & Schwarz). The internal memory of the device allowed for the acquisition of 18462 segments of 5  $\mu\text{s}$  record length at a sampling rate of 1 GSa/s. For all accessible settings of the divider, i. e., for repetition rate setting from the sub-hertz up to 5.2 kHz, recording of consecutive traces was possible. For the maximum divided-down repetition rate  $f_{\text{amp}} = 5.2$  kHz, these parameters enabled a recording of the CEP for about 3.5 s, corresponding to a lower cut-off at 0.28 Hz. The interferogram phase was extracted from each segment by numerical demodulation with the Takeda algorithm [Tak82]. Further details on the data processing are given in Appendix B.

### 2.5.3 Results

Three sets of CEO beat traces measured in the OOL interferometer are displayed in Figure 2.13. For different values of  $f_{\text{ceo}}$ , each panel displays the data of 18462 traces in the form of a colour-coded histogram. The oscillator CEO frequency was left entirely free-running for these measurements. A clear sinusoidal modulation corresponding to the CEO beat can be seen in all panels, its frequency determined by

$$f_{\text{ool}} = (f_{\text{ceo}} - f_{\text{drv}}) \bmod f_{\text{rep}}, \quad (2.9)$$

showing that CEP stability is established. The input CEO frequency varies considerably between the panels, demonstrating that the scheme establishes CEP stability without the need for a slow CEO control loop. The drift was limited to up to 14 MHz, determined by the available RF band-pass filters applied to the kHz-spaced comb (green filter trace in Figure 2.12). In contrast, when  $f_{\text{ceo}}$  was replaced by a fixed RF source of similar mean frequency, the output CEP drifted freely, resulting in practically random phase, as shown in Figure 2.14a.

Note that, since the pulsed-mode FF stabilisation scheme relies on a fixed AOFS driver frequency, the OOL beat measured in the diffracted signal shows the same frequency drift as the in-loop  $f_{\text{ceo}}$ . For subsequent amplification, however, it is the phase of one single pulse that is important. At zero delay, i. e., in the case of instantaneous correction of the measured phase error, the stabilised phase would suffer from measurement errors only. Realistically, the inevitable group delay (GD) of both the band-pass filter and the AOFS prevents the correction of phase noise upwards of a certain frequency, and introduces additional phase noise through variations of  $f_{\text{ceo}}$

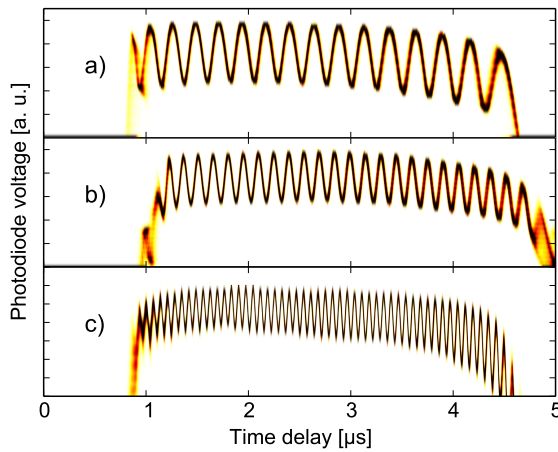


**Figure 2.13:** Histograms of phase evolution recorded in OOL f-to-2f, 18462 traces each. Panels show data for different values of  $f_{\text{ceo}}$ . a) 17.9 MHz, b) 20.5 MHz, c) 28.0 MHz.

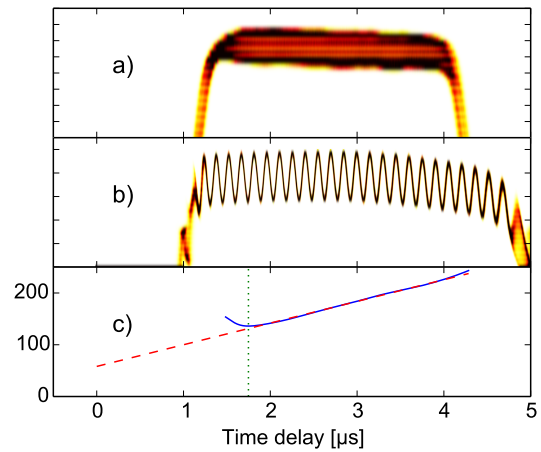


**Figure 2.14:** Histograms of 18462-trace sets. a)  $f_{\text{ceo}}$  replaced by fixed RF signal. b) CEP-stable operation. c) RMS CEP jitter [mrad] for data in b) and extrapolation to zero delay.

(Section 2.3.2). In the histograms displayed in Figures 2.13 and 2.14, this leads to increasing blur with time delay. The blue trace in Figure 2.14c shows the RMS phase variation for each time delay bin of the 18462 traces in the histogram above, indicating a linear increase of the CEP jitter with time delay. The minimum measured jitter at  $1.75 \mu\text{s}$  delay amounts to 136 mrad, which is on par with the values achieved with conventional CEP stabilisation [Ver12, Ver14].

The observed CEP error after stabilisation can be thus separated into two components. On one hand, a drift component is caused by changes of the free-running  $f_{\text{ceo}}$  that linearly increases with time delay. On the other, residual phase error at zero delay is the result of measurement noise both in- and out-of-loop. A slow feed-back loop as used in Section 2.4 practically eliminates the impact of the first contribution. The second component, however, can only be mitigated by careful design of the interferometers and cannot be avoided entirely. Extrapolation of the measured phase noise to zero delay allows an estimation of the measurement noise contribution. The red dashed line in Figure 2.14c reveals an RMS jitter of about 58 mrad. This demonstrates that the modified FF technique maintains the performance of the original single-frequency variant. The zero-delay jitter value can be approached by minimizing the GD in the signal processing chain. In the case presented here, the main contribution stems from the narrowband surface acoustic wave filter (red band-pass in Figure 2.12). This device was chosen to obtain long diffracted pulse trains in order to facilitate numerical evaluation. For practical applications, it should be replaced by conventional, less steep filters. The experiment described in Section 2.3.1 showed that the overall GD in a non-optimised arrangement is on the order of  $1 \mu\text{s}$ . Further reduction of the GD was demonstrated already [Kok11], and should enable stabilisation with pulsed-mode FF to less than 100 mrad residual CEP error on the time-scale of seconds. Taking into account these two contributing factors, the retrieved phase  $\Phi_{\text{ce}}^{(k)}(\Delta t)$  for every recorded time segment ( $k = 1 \dots 18462$ ) can be written in the form

$$\Phi_{\text{ce}}^{(k)}(\Delta t) = \Phi_0^{(k)} + 2\pi f_{\text{ceo}}^{(k)} \Delta t, \quad (2.10)$$

where  $\Delta t$  denotes the temporal delay within the recorded data segment.

The black and red traces in Figure 2.15a show the total measured phase noise  $\Phi_{\text{ce}}^{(k)}(\Delta t)$  and the phase noise induced by the frequency drift  $2\pi f_{\text{ceo}}^{(k)} \Delta t$ , respectively, at  $\Delta t = 1.75 \mu\text{s}$ . There is visible correlation between the two traces, revealing that frequency drift does play a role even within a short measurement time.

A frequency-resolved analysis of the phase noise yields further insights. The PSD, plotted in Figure 2.15b, indicates near-perfect agreement between the total phase noise and the frequency drift induced phase noise below 200 Hz, corroborating strong correlation on this time scale. The upward trend of the frequency-induced CEP noise towards the very lowest frequencies remains elusive, however, because it is not mirrored in the overall noise. In the regime of acoustic noise, narrow-band spikes lead to steps in the IPN that are common to both traces. This clearly demonstrates that, up to the acoustic band, residual CEP drift in the output is primarily caused by the delay-dependent contribution from changes in  $f_{\text{ceo}}$ . Upwards of 500 Hz, both PSD traces

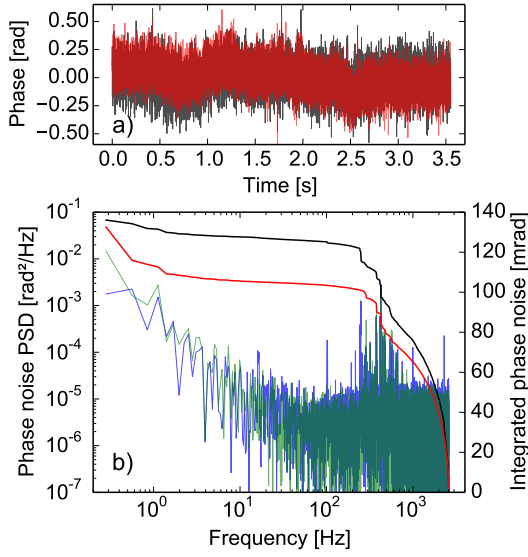


**Figure 2.15:** Analysis of short-term phase noise (0.285 Hz–2.6 kHz) for total phase noise (black traces) and contribution of  $f_{\text{ceo}}$  drift (red traces) at  $\Delta t \approx 1.75 \mu\text{s}$ . **a)** Time domain data. **b)** Fourier analysis of data in a). *Blue/black trace:* total PSD/IPN. *Green/red trace:* drift only.

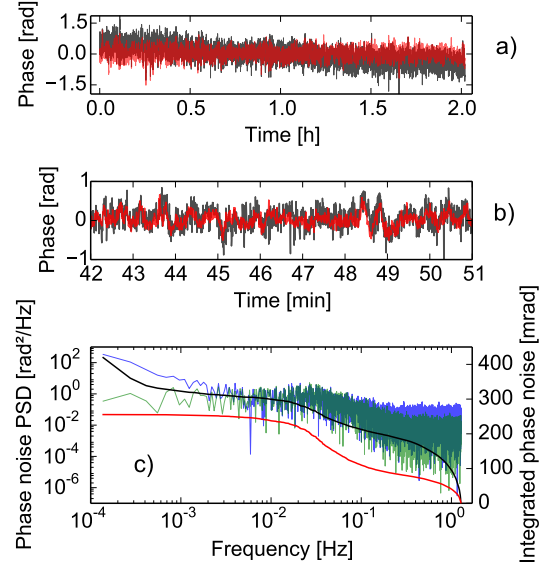


**Figure 2.16:** Analysis of long-term measurement (1.26 mHz–1.25 Hz) for total phase noise and contribution of  $f_{\text{ceo}}$  drift (trace colours as in Figure 2.15). **a)** Time domain data. **b)** Detail of a). **c)** Fourier analysis of data shown in a).

exhibit a nearly constant noise floor, which represents the detectivity limit of the measurement scheme ( $\approx 10^{-5} \text{ rad}^2/\text{Hz}$ ). This figure is somewhat higher than in the measurements presented in Section 2.4 (see Figures 2.8b to 2.9), where the noise floor is found on the level of  $10^{-6}$  to  $10^{-8} \text{ rad}^2/\text{Hz}$ . The reason lies both in the interferometer, inducing amplitude-to-phase coupling in the PCF, as well as to digitisation noise in data acquisition and processing. As a consequence of integrating over the instrument noise limit, the total IPN (black trace in Figure 2.15c) shows a smooth increase without apparent steps down to the region where noise-induced by drift of  $f_{\text{ceo}}$  becomes important. Note that the overall IPN of less than 140 mrad already is at the lower end of CEP noise values measured using spectral interferograms [Kak01].

To investigate the behaviour of the pulsed-mode FF technique for longer measurement times, the divider stage was set to obtain  $f_{\text{amp}} = 2.5 \text{ Hz}$ , extending the recording time of the data acquisition to over 2 hours. In order to avoid excessive phase drift, the slow feed-back correction was activated to keep  $f_{\text{ceo}}$  roughly constant. Time and frequency domain data are shown in Figure 2.16. Again, the frequency drift component prevails as can clearly be seen from the agreement of the phase noise traces in Figure 2.16b. On the time-scale of an hour, however, a slow de-phasing between measured phase noise and frequency noise occurs. This effect is most likely induced by a slow drift of the f-to-2f interferometer and therefore represents no actual CEP noise. The measurement also demonstrates that the temperature control implementation of

a feed-back correction is slow indeed. The red IPN trace in Figure 2.16c levels out only upwards of 10 mHz, corresponding to a loop bandwidth of minutes. As an alternative to employing such a slow correction loop, CEP-stable amplifiers often provide some form of feed-back correction to correct CEP variations on a comparable time-scale.

#### 2.5.4 Outlook

Pulsed-mode operation of the cavity-external CEP stabilisation technique substantially widens the applicability of the method for seeding low repetition rate amplifiers. This is particularly true for high-energy systems aiming beyond the millijoule level, as these often rely on grating stretchers that require a highly stable beam pointing. Due to the minuscule variation of the AOFS drive frequency, pulsed-mode FF CEP stabilisation can be used without introducing CEP jitter through pointing variations. Moreover, such systems are often part of large-scale facilities with a 24-hour schedule of experiments. Demanding a high degree of user interaction and supervision, CEP stabilisation of laser amplifiers has, up to now, remained out of question for most large user facilities. Within the last few years, several products have been introduced into the ultrafast laser market that claim to be more or less independent of user interaction. Unfortunately, none of these offers a stable CEP. These lasers commonly feature a hermetically sealed laser cavity, which can be expected to benefit the intrinsic stability of the CEO frequency. At present, the emission spectra from such automated systems are not sufficiently broad to allow the use of monolithic interferometers (see Section 2.3.1), but the operation of a fibre-based f-to-2f device might, with careful design, provide comparable performance.

In order to investigate the feasibility to CEP-stabilise such an oscillator using the pulsed-mode

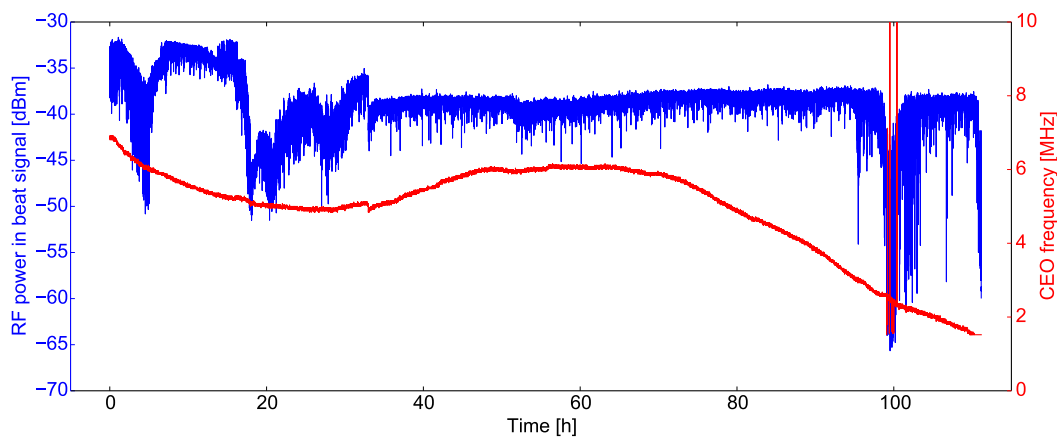


**Figure 2.17:** Free-running CEO frequency of a Ti:sa oscillator with hermetically sealed cavity (element PRO 500, Femtolasers) as detected in a fibre-based f-to-2f. *Red trace:* Beat signal frequency. *Blue trace:* RF power level.

FF technique, an available laser oscillator (element PRO 500, Femtolasers) was fitted with the  $f$ -to- $2f$  interferometer used for the experiments in the preceding section. A beat signal was easily obtained with a SNR of  $> 35$  dB (RBW 100 kHz), and showed high intrinsic stability. Applying and maintaining slight pressure on the edge of the laser housing prompted a shift in  $f_{\text{ceo}}$ . Within a few seconds, however, the beat signal returned to its initial value. The laser output power is actively stabilised, which suggests that the change in frequency was mediated solely by a change in intra-cavity power, and not by dispersion or geometrical effects. Shutting the laser down and restarting it resulted in an identical CEO frequency.

The laser was left unattended for almost five days while the CEO beat signal frequency and RF power were measured by an RF spectrum analyser, the data being polled at 1 Hz by a data acquisition PC card. As can be seen from the data displayed in Figure 2.17, the frequency excursions (red trace) were limited to less than 6 MHz within 110 hours. The maximum slope was below 100 kHz/h. Using this signal as input to a CEP stabilisation system as presented in Section 2.5.2 would have resulted in a 110-hour CEP stable pulse train.

The fluctuations in the beat signal RF power (blue trace) suggest that the limiting factor for this application is indeed the CEO frequency measurement in the  $f$ -to- $2f$  interferometer, rather than the laser itself. Reliably coupling the oscillator output into a PCF of less than  $2\ \mu\text{m}$  mode field diameter obviously requires a stable mechanical construction, but does not present a fundamental difficulty. Consequently, in combination with a CEP stabilisation unit based on the pulsed-mode FF technique, such a laser could become a platform for a maintenance-free source of CEP-stable pulses.

## 2.6 Summary

The adaptation of cavity-external CEP stabilisation for use with few-cycle pulse has culminated in a system capable of unparalleled stabilisation performance and robustness at the same time. This could be accomplished because adverse effects of the AOFS could be compensated, resulting negligible impact of the stabilisation system on the spatio-temporal properties of the pulses. This enabled the use of monolithic DFG-type interferometer, practically eliminating drift in the OOL measurement. The addition of a slow feed-back correction enabled day-long CEP-stable operation of the oscillator while maintaining its record-setting short-term stability. The work presented in this chapter thereby overcomes the stability-versus-robustness dilemma that plagues conventional CEP stabilisation. Moreover, a modification of the signal synthesis scheme was demonstrated that further enhances the applicability of FF CEP stabilisation to high-energy, low repetition rate amplifiers.

An oscillator stabilised using FF CEP control in either variety presents an ideal seed source for CEP-stable amplification to the millijoule regime and beyond. This application is discussed in detail in Chapter 4. In the following chapter, the results gathered with Ti:sa oscillators and low average power are applied to DPSS lasers providing higher average power and pulse energy.

## Chapter 3

# Towards CEP Stability of High Repetition Rate XUV Driver Lasers

Attosecond science relies on highly nonlinear processes. The low efficiency of generating coherent XUV radiation leads to long integration times and low signal-to-noise ratio, making some experiments tedious and others impossible. Although a more robust and precise CEP stabilisation may be a great benefit to present-day attosecond driver lasers at kilohertz repetition rate, the logical next step is to increase the repetition rate and average power. It is here that the current technological platform, Ti:sa chirped-pulse amplification (CPA, [Str85]), meets its economical and physical limits. First, Ti:sa requires the pump wavelength to be around 500 nm, which at present can only be accessed effectively by expensive frequency-doubled solid-state lasers. Second, the large difference of pump and laser wavelength means that more than a third of the pump energy ends up as waste heat that needs to be removed from the laser crystal. Consequently, interest in alternative driver laser sources has surged in recent years. Flanked by developments in diode lasers, rare-earth-doped media have become proven sources of sub-picosecond pulses up to the kilowatt level. Through spectral broadening and subsequent temporal compression, the pulse duration offered by such sources can be reduced to a few tens of femtoseconds, leaving only CEP stability to be accounted for. Furthermore, passive enhancement techniques have been proposed that ideally complement the low conversion efficiency of XUV generation. This chapter presents some of the first ventures into the CEP stabilisation of power-scalable laser sources with potential use in high-order harmonic or even attosecond pulse generation at megahertz rate.

First, a short overview is given in Section 3.1 of the concepts put forward to harness high average power IR lasers for XUV generation. CEP detection and stabilisation is shown to present a challenge in several respects. This motivates the exemplary investigation into the different aspects of CEP stabilisation that play a role for the respective concepts. Section 3.2 portrays the detection and stabilisation of the CEO frequency of a thin-disk laser oscillator. To this end, temporal compression of the pulses is necessary first. A different approach is covered in Section 3.3, dealing with a fibre-based master-oscillator power-amplifier (MOPA) system that is intensity-enhanced in a passive cavity. The task at hand was the full frequency comb

stabilisation of the system. Different means of CEO stabilisation are compared, gaining insight into the CEP properties of fibre amplification and the passive cavity alike.

### 3.1 Concepts

The approaches towards high average power CEP-stable laser sources treated in this chapter are all based on Yb-doped diode-pumped gain media. These ideally lend themselves to power scaling, as they can be pumped by laser diodes whose price has been dropping in the recent years as constantly as the available power has been rising. With picosecond pulses becoming established tools in industrial manufacturing, this trend can be expected to continue. Strictly speaking, even Ti:sapphire can be pumped by diodes in the blue to green spectral region, which has recently become accessible with laser diodes. Although some progress has been made in this direction (see [You13, Saw14]), the lack of high-power diodes and the large difference of pump and lasing wavelength still render this approach infeasible. Pumped at a wavelength around 980 nm and supporting an emission spectrum roughly between 1010 and 1050 nm, Yb offers a comparatively low quantum defect. This is complemented by the high thermal conductivity of the available host materials, even though it does fall short of that of sapphire ( $1.3 \cdot 10^4$  W/K in YAG as opposed to  $4 \cdot 10^4$  W/K in sapphire, both at 300 K [Web03]). Furthermore, several geometries of the laser media allow for effective thermal management. On the one hand, a gain medium in the shape of a thin disk [Gie94] or a flat slab [Kan83] allows for quasi one-dimensional heat flow. Amplification in optical fibres, on the other hand, reduces the thermal load by distributing the inversion along the propagation direction. When the advent of photonic crystal structures made it possible to maintain single-mode operation even while increasing the effective mode area [Bir97], high average powers became accessible here as well. All of these concepts have been demonstrated to provide pulses with picosecond-scale duration at several hundred watt of average power [Sar14, Rus09, Eid10].

However, the gain bandwidth of these media supports few-hundred femtosecond pulses at best. This makes the detection of the CEO frequency difficult, as extensive spectral broadening is needed to generate the optical octave needed in self-referencing (Section 1.3.1). In particular, the process employed must maintain temporal coherence, lest no interference of the  $f$  and  $2f$  components occurs. The most convenient way to achieve this is with so called highly-nonlinear PCF (see Section 2.3.1). As a rule of thumb, octave-spanning coherence can be expected when the launched pulses are shorter than 100 fs [Gen07], which usually is not the case for high-power lasers. Two approaches to this problem will be treated. In Section 3.2, the use of temporal compression is shown to enable the measurement of the CEO frequency of a thin-disk laser. This is not an option when attempting to CEP-stabilise the low-power seed laser at the beginning of a fibre amplifier chain, as is presented in Section 3.3, due to insufficient pulse energy. Instead, a specially designed auxiliary amplifier is demonstrated to provide broadening and amplification in one step. Additional obstacles must be overcome for Yb-based systems to achieve CEO stabilisation. The upper-state lifetime of the lasing transition in Yb is on the

order of a microsecond, a factor of thousand longer than in Ti:sa. Therefore, an oscillator with such a gain medium will exhibit relaxation oscillations in the kilohertz range, where much environment noise is concentrated. Furthermore, any attempt at CEO control via modulation of the pump intensity suffers from an asymmetric step response. Reductions in pump intensity lead to an exponential decay of the inversion with a millisecond time constant, whereas higher pump intensity affects the gain without this quasi-low-pass filtering.

Even with high average power and pulses lasting a few hundred femtoseconds, the intensity of such sources usually is not high enough to allow for the generation of XUV via high-harmonic generation (HHG). In the following paragraphs, three routes towards  $10^{13}$  W/cm<sup>2</sup> intensity are introduced briefly.

### 3.1.1 Intracavity HHG in oscillators

In order to maintain mode-locking (or even lasing), the intracavity energy of the circulating laser pulse can never be coupled out entirely. Although certain designs combining very high pulse energy with very low repetition rate achieve an output coupling of around 90 % [Neu08], this ratio customarily does not exceed 50 %. Inside the resonator, the intensity is therefore higher by at least a factor two. While this presents a limitation to the achievable output power of the oscillator due to optical damage, it is potentially favourable for any application that can take place *within* the cavity. HHG is an ideal candidate because of its small conversion efficiency and correspondingly low back-action to the laser process. Intracavity HHG has recently been demonstrated with a Ti:sa oscillator [Ser12], and could profit greatly from the transition to DPSS gain media. At the LMU, the work of Oleg Pronin was aimed at the design of suitable oscillators based on thin-disk technology and matching XUV output couplers [Pro12a]. It culminated in the development of a Kerr lens mode-locked thin-disk oscillator that delivered an (extracavity) pulse energy of 1  $\mu$ J in 200 fs pulses. With moderate modifications, the intracavity energy could be expected to reach 100  $\mu$ J, which in combination with an intracavity focus of 10  $\mu$ m radius would yield the desired intensity in excess of  $10^{13}$  W/cm<sup>2</sup> – at a repetition rate of several tens of megahertz. In the early days of HHG, such intensities were available on a once-per-per-minute basis [L'H93].

Still, it will take considerably shorter pulses to make CEP control necessary. However, in combination with some form of gating technique [Chi14] this could be the case, especially when more broadband varieties of host media become available, such as various sesquioxides [Die13]. Until then, such laser provide ideal grounds for external pulse compression, and seeding of even higher-power amplifiers. In both these roles, CEP control will be needed. Consequently, two approaches towards temporal compression and CEP stabilisation of the output pulses from a KLM thin-disk laser are presented in Section 3.2.

### 3.1.2 Average power scaling

While the pulse durations available from high-power oscillators remain insufficient for direct intracavity HHG, one option is external compression of the pulses. With the output power rising continuously, efficient compression schemes show the potential to raise the pulse intensity enough to use such sources without resorting to intracavity techniques. Spectral broadening in large-mode area (LMA) PCF [Gan11] or gas-filled hollow core PCF [Ema13] indeed provide a route that leads to few-cycle pulses on the microjoule level of energy. Similar geometries have already been shown to be suitable for HHG [Ver11]. As will be shown in Section 3.2, pulse compression down to the few-cycle regime is feasible in this fashion, eventually paving the way for a CEP-stabilised, few-cycle oscillator with the highest energy demonstrated so far.

Yet another route towards CEP-stable pulses at higher repetition rate can be taken by using such an oscillator as a two-fold seed source. One part of the output is compressed to few-cycle duration, while the remainder is amplified in a narrow bandwidth to serve as a pump pulse to an optical parametric chirped-pulse amplifier (OPCPA) seeded by the first part [Wit12]. Using an all-ytterbium architecture allows for considerably higher seed energy in the OPCPA, enhancing the contrast of the pulse against parametric fluorescence. Present-day OPCPA systems commonly derive both the signal and the pump seed from a Ti:sa oscillator, which leads to very low seed energy especially for the pump pulse at 1030 nm. When using two different oscillators for pump and seed pulses, tremendous effort is necessary for synchronisation of the two [Tei05], which compromises robustness. These issues were elegantly circumvented if few-cycle pulses could be obtained from Yb-based sources directly. Yet again, in order to cover all scenarios in attosecond experiments, such a seed source would need to be CEP-stable. The laser presented in Section 3.2 addresses both of these requirements.

### 3.1.3 Enhancement in passive resonators

A third route towards a megahertz-rate attosecond pulse source arises when the generation of few-cycle pulses is separated from their intensity enhancement inside a cavity. Thus, a power-scalable system can be used to provide high-energy pulses which are compressed by the means outlined above. This pulse train can then be coupled into a second cavity, its length matched to that of the repetition rate of the laser system, to obtain coherent stacking of up to thousands of pulses and correspondingly increased intensity. Systems of this type have been used to generate a frequency comb in the ultraviolet [Jon05, Goh05b], megahertz sources of 100 eV XUV radiation [Pup13] and have recently enabled megawatt-level intracavity average power [Car14]. Of all approaches mentioned so far, passive enhancement cavities hold the highest potential for the generation of isolated attosecond pulses (IAP) at megahertz repetition rate. The immense capabilities of such sources comes at the price of high complexity. Yet, concepts have been proposed that address some of the issues at hand. The combination of shorter intracavity pulses with gating techniques holds the potential to yield the corresponding continuum XUV

spectra, and methods have been introduced to couple out the XUV radiation without introducing spatial dispersion [Mol06, Wei11, Pro11b]. Still, the necessary interferometric stabilisation of the cavity length becomes increasingly challenging with rising power and bandwidth. Mirrors with extremely low GDD and high reflectivity are required in order to keep the pulses from dispersing over hundreds to thousands of round-trips. The broader the spectrum to be locked to the cavity, the higher also the demands on CEO frequency stability. Whereas coarse CEO control is sufficient to achieve coherent stacking of 100 fs pulses, full stabilisation of both frequency comb parameters –  $f_{\text{rep}}$  and  $f_{\text{ceo}}$  – will eventually be required. The experiments presented in Section 3.3 investigate the possibility of simultaneously stabilising the offset and repetition rate of a MOPA system, and yield first results regarding the influence of a stable CEP on the cavity lock.

## 3.2 CEP-stable few-cycle pulses from a thin-disk oscillator

For DPSS lasers to become an alternative to Ti:sapphire oscillators, they have to provide similarly low intensity noise operation. This was found to be a problem especially in high-power thin-disk lasers mode-locked by semiconductor saturable absorber mirrors (SESAM). Fortunately, during the author's stay at the LMU, Oleg Pronin and his team at Alexander Apolonski's group of Department of Experimental Physics succeeded in constructing a thin-disk laser with outstanding energy stability. This was accomplished by resorting to Kerr lens mode-locking instead of a SESAM [Pro11a]. The decision was made to pursue pulse compression to the few-cycle regime and subsequently CEO stabilisation with this system. The work presented in this section was therefore achieved in close cooperation with Oleg Pronin and Marcus Seidel, who continued the experiments after the author's stay at the LMU had ended.

At that time, the KLM thin-disk oscillator delivered a maximum output energy of about 420 nJ at a repetition rate of 40 MHz, corresponding to an average power of 17 W. The pulses were confirmed to have a duration of about 250 fs FWHM by means of SHG autocorrelation (AC). They were of secans-hyperbolic-squared shape, as is characteristic of soliton pulse formation [Sie86]. The pulse-to-pulse energy noise was measured to be below 0.8 % RMS. The laser in different regimes of pulse formation is described in detail in [Pro11a] and [Pro12b].

### 3.2.1 Spectral broadening and temporal pulse compression

All experiments described in this section exploited spectral broadening through self-phase modulation in large-mode area (LMA) fibres [Gri82]. This specific fibre type employs photonic crystal structures to maintain single mode operation even for mode field diameters (MFD) of up to 50  $\mu\text{m}$ , thus allowing the propagation of microjoule-level sub-picosecond pulses without optical damage. The material dispersion of the fused silica fibres was compensated by means

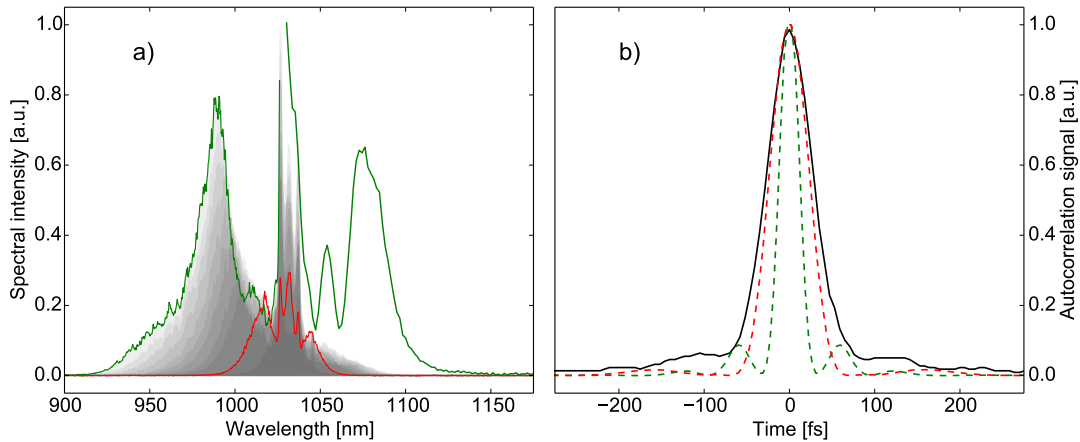


**Figure 3.1:** Results obtained by single-stage LMA fibre broadening and temporal compression of the 250 fs input pulses from the KLM thin-disk laser. **a)** Set of output spectra for input powers varying from 2 W (dark) to 14 W (light grey). *Red trace:* 5 W, maximum spectral width supported by CM39 mirrors. *Green trace:* maximum available input power (14 W). A second spectrometer was necessary to measure the IR part of the spectrum. **b)** Measured (black trace) and calculated (red dashed trace) intensity AC of the output pulses limited by the CM39 mirror bandwidth. *Green dashed trace:* AC of the Fourier-limited pulse corresponding to the green trace in a). Assuming Gaussian pulse shapes, the durations amount to 45, 35, and 18 fs, respectively.

of dispersive mirrors (DM), designed and manufactured by Volodymyr Pervak and his team at the LMU.

The first compression experiment was aimed at achieving an output pulse duration of approximately 50 fs because mirrors supporting the corresponding bandwidth were readily available. To this end, the laser output was attenuated by a waveplate and a polariser before being coupled into the fibre within a lens of 30 mm focal length. The fibres were placed in a copper V-groove holder, adjustable in three dimensions by differential micrometers. All fibre samples were cleaved manually with a fibre scribe. For collimation, a 30 mm achromatic lens was used. Figure 3.1a shows the set of spectra achieved with an LMA25 fibre of 65 mm length (NKT Photonics) for varying input power. The overall throughput of above 75% (including input and collimation lenses) was found to be independent of the input power. The output spectrum obtained from coupling the full oscillator output into the fibre significantly exceeded the bandwidth of the available CM compressor (design CM39, 980–1080 nm [Pro12a, p. 76]). The input power was thus limited to 5 W (125 nJ) at first. Six reflection on these CM provided suitable dispersion compensation and resulted in 3.6 W average power (90 nJ) after the compressor. An SHG intensity AC (PulseCheck, APE) yielded a trace with a duration of 64 fs FWHM (Figure 3.1b, black solid curve). Under the assumption of a Gaussian pulse shape, this leads to a pulse duration of 45 fs, which is close to the Fourier transform limit of 35 fs. A suitable set of dispersive mirrors would allow the compression of the entire output spectrum obtained with maximum power, the transform limit of which was calculated to about 18 fs (Figure 3.1b,

green dashed trace). Preliminarily, the fibre length was instead reduced to 30 mm, which led to a pulse duration on the order of 40 fs at an input power of 14 W.

Aiming for spectral broadening to generate few-cycle pulses, attempts were made at expanding the bandwidth obtained after the fibre. A second fibre stage was added, modelled after the first one. Higher intensity was achieved by reducing the fibre core MFD to 15  $\mu\text{m}$ . Input coupling was achieved with achromatic lenses of 19 or 30 mm focal length. With an LMA15 fibre of 17 mm, up to 14 W of input power from the first stage resulted in about 8 W output from the second one. The obtained spectrum, displayed in Figure 3.2, allowed for a Fourier limit as low as 16 fs. With second set of negative-dispersion mirrors (design PC102L), compression down to 18 fs was achieved as measured by intensity AC (Figure 3.2, solid black trace). The mirrors were used in double-angle configuration, with 6 reflections under  $8^\circ$  and further 4 under  $22^\circ$  angle of incidence. However, frequent fibre damage occurred in this setting. Although the addition of a 12 mm block of SF57 glass before the second fibre stage improved matters [Gan11], this illustrates that the approach was already close to its limit in terms of input energy. Moreover, the fibre throughput and spectral structure was found to depend strongly on the individual pieces employed. As will be portrayed briefly in the end of this section, SPM in bulk material proved a superior alternative to LMA fibre broadening at this intensity. Pulses of even higher energy must usually undergo broadening in gaseous media. The associated techniques and their influence of the CEP are the subject of Section 4.4.

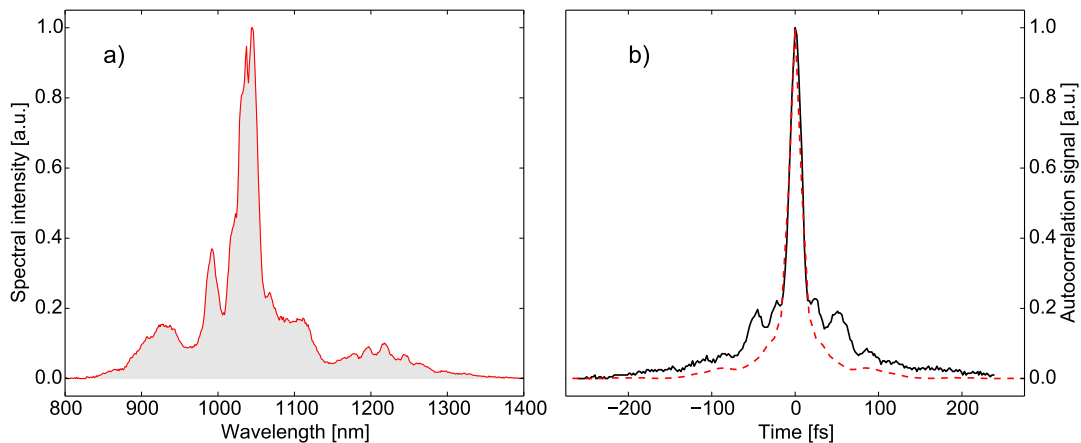


**Figure 3.2:** Results obtained by two-stage LMA fibre compression. Input to first stage (LMA35, 60 mm): 19 W, 250 fs. Input to second stage (LMA15, 17 mm): 14 W, 40 fs. **a)** Output spectrum after second stage, 8 W after compressor. **b)** Measured (black trace) and calculated (red dashed trace) intensity AC of the output pulses. Assuming Gaussian pulse shapes, the durations amount to 18 and 16 fs, respectively.

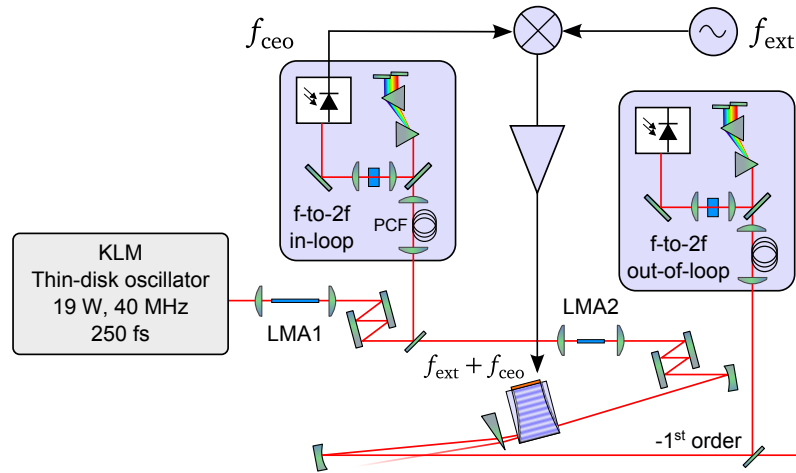


**Figure 3.3:** Set-up for pulse compression and CEO stabilisation of a thin-disk laser. LMA1 and LMA2 are the fibre broadening stages described in the text, yielding 14 W, 40 fs and 8 W, 18 fs, respectively. Both interferometers use PCF for supercontinuum generation. The stabilisation unit is otherwise identical to that used in Section 2.4.4.

### 3.2.2 CEO frequency detection and cavity-external stabilisation

As mentioned above, in order for fibre-based supercontinuum (SC) generation to maintain coherence across the octave bandwidth needed for self-referencing, the input pulse duration may not exceed a certain value. This is due to the fact that the early evolution of the SC must be dominated by coherent soliton dynamics rather than by modulation instability [Gen07]. Although both regimes can yield octave-spanning SC, the spectral edges are not temporally coherent in the latter case. Coherence can be ensured by launching pulses with a low soliton order, i. e., having as low as possible duration for a given energy and fibre geometry [Agr08, Chs. 5&6]. Following the guidelines laid down in [Pek11] for the generation a coherent octave-spanning spectrum, a pulse duration of roughly 100 fs was found to be sufficient in the case presented here. The pulses obtained in the first compression stage were thus short enough to for CEO frequency detection via self-referencing.

The experimental layout is depicted in Figure 3.3. After the first compression stage, an f-to-2f interferometer was placed. The device used a 15 cm piece of PCF (NL-3.7-975, NKT Photonics), with approximately 500 mW average power being sufficient to generate an octave-spanning spectrum. The interferometer itself was built in quasi-common-path geometry [Gre09], using a pair of prism to introduce the time delay between the visible and IR components of the spectrum. After frequency doubling in a PPLN crystal (SHG-1375-1, Covesion), the fundamental and frequency-doubled components were filtered at about 680 nm and superposed on an avalanche photodiode (APD110, Thorlabs). A CEO beat signal was observed with an SNR of more than 35 dB (RBW 100 kHz), as depicted in Figure 3.4. Conversely, no CEO signal could be found when bypassing the LMA fibre compression stage. The CEO frequency varied strongly at

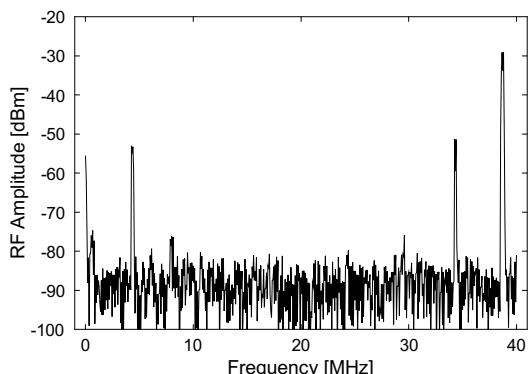


**Figure 3.4:** RF spectrogram of the IL f-to-2f beat signal. The CEO beat and its mirror frequency are visible with an more than 35 dB SNR (100 kHz RBW).

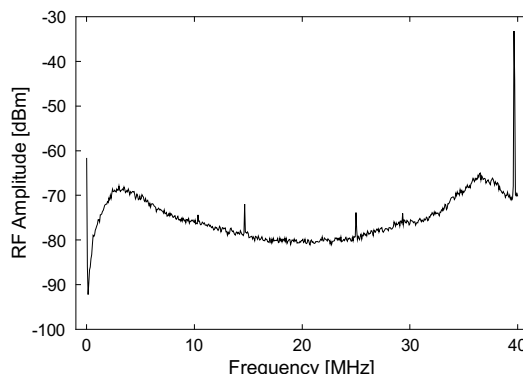


**Figure 3.5:** Stabilised CEO beat signal at 14.5 MHz measured in the OOL f-to-2f, masked by strong detection noise. 10 kHz RBW, 43 ms sweep time, 100 sweeps average.

acoustic frequencies, the modulation amplitude amounting to about 4 MHz, depending on the environmental conditions. The frequency excursions could be reduced to 1 MHz by reducing the air flow and the water flow to the laser disk of the oscillator. The CEO frequency was sensitive to the pump intensity, although only a few MHz range was accessible before mode-locking was impaired. Changing the angle of the Kerr medium in the cavity was found to provide a more convenient way of adjusting the offset, allowing a range of several  $f_{\text{rep}}$  without causing instability. This mechanism was found not to influence beam pointing and average power significantly, which suggests that the effect was rather due to the changing nonlinear phase accumulated by the pulse when the propagation length inside the Kerr medium varied.

The considerable frequency fluctuations and the narrow available range of pump modulation made the FF technique an apparently suitable choice for CEO stabilisation of the laser. The stabilisation set-up introduced in Chapter 2 was transferred directly to the thin-disk laser, with the DFG interferometers replaced by two f-to-2f devices as described above. No slow loop was used, and some RF filters were adapted to fit the repetition rate of this system. With the AOFS at a constant drive frequency, an OOL signal was obtained in the second interferometer at equal SNR as in the first. However, when using the sum of a fixed frequency  $f_{\text{ext}}$  and the IL signal  $f_{\text{ceo}}$  to drive the AOFS, the frequency excursions of the latter proved too large for FF stabilisation to work properly. The RF spectrogram obtained from the OOL measurement, shown in Figure 3.5, gives hints as to the possible reasons. In the course of the 4.3 s measurement (100 sweeps of 43 ms), the CEO frequency of the output remained stable enough to yield an SNR of 10 dB. The signal was masked by tremendous noise, however. Several effects contributed to this, all of which can be traced back to the IL frequency jitter. Most importantly, the pronounced IL frequency fluctuations translated into angular jitter, which in turn led to amplitude noise in the light launched into the SC PCF in the OOL interferometer. Being a highly nonlinear process, the SC generation acted as a noise amplifier [God13]. Furthermore, the IL frequency excursions

exceed the pass band of the narrow RF filters before the power amplifier. This causes amplitude noise on the RF drive power and on the diffracted light, again adding noise in the PCF. Third, the delay induced by the finite speed of sound in the AOFS turns frequency changes into phase changes (Section 2.3.2). Consequently, attempts at measuring the stabilisation performance by means of phase comparison, as was done in Chapter 2, remained unsuccessful.

### 3.2.3 Further developments

The experiments presented in this section laid the groundwork for further efforts by Oleg Pronin and Marcus Seidel towards a CEO-stable thin-disk laser. They refined the compression stages, eventually reaching 17 fs pulses with more than 0.5  $\mu\text{J}$  energy in one stage. A second stage based on SPM in bulk fused silica resulted in 10 fs pulses, corresponding to less than three cycles of the carrier wave under the pulse envelope half-width. CEO control was achieved using an intracavity acousto-optic loss modulator, thereby circumventing the bandwidth issues associated with pump intensity modulation. OOL phase stability was shown to be better than 300 mrad RMS (1 Hz–500 kHz). This demonstrates that high-power DPSS oscillators can retain the properties of Ti:sapphire lasers at about two orders of magnitude higher pulse energy and average power. The results are the subject of a manuscript in preparation [Pro14].

## 3.3 Cavity-enhanced fibre amplifier seeded by an Yb:KYW oscillator

When Ioachim Pupeza and his team at LMU first succeeded in producing XUV radiation in the 100 eV (12.3 nm) range using their enhancement cavity [Pup13], this was enabled by decreasing the duration of the coherently stacked pulses. The driver laser was a master-oscillator power-amplifier (MOPA) system described in detail in [Eid08]. It consisted of a SESAM mode-locked Yb:KYW oscillator, a two-stage fibre CPA, and an LMA fibre compression stage similar to that described in Section 3.2. It delivered pulses of down to 33 fs duration at a repetition rate of 78 MHz and an average power of about 40 W. The set-up is shown schematically in Figure 3.6. In order to match the comb lines of the seed laser to the longitudinal modes of the enhancement cavity (EC), the length of the seed oscillator was locked to that of the EC. Whereas pure repetition rate control had proved sufficient when locking pulses in the 100 fs range, the influence of the CEO frequency became apparent for shorter pulses. For instance, precise positioning of the intracavity fused silica wedges in the oscillator was necessary to achieve sizeable enhancement.

Being a resonator with (albeit low) dispersion and nonlinearity, the EC must be understood as having a “comb offset” of its own, meaning that its resonances are not simply multiples of its free spectral range, but rather carry an offset like the modes of a mode-locked laser as depicted in Figure 1.3. This is not immediately apparent, as one might expect a cavity that allows pulses to propagate without stretching for upwards of a thousand round-trips to be

largely dispersion-free. However, a even minuscule amount of residual GDD in the range of  $1 \text{ fs}^2$  is enough to give rise to such an offset, as is straightforwardly calculated from Equation 1.4. The geometric phase shift or Gouy phase [Lin04] and the dispersion of the HHG medium add to this figure. For a comb with narrow bandwidth, control over one of the two parameters – the repetition rate, in this case – is sufficient to achieve overlap with the modes of the EC. With broader spectra, the overlap becomes increasingly dependent on the CEO frequency of the seed pulse train. The generation of IAPs as the long-term goal eventually demands that the laser system provide and the EC accommodate pulses with constant CEP, i. e., a zero-offset comb. Means of CEO control thus need to be investigated for both seed laser and enhancement cavity. As a first step into this direction, the investigation presented in this section addressed the seed laser. In order to access intra-EC pulse durations as low as 20-30 fs, it was decided to attempt an active CEO stabilisation of the system. The experiments described on the following pages were performed together with Simon Holzberger of the Pupeza group at the LMU.

### 3.3.1 Oscillator CEO detection and stabilisation

Stabilisation of the CEO frequency of the MOPA system was subject to several constraints. First, the Pound-Drever-Hall (PDH) technique employed for the repetition rate locking of the oscillator relies on side-bands imprinted on the repetition rate by phase modulation [Dre83]. In the LMU EC, this is accomplished by an oscillating mirror before the amplifier stages. As these side-bands directly transferred to the CEO frequency, its detection had to take place before this point. Second, the seed oscillator delivered too long pulses to allow for the direct use of a PCF-based f-to-2f interferometer. Nonlinear compression to less than 100 fs was not an option because the oscillator delivered insufficient energy ( $< 4 \text{ nJ}$ ). The low power in turn is a

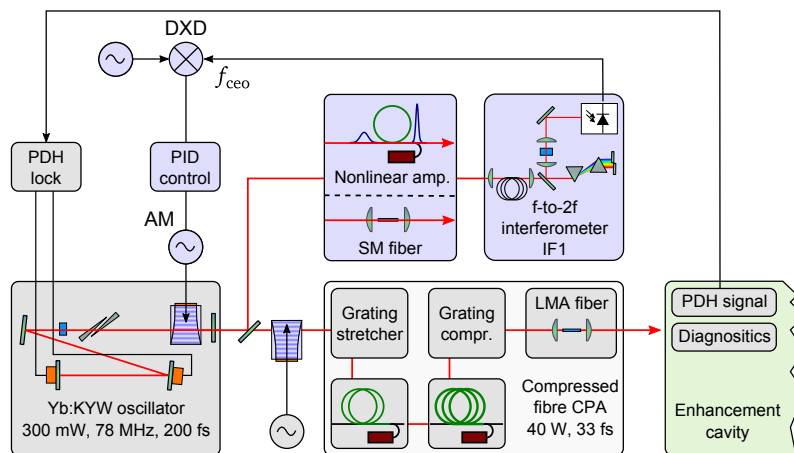


**Figure 3.6:** Experiment layout of the EC seeded by a frequency comb from a MOPA system. Boxes with a blue background are components used for CEO frequency stabilisation. The EC diagnostics included an autocorrelator, spectrometers, and several photodiodes for monitoring the pulse train locked to the EC. PDH lock details omitted for clarity. SM: single-mode. DXD: digital phase detector.

concession to the repetition rate lock, as it allows for the actuated mirror to be small and of low mass and hence not compromise the Piezo actuator bandwidth.

Consequently, it was decided to add a separate fibre amplifier stage that would simultaneously provide spectral broadening. The system was designed by Tino Eidam of the group of Jens Limpert at the IAP in Jena. It consisted of a 1 m piece of Yb-doped double-clad LMA PCF with signal and pump core diameters of 40 and 170  $\mu\text{m}$ . A third of the oscillator output power (approximately 100 mW) was split off to seed the nonlinear amplifier, resulting in about 3 W output power when pumped by about 15 W from a fibre-coupled laser diode. The spectrum supported a pulse duration of about 70 fs, and the pulses were compressed to 79 fs with a CM compressor (design HDI301, provided by Olga Razskazovskaya and Volodymyr Pervak). Using a fraction of the compressed output, a beat signal could be readily obtained in an f-to-2f interferometer (IF1 in Figure 3.6) identical to those employed in the thin-disk experiment (see Section 3.2.2). The frequency excursions of the laser CEO signal were limited to about 300 kHz on a time-scale of milliseconds, which is about one order of magnitude less than in the case of the thin-disk laser presented in Section 3.2.

Intracavity loss modulation yielded promising results on the KLM thin-disk laser (Section 3.2.3). The approach was therefore adopted in this experiment, as sketched in Figure 3.6. The Yb:KYW seed oscillator was fitted with an AO modulator that would induce losses of up to 1% at an RF drive power of 5 W (custom model, Gooch & Housego). Using a digital phase detector (DXD100, Menlo Systems) and a proportional-integral-derivative (PID) controller (D2-125, Vescent Photonics), a feed-back loop was closed on IF1 to lock the laser CEO frequency to an RF reference at 10.7 MHz. In the thin-disk experiment, a similar loop was shown to provide a CEO

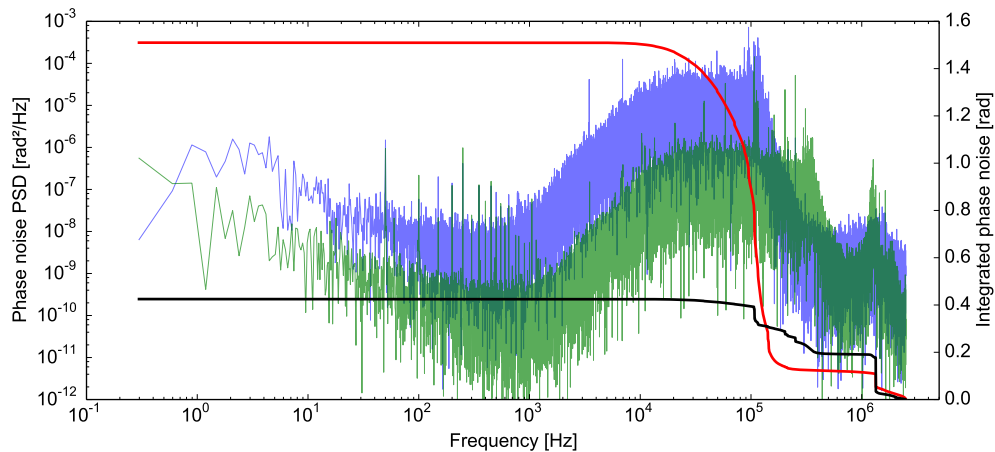


**Figure 3.7:** Frequency analysis of IL error signals (output of phase detector DXD in Figure 3.6) obtained from IF1 using different means of spectral broadening. Sampled at 5 MHz for 3.36 s. *Blue/red trace:* PSD/IPN after nonlinear fibre amplifier. Residual phase noise: 1.51 rad. *Green/black trace:* PSD/IPN after passive single-mode fibre. Residual phase noise: 425 mrad.

phase stability on the order of 200 mrad [Pro14], with its bandwidth estimated to several tens of kilohertz. However, the overall IPN obtained in this case amounted to more than 1.53 rad within 3.36 s, which is surprisingly high considering the higher intrinsic stability of this laser. The frequency analysis of the closed-loop error signal is shown in Figure 3.7 (blue/red trace). The plot indicates that most of the residual noise was accumulated in a wide band between 50 and 150 kHz. This is well beyond the range to be expected from the 0.3 ms upper-state lifetime of the lasing transition. Repetition rate stabilisation was disengaged for this experiment, and high-frequency oscillation of the loop was ruled out.

### 3.3.2 CEP noise induced in fibre amplification

The wide bandwidth and smooth rise of the IPN curve rather suggest a stochastic effect to be the underlying cause. Amplified spontaneous emission (ASE) in the nonlinear amplifier stage might serve to explain this. The noise amplification properties of the supercontinuum generation, already encountered in Section 3.2.2, further aggravate the situation. In order to exclude this source of noise, the full power of the oscillator was coupled into a short piece of single-mode fibre, with SPM providing just enough spectral broadening to allow compression to about 100 fs afterwards. Feeding this pulse train to the f-to-2f interferometer and using the obtained signal to close the feed-back loop resulted in the data shown in Figure 3.7 (green/black trace). This time, the bandwidth in question only added some 200 mrad to an overall IPN of 431 mrad, with the strong feature at about 100 kHz shrunk to 70 mrad. The nonlinear fibre amplifier can thus be assumed to be the source of the added noise. It remains unclear which effect – amplitude-to-phase coupling via SPM or fluctuations due to ASE – is the underlying cause. Other experiments involving nonlinear spectral broadening with a wide range of pulse energy (e. g., see Sections 3.2.1 and 4.4) suggest that the former is entirely compatible with CEP stabilisation. On the other hand, further investigation is necessary to clarify the impact of ASE on the CEP or its detection. It is remarkable, however, that the two phase noise PSD curves are offset by almost two orders of magnitude, yet are of a very similar shape apart from narrowband features. This further corroborates the assumption that the underlying noise source is essentially frequency-independent, such as should be expected from ASE. In that case, the high loop bandwidth provided by the loss modulation CEO actuator would have further increased the in-loop CEO noise in attempting to correct a random error. Unfortunately, the seed oscillator power was not sufficient to seed both the passive broadening stage and the main amplifiers simultaneously, which would have enabled an isolated CEP characterisation of the two linear amplifiers.

Instead, a direct phase comparison was performed between identical f-to-2f interferometers. The first was placed behind the nonlinear amplifier as described above, the second after the entire fibre amplifier and compression stage (IF2 in Figure 3.8). The output of the second interferometer was mixed down to account for an auxiliary frequency shifter placed behind the stretcher, and then compared to the output of the first with a phase detector. The CEP

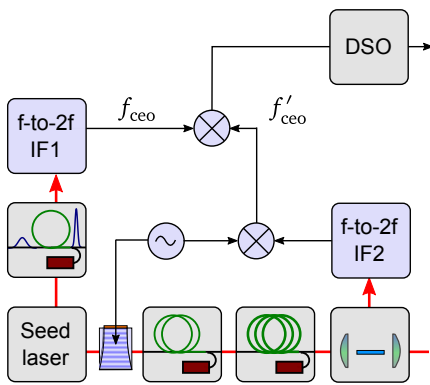


**Figure 3.8:** Layout for measuring the CEO noise contributions of the fibre amplifier stages. The phase difference of IF1 and IF2 is displayed in Figure 3.9.

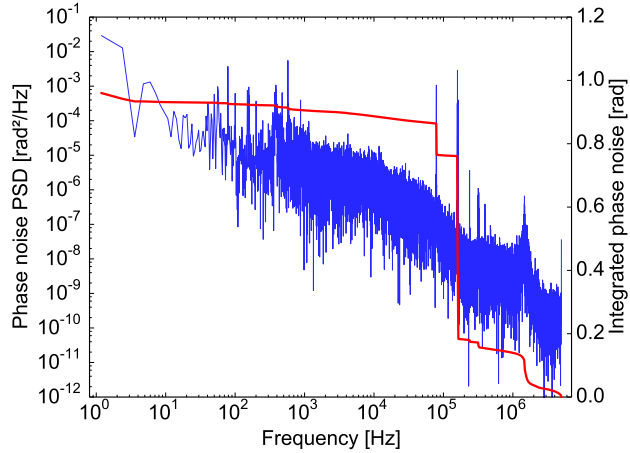


**Figure 3.9:** Phase comparison of CEO signals obtained by f-to-2f interferometers before and after the main MOPA fibre amplifiers. The RMS phase deviation between the two amounted to 970 mrad within 0.84 s.

stabilisation loop was left open in this experiment. The Fourier transform of the measured phase difference is displayed in Figure 3.9. Again, the phase difference is on the order of 1 rad, but this time the prominent feature at about 160 kHz is of a much lower bandwidth than in Figure 3.7, with its higher harmonics present at lesser intensity. However, none of these sharp spikes appeared in the measurement of the nonlinear amplifier alone (Figure 3.7, blue trace). This suggests that the dominant contribution in this measurement came from the linear amplifiers, with only a background being due to the nonlinear stage. Without the feed-back loop adding noise, its contribution is limited to the slow rise of the IPN curve, contributing on the order of a few hundred millirad. The spikes could be assumed to stem from the switching power supplies of the high-power laser diodes. Upwards swings in pump power translate directly into gain changes and do not experience the low-pass filtering caused by the millisecond-scale upper state lifetime.

In combination, these two experiments illustrate that the CEO phase-stable amplification of ultrashort pulse trains in fibres still holds numerous open questions. While in principle, the role of ASE (for low seed levels) and amplitude-to-phase coupling (at high output power) require further investigation.

### 3.3.3 Effect of CEO lock on enhancement cavity

A seed oscillator with a moderately increased power level of about 1 W would already have enabled the MOPA to be CEO-stabilised on the passively-compressed output of the oscillator. As no such seed laser was available, feed-back on the CEO frequency was instead closed on

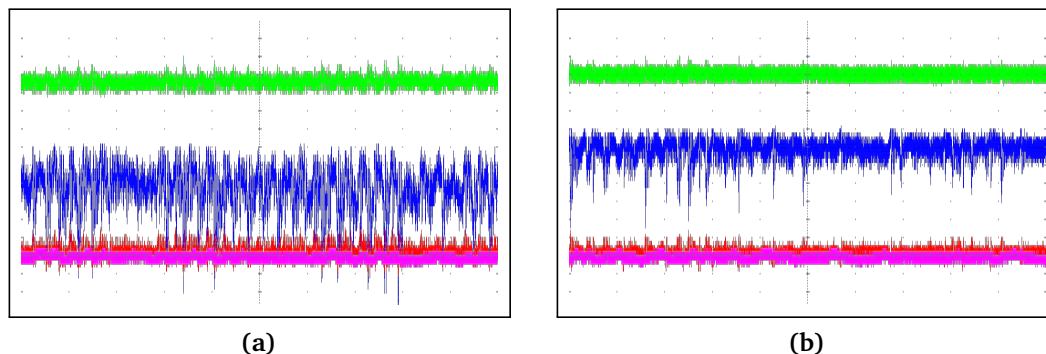


**Figure 3.10:** Oscilloscope screenshots of EC lock parameters for 33 fs input pulses. Time span 40 ms each, identical scaling. *Green trace:* power reflected by EC. *Blue:* power level within EC. *Red:* error signal of length lock. *Magenta:* signal applied to Piezo actuator. **a)** CEO lock disengaged. Intra-EC pulse duration: 41 fs. **b)** CEO feed-back loop closed on signal after nonlinear fibre stage. Intra-EC pulse duration: 39 fs.

the  $f$ -to- $2f$  signal after the nonlinear amplifier stage (IF1). The full power of the laser system resulted in a train of 33 fs pulses at an average power of 40 W after the LMA compression stage. In order to lock the output to the EC, the repetition rate lock was engaged as well. With a residual phase noise on the order of 1 rad, the system could hardly be called phase-stable, yet even this coarse means of frequency stabilisation led to a visibly improved stability of the enhancement. Oscilloscope screenshots of four lock parameters are shown in Figure 3.10 with the CEO lock turned off (a) and on (b). Most notably, the locked power level within the EC was significantly less noisy. Simultaneously, the pulse duration of the pulses transmitted through the cavity (which are of essentially identical shape as those inside) was measured to be slightly lower when both comb parameters were locked (39 vs. 41 fs), meaning that a broader comb could be locked to EC resonances. In addition, the mean time to lock failure was found to be higher in this case as well. Whereas such a broad input spectrum could scarcely be held locked to the EC for more than a few tens of seconds with only one comb parameter stabilised, the coarse CEO lock extended this time to a few minutes.

In summary, the experiments presented in this section have provided experimental evidence that an enhancement cavity designed for increasingly broad spectra and short pulse durations profits measurably from stabilisation of both comb parameters at once. Even a coarse lock of the comb offset resulted in increased stability of the power and higher spectral width locked in the EC. Although further investigation is necessary to pinpoint the reason for the high residual CEO phase noise of the MOPA system, the data suggest that it is a by-effect of fibre amplification. Cues towards ASE and pump diode noise were found in the noise spectra, providing the basis for possible remedies. Higher seed power could enable an amplification-free CEO measurement, and pump power supplies chosen for low switching noise could reduce the noise induced in power amplification.

### 3.4 Summary and outlook

An array of concepts exist that aim to generate attosecond pulses at megahertz repetition rate, all of which are based on diode-pumped laser systems in combination with a scalable thermal management. This chapter gave an overview of the concepts and introduced the various points at which CEP stabilisation is a crucial factor for further progress. Exemplary experiments on CEO frequency measurement and stabilisation were conducted. The systems in question cover two laser architectures that can be expected to be at the core of a future source of megahertz XUV radiation. First, the output of a thin-disk laser was shown to be compressible to few-cycle duration, with CEP stabilisation being the logical next step. Although the cavity-external technique was found inapplicable in this case, the experiment later led to the first demonstration of a CEP-stable thin-disk laser. In conjunction with external compression, the laser provided waveform-controlled few-cycle pulses comparable to that of state-of-the-art Ti:sapphire oscillators, but at two orders of magnitude higher energy and average power. Another attractive future application of such an oscillator is intracavity high-harmonic generation. With moderate power scaling, the presented laser system would provide the necessary intensity level, leading to an XUV source of considerably reduced complexity as opposed to amplifiers or enhancement cavities. In combination with novel approaches for CEP stabilisation [Bal14], it might even provide phase-stable XUV pulses. The second system presented in this chapter was based on a master-oscillator power-amplifier architecture that combined a conventional bulk oscillator with two stages of fibre CPA. It was intended for the use of EC seeding, an approach that perfectly complements the low efficiency of HHG. However, this scenario calls for simultaneous stabilisation of both frequency comb parameters, and thus places numerous constraints on the employed seed laser. Detection of the CEO frequency was demonstrated by use of a nonlinear fibre amplifier, but only radian-level phase stability of the CEO could be achieved in a feed-back configuration. However, even this coarse level of stabilisation was sufficient for a visible improvement of the EC lock parameters. The findings highlight the necessity for full comb stabilisation in order to reach cavity enhancement of pulses lasting as short as a few tens of femtoseconds. The obstacles encountered in CEP-stabilisation of the system could be traced back to the fibre amplifier stages, and clues for further investigation were given. Mitigation of these obstacles can be expected to pave the way towards the EC locking of pulses approaching the 10-20 fs range. In combination with gating techniques and novel output coupling methods, cavity enhancement could even make isolated attosecond pulses available at megahertz repetition rate.

Coherent enhancement techniques left aside, the laser sources treated in this chapter produced pulses on the microjoule level of energy. However, with the rapid development of power-scalable ultrafast lasers in mind, the advent of millijoule-level, megahertz rate laser systems appears but a matter of time. CEP control at this level of energy is the subject of Chapter 4.

## Chapter 4

# CEP Stability and Robustness for High Energy Pulses

The next generation of laser sources for attosecond science, some candidates for which were presented in the preceding chapter, combine power scalability with novel approaches to mitigate the intrinsically low efficiency of highly nonlinear processes. Without doubt, these technologies hold the potential to revolutionise the field, and the first steps on the way towards CEP stabilisation of such sources have been made. The vast majority of experiments conducted so far required a driver pulse energy on the order of a millijoule, with more energy generally considered beneficial. Regardless of what technological route is chosen to produce these pulses, they all face similar challenges when it comes to CEP stabilisation (Figure 1.2). Be it a conventional laser amplifier, an OPCPA pumped by a high-power DPSS laser or the temporally compressed output of a high-energy oscillator, experimental progress will depend on the availability of CEP-stable operation which is robust on a long time-scale, and at the same time provides as low residual CEP noise as possible. In addition, present-day and future sources alike require temporal compression to obtain few-cycle pulses, which in turn will have an impact on the CEP. The work presented in this chapter addresses these three points. Although the sources investigated here are based on conventional CPA, the conclusions apply to all technologies aiming to achieve high pulse energy.

After an overview of the multi-pass amplifier layout and the measurement schemes employed in this chapter, the use of cavity-external CEP-stabilised oscillators as seed sources is investigated in Section 4.2, putting its CEP stabilisation robustness to test. Section 4.3 then focuses on the origin of as well as possible remedies to noise induced in amplifiers. It presents the results of a cooperative experiment with the company Fastlite, in which the CEP noise of a 10 kHz amplifier was measured at the full repetition rate. In combination with a novel CEP actuator, the experiment pushes the limits of CEP stability for amplifier systems. The last section then concentrates on the impact of pulse compression on CEP stability. Section 4.4 introduces a novel scheme to measure the impact of nonlinear CEP changes induced in the most wide-spread method of high-energy pulse compression. The results obtained with it give insight into the origins of the additional phase noise and provide guidelines for future CEP-preserving means of temporal pulse compression.

## 4.1 Multi-pass amplifier system layout

The millijoule-energy pulses whose CEP properties are treated in this chapter were produced by means of conventional chirped-pulse laser amplification (CPA, [Str85]). The laser amplifier systems employed to this end provided different levels of pulse energy and repetition rate, but shared a similar design. The same applies to the CEP measurement principles. The subsequent sections of this chapter will therefore refer to the description given here.

The common platform of all systems was a commercial Ti:sa multi-pass amplifier design (Femtopower series, Femtolasers). Figure 4.1 shows a schematic representation of the layout. At the beginning of the amplifier chain, a KLM Ti:sa oscillator (rainbow series, Femtolasers) provided the seed pulses. All models were pumped by low-noise DPSS CW lasers at 532 nm, placed within the laser housing and fitted with an active beam pointing stabilisation. The cavities relied on mirrors for dispersion management and a pair of fused silica wedges for fine tuning. They delivered pulses of less than 7 fs duration at a repetition rate between 70 and 78 MHz and an average output power of 250 to 550 mW. The bandwidth of more than 300 nm at -10 dB was needed for detection of the CEO beat in a DFG interferometer. CEP stabilisation of the oscillator was accomplished with the cavity-external shifting technique (Sections 4.2 and 4.3) or conventional feed-back to the pump laser intensity (Section 4.4). The spectral content at the amplifier input was reduced by appropriate mirrors to a bandwidth of 100 nm at a centre wavelength of 800 nm. Following a Faraday isolator, the pulses were stretched to a few tens of picoseconds using a variable length of bulk SF57 glass depending on the desired pulse energy. The stretching factors were thus kept on the order of  $10^3$ , which enabled a compact compressor design. The gain medium was placed in an evacuated chamber and cooled to about 150 K using a low vibration chiller. Different models of pulsed pump lasers were available for the amplifier. The nanosecond-duration pump pulses were triggered by a master clock derived from the oscillator repetition rate. After four passes through the gain medium, the pulse train was reduced to the intended amplifier repetition rate with a Pockels cell. An

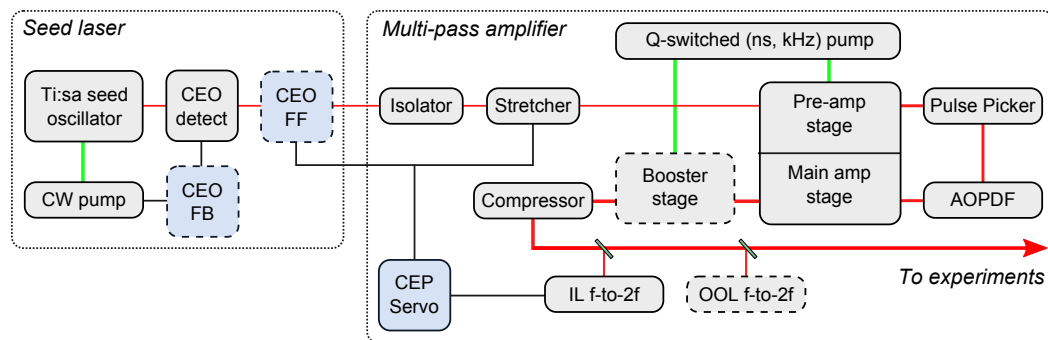


**Figure 4.1:** General layout of the millijoule CPA systems and subsequent CEP measurement as used in this chapter. FB: Feed-back stabilisation. *Red lines:* 800 nm beams. *Green lines:* 515 or 532 nm beams. *Black lines:* electronic connections.

acousto-optic programmable dispersive filter (AOPDF, low-jitter Dazzler HR, Fastlite) provided compensation of higher-order dispersion in the compressor as well as spectral shaping. The latter was used to partially counter the effect of gain narrowing. Both Pockels cell and AOPDF were triggered with individually adjustable delay by the same master clock that controlled the pump laser. A telescope assembly was inserted between the 9<sup>th</sup> and 10<sup>th</sup> pass to allow for adjustment of the beam waist in the gain medium. With the exception of the system used for the experiments described in Section 4.4, all were of single-stage design. After up to ten total passes through the gain medium, the pulses were re-compressed. Alternatively, a second amplifier stage of similar layout was inserted at this point, with compression instead taking place after it. The compressor consisted of transmission gratings in a double-pass configuration, yielding an overall throughput of 80 %. Different sizes and grating separations were available matched to the output pulse energy. The entire system including seed oscillator, amplifier and their respective pump sources was placed in an enclosure protecting it from air currents and accumulation of dust.

All CEP measurements presented in this chapter were performed with two interferometers simultaneously. The devices were based on collinear f-to-2f geometry [Kak01], extracting the CEP from the phase of a single-shot interferogram (see Section 1.3.2). A variety of different spectrometers were used, but were always configured such that only a single pulse could contribute to the interferogram. No averaging whatsoever was applied.<sup>1</sup> One device provided the in-loop (IL) signal, which was used for feed-back correction of the CEP with different actuators at the amplifier input. The second device provided an independent, out-of-loop (OOL) measurement of the CEP. This double measurement served two purposes. First, it allowed for a more realistic estimate of what CEP stability can be expected at the location of the experiment. Every kind of measurement adds noise, and as will become clear in Section 4.3, this noise can be significant. However, its contribution is masked when the device is used in an IL role, correcting its own error. Of course, the OOL measurement will also add noise, such that the actual value of the residual noise lies in between the two. Second, it ensured that certain lock faults, such a  $2\pi$  phase jump, a loss-of-signal event or a software error would not go unnoticed. This could potentially be the case if only one device was used. In subsequent sections, the experimental layout descriptions will provide further detail on the above points.

---

1 All measures of CEP noise given in this chapter are based on “single-shot values”. There exists surprising creativity in the laser development field as to what qualifies as such. Here, the term denotes a set of measurements in which each measurement carries information on the CEP of one pulse only. This definition excludes several popular means of achieving deceptively low CEP noise, including (but not limited to) setting the spectrometer integration time higher than twice the pulse-to-pulse delay, or taking the rolling average of the CEP of a number of consecutive (“single-shot”) measurements.

## 4.2 Day-long operation of CEP-stable amplifiers

One of the prime motivations for the work presented in this thesis was to enable truly long-term measurements in experiments that rely on a constant CEP. Even though the problem had been realised already in early ventures into the microcosm [Sch04], robust constant-CEP operation of laser amplifiers over several hours has remained elusive. One boost in long-term locking robustness was due to the introduction of monolithic DFG interferometers as described in Section 2.3.1. A further extension of unlock-free operation could be achieved with the addition of differential actuators for feed-back control (e. g., CEP-O-Clock, Femtolasers). This enabled the oscillator to remain mode-locked in the presence of large drifts of the feed-back stabilisation correction signal over time, which otherwise would have resulted in insufficient intra-cavity energy for KLM action. Yet, even commercial systems based on feed-back stabilisation scarcely offer more than a few hours of operation without a loss-of-lock event. The reason for this lies in the property of a PLL to balance robustness and stability (see Section 1.4), combined with the fact that effects causing extreme phase excursions are present in any natural environment. Such outliers are rare on the time-scale usually considered when analysing CEP stability, and hence can be safely ignored. This assumption fails in an environment where people move about, machinery is operated, and the sheer amount of noise sources and interactions make predicting CEP noise impossible. Surely, one could tailor the PLL parameters to accommodate these rogue events, but the price to pay in terms of CEP stability would be so immense that the stabilisation system would be useless for its intended application.

An elegant workaround has been found for experiments that do not actually require the CEP to be constant, but only known and evenly distributed [Küb13]. In this case, a single-shot measurement of both the CEP and the experimental outcome allows for so-called phase-tagging [Wit09]. However, this is not an option for experiments that employ the IR pulse to generate radiation in the XUV spectrum, where the properties of the latter are critically dependent on the CEP of the driver pulse. Cavity-external CEP stabilisation ideally lends itself to this task. In principle, it maintains a fixed phase relation for as long as the oscillator is mode-locked, and has been demonstrated to provide a stable CEP for considerable time in the experiments treated in Chapter 2.

### 4.2.1 High energy system

The first attempt at using an FF-stabilised Ti:sa laser to obtain long-term CEP-stable high-energy pulses was performed on a CPA system as outlined in Section 4.1, delivering 2 mJ pulses at 1 kHz repetition rate. The seed oscillator (rainbow CEP4, Femtolasers) was pumped by a DPSS ring laser (Verdi V6, Coherent), and was CEP-stabilised using a commercial implementation of the FF technique as outlined in Chapter 2. It provided a frequency comb with  $f_{\text{ceo}} = 0$ , i. e., a train of pulses with constant CEP. The single-stage amplifier (Femtopower HE, Femtolasers) was pumped by 22 mJ from a q-switched DPSS laser (Evolution 30, Coherent). The overall

conversion efficiency in amplification amounted to 9.1%. After the compressor, the pulse duration was measured to less than 20 fs via FRAC.

Beam splitters directed a small fraction of the output to two collinear f-to-2f interferometers. One of them, integrated into the amplifier housing, was a commercial device (APS800, Menlo Systems) with an acquisition rate of about 268 Hz. The spectrograms were transferred to a PC for CEP extraction in the proprietary software delivered with the interferometer. Care was taken to ensure that the software logged single-shot phase values and did not apply averaging of any sort. This device was used in an OOL role. The other interferometer was home-built in an all-reflective optical layout, and was placed outside the amplifier due to insufficient space. It was equipped with a different spectrometer (USB2000+, Ocean Optics), reaching an acquisition rate of 345 Hz. The data were evaluated and logged using another software suite running on a second PC, although under the same requirements with respect to averaging. This interferometer was chosen as the IL device. A PI servo integrated into the program could be used to control a Piezo actuator changing the insertion of a prism into the stretcher. This mechanism represents a standard way of correcting for slow CEP drift. Due to the prism mass and the relatively low acquisition rate, its loop bandwidth does not exceed a few tens of hertz. Both devices were triggered independently by a signal derived from the q-switch of the amplifier pump laser. The integration times of both devices allowed only one amplifier shot to contribute to each CEP measurement.

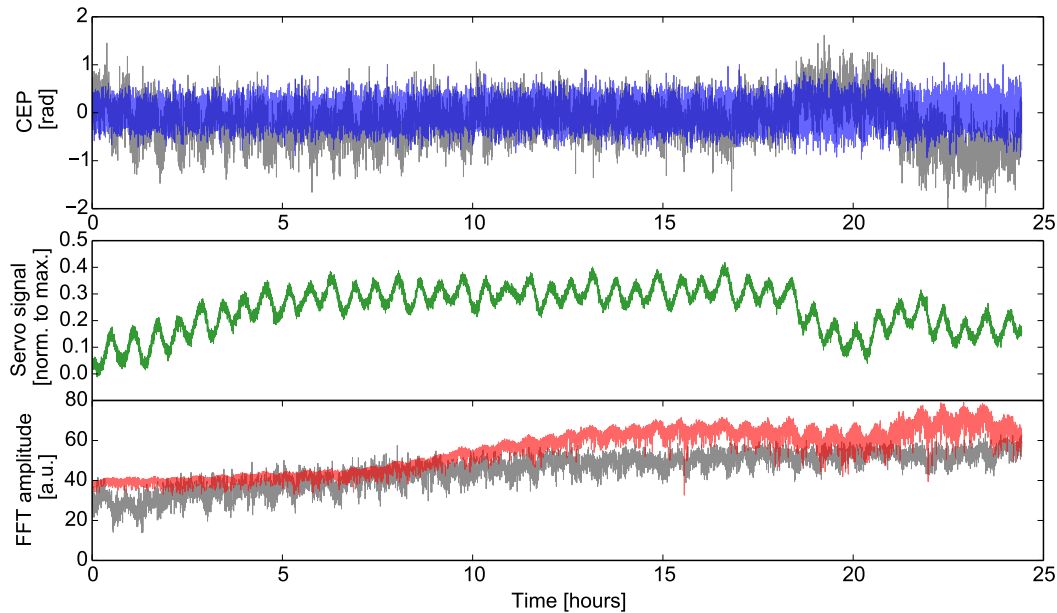


**Figure 4.2:** Long-term measurement of the CEP in a 2 mJ, 1 kHz CPA system seeded by a FF CEP-stabilised oscillator. Panels show measured CEP, applied correction signal and FFT amplitude. *Coloured traces:* IL data ( $\sigma = 266$  mrad). *Grey traces:* OOL data ( $\sigma = 466$  mrad).

The results are plotted in Figure 4.2, showing the measured CEP and the Fourier amplitude of the  $f$ -to- $2f$  interferogram fringe frequency for each interferometer, as well as the applied correction signal. As is immediately obvious, all traces of both IL and OOL data are free from discontinuities. This means that over a period of more than 24 hours, no event has occurred that significantly changed the CEP of the output pulses. Fringe visibility was never lost, and there were no phase jumps. The standard deviation of the CEP in the IL and OOL datasets over the measurement duration of 24.4 hours amounts to 266 ( $3.03 \cdot 10^7$  shots) and 466 mrad ( $2.36 \cdot 10^7$  shots), respectively.<sup>2</sup> See Appendix B for details on numerical evaluation. An experiment performed after this system could have relied on the availability of a high-energy pulse with an essentially constant waveform.

The oscillations of the servo signal (green trace in Figure 4.2) show the same period as the variation in ambient air temperature and humidity caused by the laboratory air conditioning system. Similar oscillations can be seen in the OOL CEP (grey trace in upper panel of Figure 4.2), measured by a device that was partially shielded from these variations by the amplifier enclosure. This suggests that much of the CEP noise measured by the OOL  $f$ -to- $2f$  was in fact caused by the two measurements being influenced by different ambient conditions. Had both been placed side-by-side, the comparison of IL and OOL results for the entire dataset would look rather more as it does for shorter measurements. For instance, 30 minutes into the measurement, a 10 minute segment yields 223 vs. 334 mrad.

#### 4.2.2 High repetition rate system

A similar measurement was performed on a high repetition rate CPA system. The seed oscillator was identical, but the amplifier repetition rate was 10 kHz. Pumped by 6.2 mJ pulses from a q-switched DPSS laser (DM60, Photonics Industries), the amplifier delivered 1 mJ pulses with a duration of 22 fs. This corresponds to a conversion efficiency of 16.1%. Further differences to the system described before were the gain medium housing and cooling mechanism, allowing for the fivefold increase in average power. Accordingly, a smaller version of the transmission grating compressor was employed, owing to the lower pulse energy in this case.

This time, both  $f$ -to- $2f$  devices were placed outside of the amplifier enclosure to minimise the influence of ambient conditions on the comparison. Again, the home-built interferometer was used as the in-loop device. As the original spectrometer did not allow for a shorter integration time than 1 ms, a different device (CCS100/M, Thorlabs) was used to ensure that only one pulse would contribute to every interference spectrogram. This led to a lower acquisition rate of 127 Hz. Feed-back correction was applied as before, using the prism actuator. The OOL device was of the same model as in Section 4.2.1, but in this configuration provided a somewhat higher measurement rate of 293 Hz.

---

<sup>2</sup> As before, when referring to statistical deviations from a constant value, RMS values are given in this work unless otherwise noted.

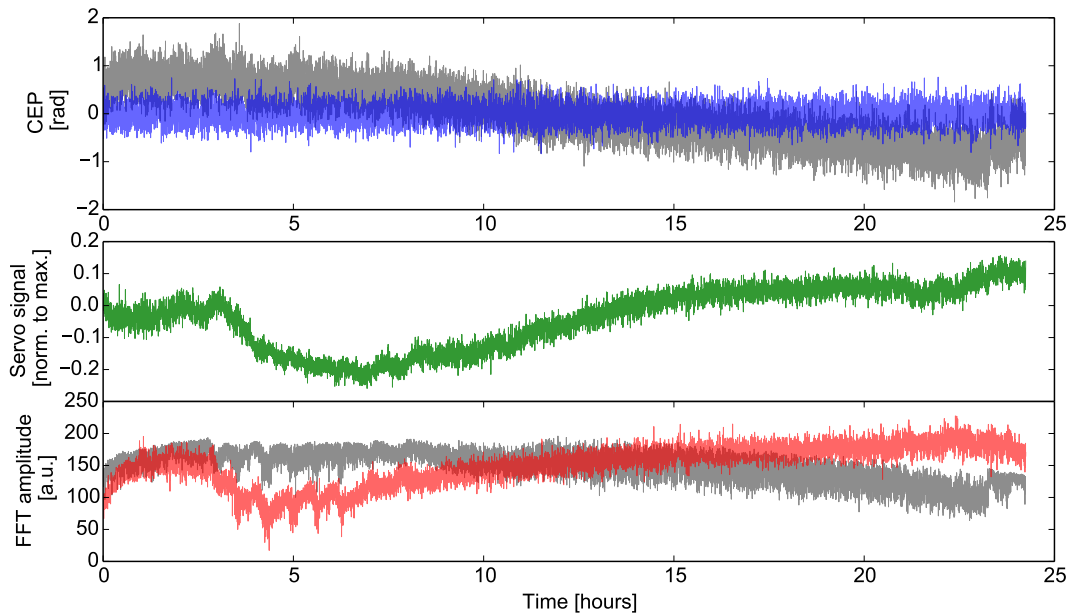


**Figure 4.3:** Long-term measurement of the CEP in a 1 mJ, 10 kHz CPA system seeded by a FF CEP-stabilised oscillator. Panels show measured CEP, applied correction signal and FFT amplitude. Coloured traces: IL data ( $\sigma = 211$  mrad). Grey traces: OOL data ( $\sigma = 588$  mrad for full set,  $\sigma = 250$  to 350 mrad for any 1-hour subset).

Figure 4.3 displays the results of a long-term measurement with this amplifier, the scaling of time and phase axes being identical to that in Figure 4.2. This system, too, was capable of maintaining a constant CEP for more than 24 hours. Just as before, both IL and OOL traces are free from discontinuities, corroborating the conclusion that an FF CEP-stabilised seed oscillator represents the ideal solution for applications that demand an extremely long measurement time.

The most notable difference compared to the dataset obtained with the high-energy amplifier is the absence of the half-hour period oscillations in both OOL CEP and the correction loop servo signal. This is due to the fact that, in this case, both interferometers were subject to the same ambient condition. Naturally, this does not mean that these did not influence the CEP. Rather, it serves to illustrate that the means of measurement itself needs to be taken into account when looking at a phenomenon that is subject to such a multitude of factors as the CEP of an ultrashort pulse. Moreover, although not necessarily visible to the eye, the residual CEP noise is lower for this system. Within an evaluation period of ten minutes, the IL and OOL datasets show a standard deviation of 210 and 251 mrad, respectively. Taking into account the entire dataset, the IL value stays virtually unchanged at 211 mrad, whereas the OOL value rises to 588 mrad. This value is obviously due to the linear slope of approximately 0.1 rad per hour. As a comparison, in any one-hour subset of the whole measurement, where this slow drift is insignificant, the OOL CEP error lies between 250 and 350 mrad. Comparison of the

panels in Figure 4.3 does not point out any visible correlations of this slow drift to the IL data. In particular, it does not relate to the combination of IL phase and servo signal. If at all, one might make out a correlation of the OOL drift to the FFT fringe amplitude seen by the device. Both keep decreasing monotonously after 10 hours, and also share the kinks occurring in the last two hours of the recording. This hints at the influence of SPM, changing the CEP when the octave-spanning continuum is produced by WLG in a sapphire plate. The corresponding decline input pulse energy to the interferometer might be due to slow changes in pointing of the output beam.

The precise origin of such drifts cannot be pinpointed with certainty without a measurement of the absolute phase between carrier and envelope of the pulse, and perhaps not even with it. However, the measurements presented here serve to sharpen the awareness towards possible origins of CEP noise, not all of which can be attributed to the system producing the pulses. These experiments have addressed the question of CEP robustness for high-energy pulses. It was demonstrated that FF CEP stabilisation of the seed lasers enables day-long operation at essentially constant CEP, even for pulses with multi-millijoule energy. The following section will deal with the issue of CEP stability.

### 4.3 Millijoule-level pulses at the limits of CEP stability

For the purpose of amplification, FF stabilisation of the seed oscillator CEP greatly enhances the robustness of the CEP lock for long measurement times. The residual CEP error obtained for such a system is on par with the best reported results obtained with feed-back stabilised seed lasers [And11a]. Regarding the superior performance of FF stabilisation in terms of CEP noise, one might expect to see a similar benefit to the CEP stability of the amplified pulses as well. Before the introduction of the FF technique, it was observed that the CEP stability of the best-performing amplifiers was slightly above that of the respective seed oscillator. Under this impression, it was argued that their performance might in fact be curtailed by the seed laser [Ste13, Bor14a]. Consequently, high hopes were placed on a technique that would ease this limitation. Yet considering the experience gathered with FF CEP stabilisation as reported in the previous section, it seemed that a more in-depth analysis is necessary.

The experiments described in this section were made possible by Vincent Crozatier of the company Fastlite. Together with Nicolas Forget, he developed the fast spectrometer enabling CEP characterisation of an amplifier at the full repetition rate. The fruitful cooperation also resulted in a publication [Lüc14c] and two conference contributions.

#### 4.3.1 Sources of CEP noise in amplifiers

Several factors contribute to the overall CEP noise measured at the output of an amplifier. First, the pulse-to-pulse phase jitter cannot fall below the seed oscillator CEP noise integrated

over the time between two pulses being picked for amplification [Goh05a]. For oscillators using feed-back stabilisation, this baseline limit commonly amounts to about 100-140 mrad RMS [Ver12, Ver14]. The results presented in Chapter 2 show that this figure can be pushed below 50 mrad with the cavity-external shifting technique. For most systems in the millijoule range, the limit set by the seed oscillator is rather a theoretical issue, as their overall residual CEP noise clearly exceeds that level, with most reported values in the range of 250-400 mrad [Rau06, Li08, Her11]. Rather, the overall CEP performance of such amplifiers is dominated by CEP noise added during the amplification process, the sources of which fall into one of two categories.

Most importantly, the CEP is affected by changes in dispersion (Chapter 1). These are often mediated by functional parts that couple dispersion to beam position. Thus, the drift or vibration of mechanical components can translate into CEP noise. This is especially severe in large grating stretcher or compressor assemblies [Kak04]. Also, beam pointing drifts and changes in ambient conditions belong into this category. These effects dominate at frequencies up to 1 kHz, often occurring in narrow frequency bands, or with a  $1/f$ -like noise signature. An exception to this rule concerns dispersion-reliant pulsed devices, such as AOPDFs (e. g., Dazzler, Fastlite) which are routinely employed for spectral shaping and compensation of higher-order dispersion. An imprecise synchronisation and triggering of these devices will result in frequency-independent dispersion jitter and, consequently, CEP noise. On the other hand are effects coupling pulse intensity to CEP through self-phase modulation (SPM). Intensity noise can be caused by pulse switching electronics or pump power fluctuations. Beam pointing drifts can also act in this fashion by varying the overlap of the pump and seed beams. Except for the latter, these effects generate stochastic or high-frequency noise. The impact of CEP noise sources from both categories can be reduced through careful design of the amplifier. It is paramount to reduce the susceptibility of the system to mechanical influences. To this end, work needs to be devoted to details, such as stable mechanical construction. Further measures include the use of bulk material for pulse stretching [Ric12]. Also, low-vibration cooling systems can be applied in favour of piston-type cryo-coolers for the amplifier gain medium, as was done in the 10 kHz amplifier presented in Section 4.2. Effects of the SPM-related category can be minimised by reducing the accumulated nonlinear phase, the so-called B-integral [Sie86, Chs. 5, 9, 10].

Some of the sources of CEP noise named here apply to laser oscillators as well, but most them are of negligible importance to the low-energy pulses circulating in a small and comparatively stable cavity. In other words, the CEP noise added during amplification,  $\Delta\Phi_{\text{amp}}$ , and that of the oscillator alone,  $\Delta\Phi_{\text{ceo}}$ , have little correlation. With that in mind, it becomes clear that an amplifier with an overall residual CEP noise of several hundred milliradian is hardly going to profit from decreased seed oscillator noise alone. Representing (at least approximately) independent stochastic errors, the two contributions add up geometrically [Mer01]:

$$\Delta\Phi_{\text{tot}} = \sqrt{\Delta\Phi_{\text{ceo}}^2 + \Delta\Phi_{\text{amp}}^2}. \quad (4.1)$$

For an overall system noise of 300 mrad, of which 150 mrad were due to the seed laser, reduction

of the latter by a factor of two leads to a total system noise of 270 mrad. Stabilisation of the oscillator to 30 mrad, as can realistically be assumed following the results from Section 2.4, only pushes the error a little closer to 260 mrad – which, for the values in the above example, is the isolated contribution of the amplifier. Expecting FF stabilisation alone to yield a significant jump in amplifier CEP stability might have been naïve, but the above example illustrates that reducing oscillator CEP noise is a necessary pre-requisite for reducing the CEP noise of millijoule-level pulses. In the following paragraphs, active correction measures will be discussed that target the amplifier contribution, too.

### 4.3.2 Spectrogram-based fast measurement of the CEP

When passive stability of the amplifier reaches its limits, active correction can be employed to cancel CEP noise in principle up to the Nyquist frequency, i. e., half the repetition rate. In practice, both measurement and actuation are hampered by other limitations, reducing the bandwidth of stabilisation loops to a few hundred hertz at best. Conventional CEP detection in a single-shot f-to-2f interferometer relies on the processing of a spectrogram [Kak01]. A similar method of phase extraction was used in Section 2.5. Processing time was of no concern in that experiment, but real-time acquisition and analysis faces problems. The signal of the charge-coupled device (CCD) used for pixel-wise detection of the angularly resolved spectra first has to be made available to a data bus, then has to be transferred to a PC for evaluation. The processing power of modern PCs is sufficient to perform the numerical part in time, but it is the CCD read-out and transfer that typically causes a time delay on the order of milliseconds.

Only within the last decade have methods been invented to determine the shot-to-shot CEP fluctuations of amplified pulses at an acquisition rate in the kilohertz range and above. Circumventing the CCD limitation, these schemes either combine the single-shot f-to-2f with a faster means of extracting the phase from the spectral interference pattern, or rely on a different CEP-sensitive effect altogether. Representing the former category, the phase information can be gained from the yield asymmetry of two photo-multipliers placed on either side of an optical element separating one interference fringe [Kok08], or from an array of photodiodes [For11]. Both techniques trade spectral resolution against read-out speed, possibly at the expense of detection errors. In contrast, the so-called phase-meter [Pau03, Say11] relies on the yield asymmetry along the laser polarisation direction of photoelectrons liberated in an above-threshold ionisation experiment [Pau01]. Unlike methods based on self-referencing, it provides an absolute phase measurement, but is applicable to very short (< 7 fs) pulses only. Requiring a vacuum apparatus and gas supplies, it is also significantly more complex.

In a cooperation with Vincent Crozatier of the company Fastlite, it was decided to pursue the first approach. In the course of developing an every-single-shot version of their pulse characterisation device dubbed *Wizzler* [Oks10, Mou10], a fast spectrometer had been developed. It was demonstrated to be capable of interferogram measurement and extraction of the phase at a repetition rate of 11 kHz [Cro11]. The prototype was based on a typical grating spectrometer.

It was built in Czerny-Turner configuration with an arm length of 75 mm and an entrance slit width of  $25\ \mu\text{s}$ . The detector was a 512 pixel CMOS array with fast read-out capability (line reading scan time  $< 85\ \mu\text{s}$ ). It received a 30 nm band centred at 520 nm. The acquired spectra could be displayed using an oscilloscope. The f-to-2f interference pattern was converted into an electronic signal which was filtered, digitised, and further processed on-board for phase extraction. The resulting  $2\pi$ -periodic phase value was provided with 12-bit precision as an analogue voltage. The internal memory of the device allowed for the logging of up to 512000 consecutive phase values. The maximum acquisition rate exceeded 10 kHz and was limited by the detector read-out and phase extraction process. In order to achieve fast CEP detection without compromising measurement precision, the device was used to replace a typical USB spectrometer in an f-to-2f interferometer.

This fast f-to-2f device was put to a test with a millijoule-class amplifier running at a repetition rate of 10 kHz, similar to the second system presented in the preceding section. The tenfold increase in repetition rate as compared to the high-energy system in Section 4.2 allowed the characterisation of CEP noise in a considerably higher bandwidth. In contrast to a system running at 1 kHz repetition rate, the noise in this case can be resolved in frequency even for the presumably most interesting acoustic range. Figure 4.4 shows a schematic overview of the experiment. As before, the seed laser was CEP-stabilised using a commercial implementation of the FF technique (rainbow CEP4, seed version, Femtolasers). The oscillator delivered approximately 320 mW of average power at a repetition rate of 76 MHz when pumped with 3.5 W from a CW pump laser (Sprout, Lighthouse Photonics). The entire power was sent through a DFG interferometer, the spectral content above 1050 nm being split off for the detection of the CEO frequency. The remainder passed the AOFS, leading to a CEP-stabilised

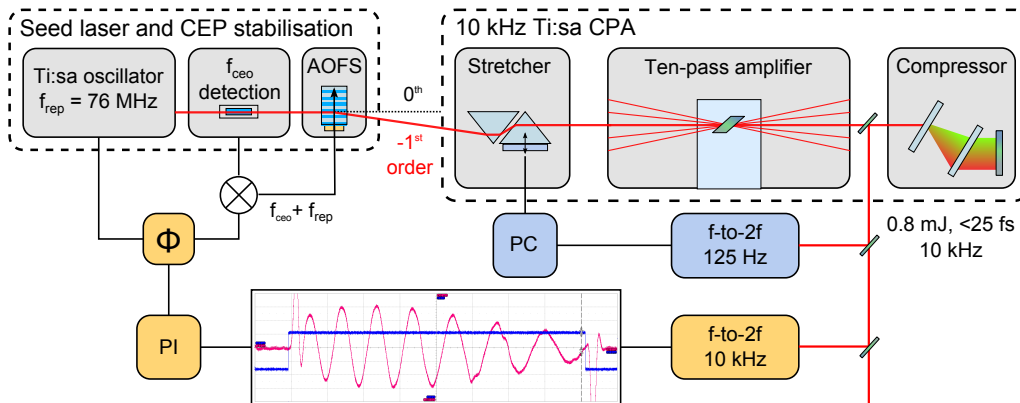


**Figure 4.4:** Schematic layout of the experiment. Seeded by an FF CEP-stabilised Ti:sa oscillator, a 9.9 kHz amplifier provides pulses with 0.8 mJ energy and a duration of 25 fs. The CEP of the amplified pulses is measured by two collinear f-to-2f interferometers running at 125 Hz and 10 kHz acquisition rate, respectively. Feed-back correction can be applied by varying either the stretcher dispersion or the RF phase of the AOFS driver signal.  $\Phi$ : RF phase shifter. PI: PI controller. Inset: Oscilloscope screen-shot of an interferogram acquired by the fast f-to-2f.

pulse train with an average power of about 200 mW. After the bulk stretcher and spectral filtering (see Section 4.1) the average seed power amounted to 50 mW. The pump laser (DM60, Photonics Industries) was set to 5.8 mJ per shot at 9.9 kHz. After the transmission grating compressor, the amplifier delivered 0.8 mJ pulses of 25 fs duration. Beam splitters directed a small fraction of the output to two home-built collinear  $f$ -to- $2f$  interferometers, both placed outside of the amplifier housing. One of the devices was identical to that employed in the long-term measurements described before (Section 4.2.2), running at a repetition rate of 127 Hz. Its signal could be employed for feed-back CEP correction via a PC, the insertion of a prism in the stretcher serving as the actuator. The other interferometer was of same optical layout, but the fast spectrometer described above was used in place of the original one. It was triggered synchronously with the q-switch of the amplifier pump laser. The integration times of both the slow and the fast device allowed only one amplifier shot to contribute to each CEP measurement.

An a first experiment, the CEP of every single shot emitted by the amplifier was measured with the fast device in an OOL configuration, investigating the impact of the conventional slow feed-back loop. The Fourier analysis of the 10 s datasets, shown in Figure 4.5, yields an exemplary display of the different sources of CEP described in Section 4.3.1. The PSD clearly shows their characteristic signatures, as the measurement noise floor amounts to slightly less than  $10^{-5}$  rad<sup>2</sup>/Hz. Power supply mains leakage occurs at 100, 200 and 300 Hz, a broad range of acoustic resonances can be seen between 120 and 600 Hz, whereas  $1/f$ -like behaviour is dominant towards low frequency. The action of the slow correction loop has but marginal impact on the residual CEP noise, reducing it from 242 (green/black trace) to 237 mrad (blue/red trace).

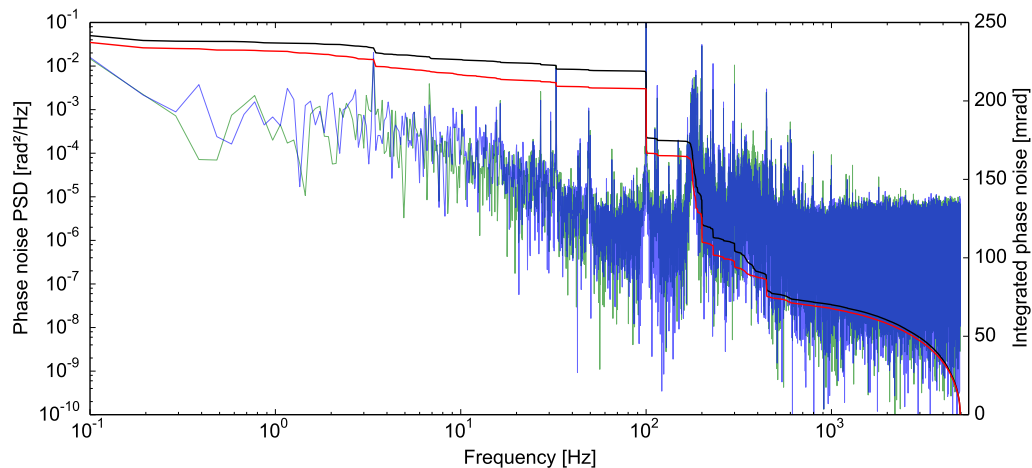


**Figure 4.5:** Characterisation of slow feed-back loop performance. Data were acquired with an  $f$ -to- $2f$  interferometer equipped with the fast spectrometer in an OOL role. The plot shows a comparison of PSD/IPN in open-loop (green/black trace) and closed-loop situations (blue/red trace).

trace). Owing to the low acquisition rate and the high mass of the prism, the slow feed-back loop can only compensate CEP error occurring in the few-hertz range. In fact, the slightly better performance in the closed-loop state cannot be due to the correction loop, as its error signal is updated only at a maximum frequency of 75 Hz. Clearly, even if it were able to provide CEP correct up to half the acquisition rate, major contributions to the total IPN come from much higher frequencies.

### 4.3.3 The acoustic grating phase as a CEP shifter

With a fast means of CEP detection available, the next logical step is to identify a suitably fast actuator. Previously demonstrated mechanisms include adding an offset to the seed oscillator stabilisation [Can09], shifting the phase in an AOPDF [For09], or in an electro-optic crystal [Gob11]. The use of FF CEP stabilisation offers an interesting alternative with favourable properties that requires only minimal modifications to the original stabilisation system. The primary task of the AOFS in FF stabilisation is to modify the *frequency* of the diffracted light. However, recalling Section 2.3.2, the acoustic wave also imprints its *phase* on that of the optical wave. Thus, by changing the phase of the acoustic wave, the AOFS can be employed not only to produce pulses with constant CEP, but also to arbitrarily set its value. This effect does not rely on material dispersion and hence leaves the pulse temporal envelope unchanged. In contrast, the use of material dispersion to influence the CEP not only changes the pulse envelope. Recently, it was shown that this wide-spread means of CEP control also causes measurement errors in f-to-2f interferometry [Kre11]. Both effects are aggravated with decreasing pulse duration, and are avoided entirely when resorting to the RF phase shift actuator.

In practice, the phase of the AOFS driving signal was controlled by a standard voltage-controlled radio frequency (RF) phase shifter (SF28A7, Sigatek), allowing  $360^\circ$  of electronic phase shift with linear voltage-to-phase response and a specified modulation bandwidth of 1 MHz. Figure 4.6 shows the voltage-to-phase action of the device. An input voltage range of approximately 5 V is sufficient for phase shift of  $2\pi$ . The insertion loss variation of about 2 dB is easily compensated by the limiter in the final stage of the FF electronics. In order to avoid potential phase noise arising from a changing input frequency to the RF phase shifter, the device was placed in the repetition rate branch of the signal chain. As the subsequent mixer is linear in the phase of both inputs, this does not limit its function (see Section 2.4.3).

For a combined test of measurement and actuation, the RF shifter was driven by a square wave of a fixed amplitude, triggered at half the amplifier repetition rate. The CEP data, acquired by the fast f-to-2f interferometer and displayed in Figure 4.7, illustrate that the actuator is fast enough to change the CEP by more than  $\pi$  from one shot to the next. The RMS deviation of the CEP values from the upper and lower targets amounted to 198 and 197 mrad, respectively ( $2 \cdot 10^4$  shots, 2 s). This is close to the free-running CEP jitter measured at that time, showing that the height of the phase jump was highly reproducible. Regarding the specified modulation bandwidth of the RF phase shifter of 1 MHz, this behaviour ought not change significantly even

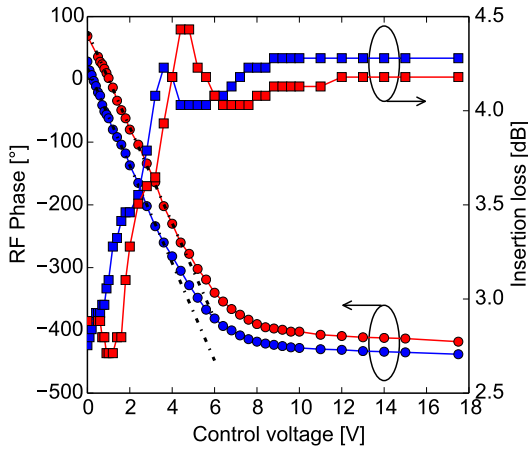


**Figure 4.6:** RF phase shifter characteristics. Phase shift (circles) and insertion loss (squares) for input frequencies 75 MHz (blue) and 90 MHz (red). The dashed lines are least-squares fits showing slopes of  $-76$  and  $-78$   $^{\circ}/\text{MHz}$ , respectively.

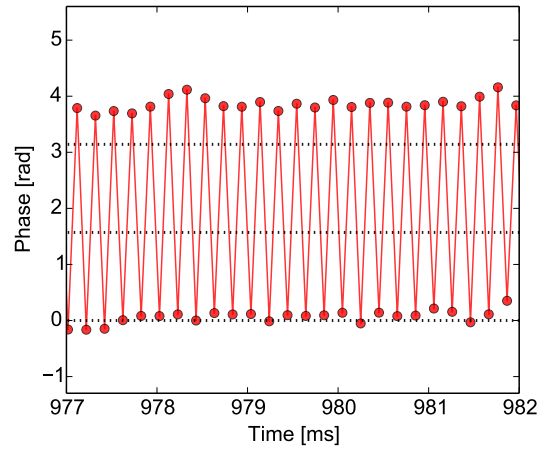


**Figure 4.7:** Demonstration of RF shifter as CEP actuator. Driven by a triggered square wave, the RF shifter allows CEP jumps of more than  $\pi$  from one amplifier shot to the next. Data recorded by the fast f-to-2f spectrometer at 9.9 kHz repetition rate.

at a repetition rate of 100 kHz. The actuator thus opens up the possibility of lock-in detection in CEP-sensitive experiments similar to the method employed in [Sch13], yet at far higher repetition rates. Shifting the modulation frequency out of the regime of acoustic and vibration noise should lead to a further increase of the sensitivity of such methods.

#### 4.3.4 High-speed CEP correction

Attempts have been made to use fast detection [Ado11], fast actuation [Can09], or both [Fen13] to close a feed-back loop correcting the CEP of amplified pulses. Albeit each has resulted in a slightly decreased residual CEP noise at the amplifier output, none of these approaches has yielded as significant an improvement as should be expected from an effective feed-back loop. Following the lines of argumentation laid down in Section 4.3.1, two reasons can explain this. Either the feed-back correction acting on the overall system noise was insufficient to cancel the noise added in amplification, and/or the oscillator CEP stability was low even before amplification. Whatever the reasons in those cases, the examples suggest that low-noise operation of both the seed oscillator and the amplifier correction loop should be verified independently.

Concerning the experiment presented here, the performance of the former had been thoroughly investigated (Chapter 2), and could safely be assumed not present a limit to the overall system. Next, the combination of the fast CEP detection (Section 4.3.2) and the RF phase shifter

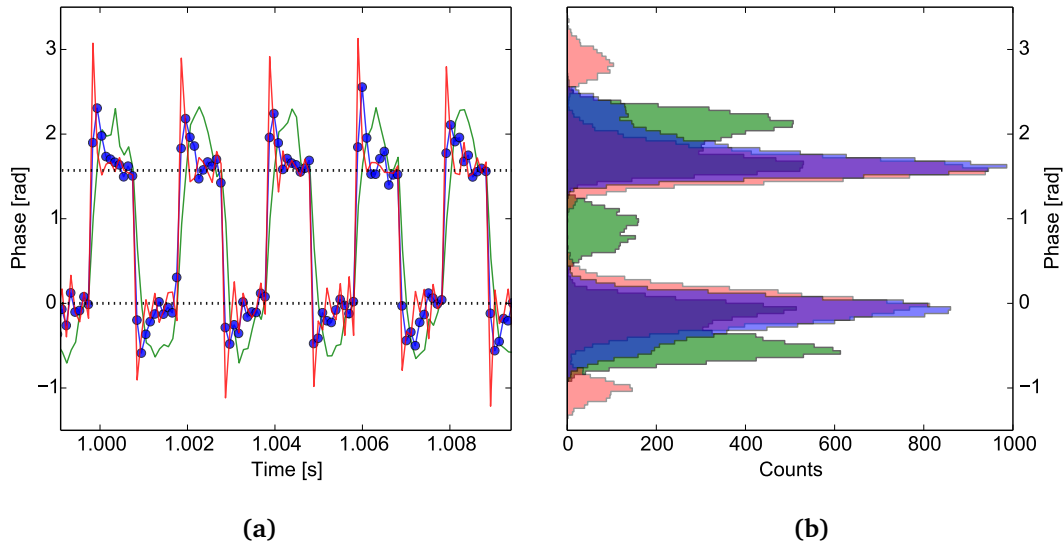


**Figure 4.8:** Closed-loop step response of the fast CEP correction feed-back loop. Trace colours correspond to low (green), optimal (blue), and high (red) proportional loop gain. **a)** Detail of recorded CEP data. **b)** Histograms of 2 s datasets ( $2 \cdot 10^5$  shots). For optimal gain, the RMS deviation from the low and high phase targets amounts to 217 and 246 mrad, respectively.

(Section 4.3.3) was put to the test. The prototype spectrometer provided an analogue voltage signal proportional to the difference between the measured CEP and an arbitrary fixed value. This voltage was passed through a PI controller (D2-125, Vescent Photonics) to generate a control signal. The integrator cut-off frequency was set to  $f_i = 5$  kHz. A simple circuit based on operational amplifiers was used to adapt the PI controller output to the linear range of the RF phase shifter, and to set its operation point by adding an offset.

For optimisation of the PI parameters, the fast feed-back loop was engaged, with the target phase being switched by  $\pi/2$  every 10 amplifier shots. Figure 4.8 shows the CEP data acquired for different settings of the proportional loop gain with the fast correction loop. The loop was able to lock to the alternating phase target for all settings, but with distinctive settling behaviour for excessive and insufficient gain. For optimised servo gain, the closed loop step response was sufficiently fast to lock to the new target within 3-4 shots, suggesting a loop bandwidth in excess of 2.5 kHz. At this setting, the standard deviation of the CEP from the respective targets was less than 250 mrad ( $2 \cdot 10^5$  shots, 2 s), which is remarkable in the presence of such significant phase jumps. These data justify the assumption that the loop should be suitable to correct most of the CEP noise measured in the free-running case.

Accordingly, the CEP correction loop was closed at the full amplifier repetition rate. The acquired data, limited by the maximum recording length offered by the fast spectrometer, are displayed in Figure 4.9. Within 52 seconds, evaluation and correction of the CEP of  $5.12 \cdot 10^5$  shots resulted in a residual in-loop phase error of 98 mrad. No notable steps occur in the IPN

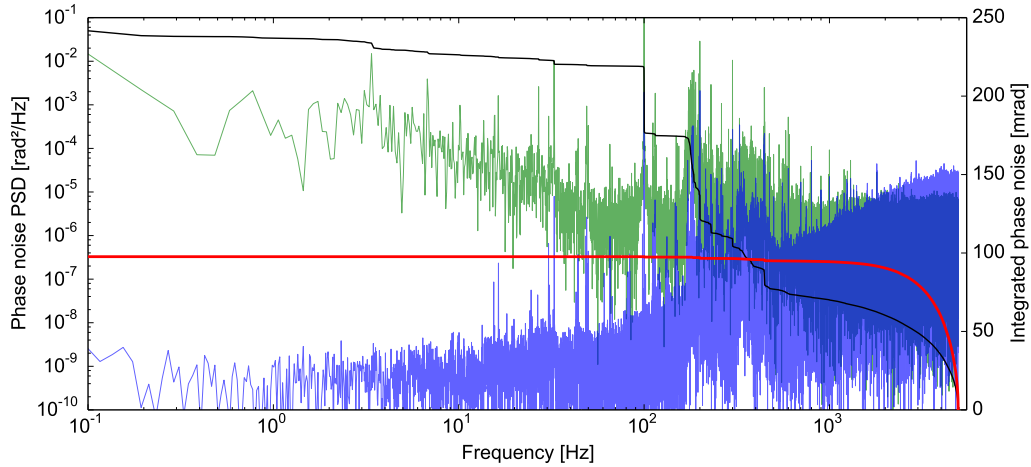


**Figure 4.9:** CEP stabilisation performance of the fast feed-back loop using full-repetition rate detection and actuation. Traces show the high-frequency part of Fourier analysis, corresponding to PSD/IPN of IL data (blue/red trace) and open-loop data (green/black trace from Figure 4.5).

curve (red trace), in stark contrast to the results achieved with the slow feed-back loop. For reference, the open-loop data measured at the full repetition rate are displayed as well. Note that all sources of CEP noise from low to high frequency are cancelled perfectly. The base level of the PSD (blue trace) keeps falling from high to low frequency, meaning that the control bandwidth spans the entire measurement range. For the lack of a second fast acquisition system, no equivalent OOL comparison could be performed. Instead, the slow  $f$ -to- $2f$  was employed for this task, yielding a residual CEP jitter of about 140 mrad. Figure 4.10 provides a visual comparison of the CEP time series and the corresponding histograms. In spite of the discrepancy between the IL and OOL values, the result still constitutes an improvement of 100 mrad over the IPN obtained with the conventional loop.

A closer look at Figure 4.9 suggests that the fast loop still offers room for optimisation. Clearly, the residual CEP noise PSD level with the loop closed exceeds that of the free-running system upwards of 2 kHz, meaning that the stabilisation system actually added noise which was not present in the other cases. A likely explanation lies in the nature of the CEP noise floor upwards of this frequency. The measurement precision of an  $f$ -to- $2f$  interferometer is limited by amplitude fluctuations transferring to the CEP by way of SPM [Li09]. Stochastic shot-to-shot fluctuations of the amplifier pump laser energy cause intensity jitter on the femtosecond output. The measured CEP noise spectrum therefore contains a white noise background at high frequency. A feed-back loop acting on such a stochastic error adds noise instead of suppressing it, and the high frequency integration stage ( $f_i = 5$  kHz) used in the experiment provided gain at a region where the  $f$ -to- $2f$  signal was already dominated by stochastic noise. Tailoring the loop filter high-frequency response to the crossover point of the two PSD curves in Figure 4.9 should result in a residual CEP jitter of less than 70 mrad. This type of filter design is likely easier to

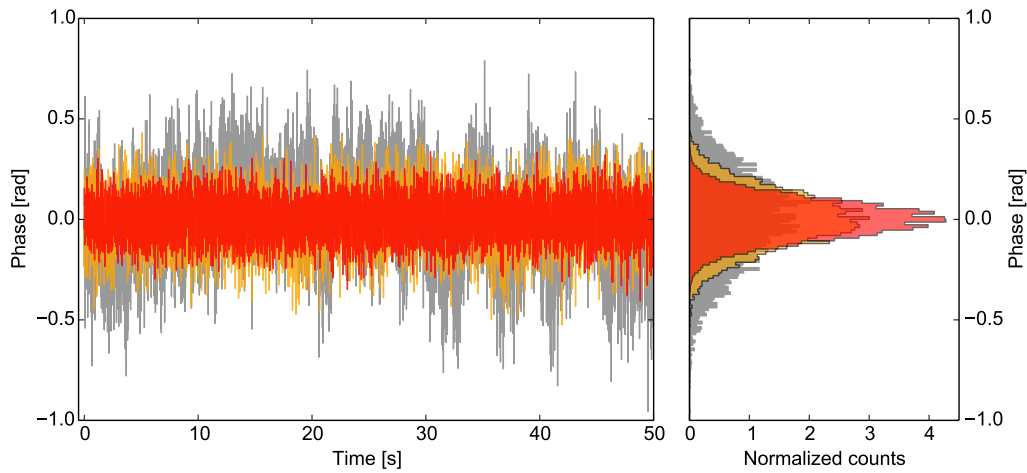


**Figure 4.10:** Time domain CEP data and histograms obtained with different feed-back loop configurations. *Red traces:* fast loop IL data, same dataset as Figure 4.9 (red/blue curve),  $\sigma = 98$  mrad. *Yellow traces:* OOL data simultaneously acquired in slow f-to-2f,  $\sigma = 146$  mrad. *Grey traces:* CEP evolution of free-running amplifier measured by slow f-to-2f,  $\sigma = 273$  mrad.

implement in the form of digital signal processing, rather than in analogue electronics, as was the case here. At the cost of a slight increase in low-frequency noise, such a filter could result in a residual CEP noise level lower than that of most conventionally stabilised oscillators, and only about a factor of two higher than can be expected from the seed oscillator employed here (see Section 2.4.4). Eventually, however, a measurement with a lower noise floor would be required to exploit the presented fast correction loop at its full potential. Given such a measurement, the residual CEP jitter could be reduced to the oscillator limit.

#### 4.3.5 Outlook

The experiments presented in this section have led to the lowest CEP jitter measured to date for a pulse train on a single-shot basis (98 mrad over 52 s,  $> 5 \cdot 10^5$  shots). This was enabled by the combination of a fast means of CEP detection with a novel fast and precise actuator. Free from crosstalk to other pulse parameters such as the spectral phase, this comparatively simple modification of the cavity-external technique not only enables fast CEP control, but also offers a route to lock-in detection for CEP-sensitive experiments at frequencies that are presently hard to access. The fact that such highly precise phase control was achieved at the level of millijoule pulse energy underlines that, given careful amplifier design and a highly stable seed oscillator, high CEP stability can be maintained even during  $10^6$ -fold amplification. The findings presented here furthermore highlight the fact that acoustic noise and vibration present the most severe limits to CEP stability already at millijoule pulse energy. When aiming at even higher energy, where a repetition rate in the kilohertz range gradually becomes infeasible, it therefore

appears sensible to maintain high-repetition rate pre-amplifiers (and hence, the opportunity for high-bandwidth correction) for as long as possible. On the other hand, much effort has lately been devoted to increasing the average power rather than the energy of ultrafast pulses, as was outlined in Chapter 3. With fibre technology pushing the repetition rate of millijoule picosecond pump pulses to hundreds of kilohertz [Kle13], parametric amplifiers driven by such systems could profit considerably from the work presented in this section.

#### 4.4 Hollow-fibre compression and its impact on the CEP

Most sources of high-energy pulses do not offer the exceptionally broad spectral bandwidth that is needed to support truly few-cycle pulses. Due to gain narrowing in laser oscillators and amplifiers [Sie86, Ch. 7], and temporal jitter [Fat12, Sch12] and phase-matching effects [Wit12] in parametric amplifiers, the overwhelming majority of light sources for attosecond experiments needs to rely on temporal compression of the pulses after reaching the desired pulse energy. The approaches presented in Chapter 3, aiming primarily at a high average power rather than pulse energy, could still rely on spectral broadening in bulk or structured solid state media. The pulse energy remained on the microjoule level, but catastrophic optical damage was still observed in all of the experiments at some point. Temporal compression beyond that energy range is therefore commonly achieved using gaseous media. Their nonlinear coefficient of the refractive index is several orders of magnitude lower than that of bulk or liquid media, thus requiring either a high intensity or long interaction length to achieve the desired spectral broadening. The former path is limited by the onset of ionisation, giving rise to absorption and defocusing effects. The most widespread technique to this end therefore employs a hollow waveguide in the form of a glass capillary filled with a noble gas, hence named hollow-fibre compression (HFC) [Nis96]. Many successful experiments exploring CEP-sensitive phenomena or involving isolated attosecond pulses (IAP) have relied on it, providing indirect proof that this form of compression essentially preserves the CEP. However, the recent trends towards up-scaling the pulse energy [Böh14] and the ever-increasing spectral bandwidth obtained in such compression schemes [Wir11] have made it necessary to look more closely into the CEP-related effects of HFC. First investigations had characterised the CEP stability of the output pulses after the compression device [Wan09, Ado11, Oke13]. Providing little information on the CEP performance of the earlier steps in the laser chain, their findings yielded but indirect insight into the spectral broadening process itself.

The experiments presented in the following were motivated by the question of whether a specific approach towards HFC energy up-scaling would fare differently in terms of CEP stability as compared to the original technique [Nis97]. Instead of filling the fibre with gas at a static pressure (SP), the use of a pressure gradient (PG) geometry had been shown to enable considerably higher throughput at high input energy [Sud05]. With the gas pressure being lowest at the fibre input and increasing with the propagation distance, the scheme reduces ionisation of the gas atoms before the waveguide. This is beneficial because the shot-to-shot

variation in the density of free electrons from ionisation would lead to stochastic fluctuations of beam pointing, and thus coupling efficiency, through filamentation [Boy09, Ch. 12]. On the other hand, the technique requires additional vacuum pumps to be connected to the fibre enclosure, thus potentially increasing noise induced through mechanical vibration. So far, there existed no means of measuring the contribution of CEP noise induced in HFC.

The method presented in this section alleviated this problem. It was conceived by Gabriel Tempea of Femtolasers, in cooperation with Thomas Oksenhendler of Fastlite. The experiments were performed at the laboratory of Mauro Nisoli at Politecnico di Milano during three campaigns in May to October 2013 together with Andrea Trabattoni and Francesca Calegari. The data gathered with it were disseminated in a joint publication [Lüc14f] and conference talks.

#### 4.4.1 In-situ single-shot interferometric measurement technique

The most straightforward way of determining the phase shift experienced by an optical signal is by linear interference with a reference replica that propagates under precisely known conditions. In principle, the CEP change introduced by HFC – or any other optical assembly – could be measured by splitting off a small fraction of the pulse energy at the fibre entrance, propagating it in vacuum over a distance equal to the path length of the fibre, and overlapping it with the main pulse at the exit of the waveguide. The experimental implementation of this scheme would be challenging, however, since timing jitter and spatial mode mismatch would diminish the accuracy of an interferometer with such long and complex arms. In the case of the CEP, however, the main contribution can be expected to be due to nonlinear effects, making it unnecessary to separate main and probe pulse spatially. Instead, they can be distinguished by their energy, allowing for the use of a collinear geometry.

In the approach described in the following, a small co-propagating replica is generated by means of a thin birefringent plate of each pulse that is coupled to the gas-filled fibre. The orientation of the plate in the plane perpendicular to the beam determines the amount of energy coupled into the pulse replica, while the delay between main pulse and replica depends on the thickness of the plate and the optical properties of the crystal. If the input pulse was linearly polarised, so is the replica, but at perpendicular polarisation direction. The main pulse experiences SPM and spectral broadening in the gas-filled hollow fibre, whereas the replica will propagate linearly, provided that its intensity is sufficiently low. This can be easily verified by measuring the spectrum in the polarisation direction of the replica and comparing it to the spectrum recorded at the entrance of the fibre. Since the Kerr effect-induced refractive index changes are highly adiabatic, they have no effect on the replica as long as it does not overlap in time with the main pulse. Dispersion affects the CEP of both pulses alike, but can safely be assumed to be constant considering that the time delay between the two pulses is on the order of a picosecond. This assumption holds while the main pulse does not cause a significant amount of ionisation in the gas, which would in fact change the dispersion by modifying the density of free electrons. As ionisation has a negative impact on the compressor throughput,

care is usually taken to avoid it in the first place, e. g., by proper choice of the gas and the fibre diameter. However, even if it should be found to play a role, the use of a pre-pulse replica rules out this limitation. In turn, the use of a post-pulse configuration allows a comparison indicating the magnitude of ionisation caused by the main pulse. Finally, linear spectral interference between the main pulse and its replica is detected by means of a polariser and a spectrograph at the output of the HFC. Fourier analysis of the spectral interferogram yields the phase difference between the main pulse and the reference replica. When single-shot spectra are acquired, the method provides a means of measuring the accumulated CEP change along the common beam path. Hence, it was dubbed in-situ single-shot interferometry (ISI).

#### 4.4.2 Experimental layout

Figure 4.11 shows the layout of the experiment. As in the preceding sections, the millijoule pulses were provided by a commercial CPA system (see Section 4.1). In this case, however, the seed laser (rainbow DFG, Femtolasers) was stabilised to  $f_{\text{ceo}} = f_{\text{rep}}/4$  using a conventional feed-back loop to the oscillator pump power (XPS800, Menlo Systems). Still, the CEO beat signal was generated in a DFG-type monolithic interferometer. Deriving the amplifier repetition rate from  $f_{\text{rep}}$  divided by a multiple of 4, the amplifier was seeded by pulses with a constant CEP. The total input power amounted to about 100 mW in the relevant spectral range. In contrast to the CPA systems used in the other experiments presented in this chapter, this amplifier was of a double-stage design. The first stage delivered up to 3 mJ at 1 kHz, and was of similar design to the one employed in Section 4.2.1. The second stage served to boost the pulse energy, with  $> 6$  mJ available for experiments after the compressor. The pulse duration was measured to 28 fs.

Immediately before the focusing optics for the HFC input coupling, a collinear single-shot f-to-2f interferometer (APS800, Menlo Systems) was placed. It could be used to close a second feed-back loop by varying the material dispersion in the stretcher by the same mechanism as described in Section 4.3, and served to measure the CEP stability of the amplifier before the HFC. The free-running CEP noise measured during normal operation of the amplifier on the time-scale of minutes ranged between 170 to 200 mrad (IL). With the loop closed, a comparable stability was kept for up to two hours, usually limited by loss-of-lock events in the oscillator CEP feed-back loop as described in Section 1.4. A curved mirror (ROC 3.5 m) was used to focus the pulses into the hollow fibre. They passed a 1.5 mm-thick calcite plate oriented such as to produce a weak, orthogonally polarised replica of approximately 60  $\mu\text{J}$  energy. A temporal separation of 900 fs between the two pulses was determined experimentally by measuring the frequency of the pulse pair spectral interference fringes. This value is in good agreement with that expected from the difference in group delay between the optical axes [Web03]. The birefringent plate was placed as far away from the fibre entrance as its clear aperture of approximately 10 mm allowed, and caused a small amount of SPM. The glass capillary had an inner diameter of 320  $\mu\text{m}$  and a length of 1 m, and was placed in a gas-tight enclosure.

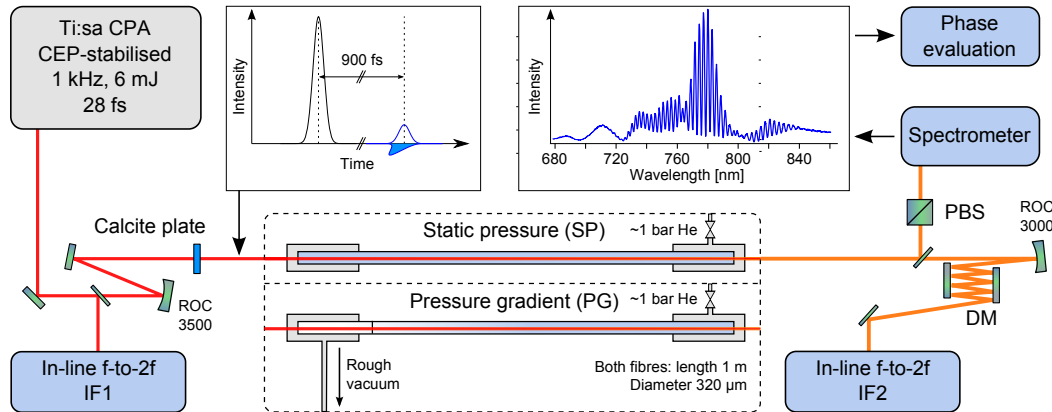


**Figure 4.11:** Experimental layout. Before the HFC, an orthogonally polarised post-pulse is generated. Spectral interference of the two is recorded after propagation in different operating modes. In the absence of dispersion changes, phase changes arise solely from nonlinear processes acting on the main pulse. Two f-to-2f interferometers provide an independent measurement of the CEP. *PBS*: polarizing beam splitter cube. *DM*: dispersive mirror compressor.

Close to the fibre exit port, a pressure valve could be used to fill the vessel with helium to produce spectral broadening by HFC under the conventional static pressure (SP) condition. Furthermore, the enclosure was connected to a scroll vacuum pump close to the fibre entrance, in order to enable operation in pressure gradient (PG) regime. The pulse energy measured after the fibre under vacuum amounted to about 3.5 mJ, corresponding to an overall transmission of about 60 %, which already includes the losses induced by the calcite plate of roughly 10 %. These appeared to be due to a slight shift of the focus position. After re-collimation by a mirror with 1.5 m focal length, the pulses were sampled by a beam splitter and coupled into a spectrometer (AvaSpec2048 series, Avantes). A polariser placed before the device was adjusted for maximum contrast of the resulting interference fringes. The spectrometer was triggered such as to record interference patterns of single amplifier shots at an acquisition rate of 500 Hz. From these interferograms, a sample of which is shown in the inset in Figure 4.11, the CEP change during propagation of a single shot was extracted numerically, yielding the ISI result.

The remaining fibre output was compressed using dispersive mirrors. Furthermore, a home-built second collinear f-to-2f interferometer was placed after the dispersive mirror compressor. Together with the device placed in before the fibre, the two devices provided an independent measurement of the CEP changes induced in HFC for comparison with the ISI technique. The former device (labelled IF1 in Figure 4.11) employed a 1 mm sapphire plate to broaden the spectrum to an optical octave. In the second f-to-2f interferometer (labelled IF2), the spectral bandwidth of the pulses was sufficiently large to obviate the need for additional broadening. It was the same device used for the IL measurements in Section 4.2, based on an all-reflective (i. e., dispersion-free) beam path up to the frequency doubling stage. This proved essential in the measurement, as dispersive elements between the mirror compressor and the frequency doubling crystal increase the time delay between the interfering spectral components.

This would lead to a reduced fringe spacing in the interferogram, causing unreliable CEP extraction as its value approached the spectrometer resolution. The beam path after the fibre exit between IF2 and the ISI detection was covered for protection against air currents. As in all measurements presented in this Chapter, both f-to-2f devices were triggered to measure single-shot interferograms. The acquisition rates amounted to 158 Hz before and 335 Hz after the HFC.

#### 4.4.3 Characterisation

In order to assess the noise floor of the ISI technique, a first measurement was performed with the fibre under vacuum. The CEP noise contribution from the HFC was indicated to be 6 mrad rms over  $10^5$  shots (200 s) at the full input energy of 6 mJ, most likely limited by the signal-to-noise ratio of the spectrometer. With the fibre in a pressure-gradient configuration, a constant backing pressure of approximately 1.5 bar helium was applied at the fibre exit, leading to an output pulse energy of 2.1 mJ. The spectra supported a bandwidth-limited pulse duration of 3.9 fs. Under these conditions, the CEP noise from nonlinearity detected by ISI increased to 40 mrad for the same measurement time. Monitoring the mean CEP shift emerging in the HFC with the ISI method while slightly varying the input pulse energy, a coupling constant of 1.19 rad/mJ, or 71 mrad/% was found (see Figure 4.12). An early investigation into the CEP properties of HFC reported a value of 128 mrad/% [Wan09].<sup>3</sup> Considering the dissimilarities between the experiments, these values are remarkably close.

During these initial measurements, the pulse-to-pulse energy fluctuations of the amplified pulses were recorded with a photodiode in front of the fibre. As a simple consistency check, the CEP jitter calculated with the coupling constant given above was compared to the ISI result. The two agreed to within 10 %, Figure 4.12 showing both datasets. The slightly higher value of datapoints obtained with the calibration factor can be explained by the favourable energy stability of the amplifier of about 0.5 % RMS, which corresponds to voltage fluctuations close to the resolution of the 8-bit sampling oscilloscope. For changes in helium backing pressure, a coupling constant on the order of 100 mrad/% relative pressure change was determined. Due to the low precision of the pressure gauge available, this value provided but a coarse estimate. Nevertheless, considering the leakage rates and backing pressures usually encountered in HFC systems, it justified the assumption that pressure-related CEP changes are limited to slow, monotonous drifts. It was furthermore found that values retrieved from the ISI measurement for this set-up were independent of whether the post- or pre-pulse replica was used. Long-life (>1 ps) plasma-related effects could thus be shown not to play a role in compression-induced CEP noise in this configuration.

---

<sup>3</sup> The opposite sign of the slope given there is due to the indirect nature of the measurement, basically taking the error signal of the IL device upon external modulation as the measurement result.

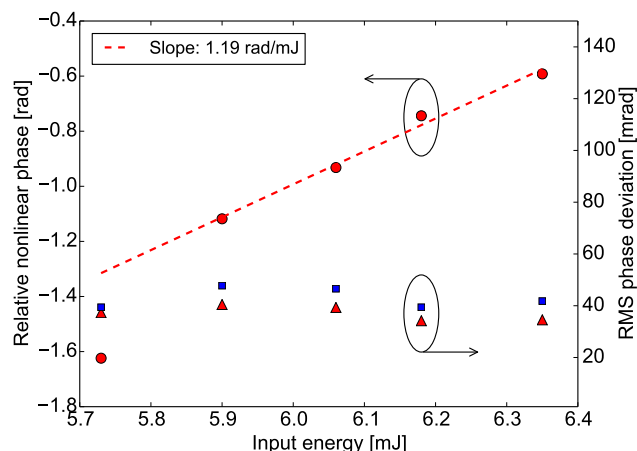


**Figure 4.12:** Mean phase change and phase jitter emerging in the HFC as measured by ISI. *Red circles:* mean phase extracted by ISI from  $10^5$  consecutive spectra each. *Red triangles:* CEP jitter extracted from the same dataset. *Blue squares:* CEP jitter calculated from shot-to-shot energy fluctuation measured simultaneously. The leftmost data point was omitted in the fit, its lower value probably due to decreased gas pressure in the fibre.

#### 4.4.4 CEP noise in pressure gradient and static pressure geometry

ISI provides an isolated measurement of intensity-related CEP noise added during the compression process. In terms of noise characterisation, this sets the situation apart from the one encountered in Section 4.3. There, only the noise level at one point along the amplification chain (i. e., after the oscillator) and that of the entire system were known. Taking into account likely origins of CEP noise in amplification, the correlation argument provided a guideline of how noise in CPA chains could be reduced (Section 4.3.1). Here however, the element in question – the HFC – could be investigated in an isolated way. In combination with the CEP measurements taken before and after the device with f-to-2f interferometers, this provided insight into the correlation properties of the added noise, and hence into its origin. In analogy to the argument used in Section 4.3, if the phase noise emerging in the HFC and detected with the ISI technique was uncorrelated to the phase noise of the input pulses, the standard deviations of the two noise contributions would add geometrically:

$$\sigma_{\text{tot}} = \sqrt{\sigma_{\text{amp}}^2 + \sigma_{\text{hfc}}^2}. \quad (4.2)$$

That would be desirable, considering that the overall standard deviation of the CEP encountered in this amplifier was typically about 190 mrad as indicated by IF1. An additional uncorrelated contribution of 30–50 mrad would therefore result in negligible extra noise, and HFC could safely be considered CEP-preserving in almost any situation. In the case of direct correlation however, i. e., if both the noise before compression and the contribution of the HFC shared a common origin, the standard deviations would add up arithmetically. In order to characterise

the correlation of the CEP noise added in the HFC process, parallel measurements of the CEP were conducted using both ISI and the two conventional f-to-2f interferometers IF1 and IF2. Due to the unequal sampling rates offered by the available spectrometers, true time-domain comparison was not possible. Considering their low sampling rates as compared to the laser repetition rate and the frequencies of likely noise sources, this would have provided little insight in the first place.

The HFC was first operated in PG configuration at identical conditions as in the experiments used for the initial test. The amplifier CEP correction loop remained open. During the 5 minute measurement, the f-to-2f interferometers IF1 and IF2 detected CEP errors of 188 mrad and 233 mrad before and after the fibre, respectively. In the same time window, the CEP error recorded by ISI amounted to 40 mrad. The frequency analysis of the high-frequency part is shown in Figure 4.13. The difference of 45 mrad between the RMS phase fluctuations detected by IF2 and IF1 is very close to the value detected with the ISI method. This leaves two possible explanations. Either the HFC adds a large amount of uncorrelated CEP noise (about 140 mrad in this case), or the noise induced is at least partially correlated to that present on the input pulses. However, there is no conceivable noise source that might account for a contribution as would have to be assumed for the first explanation. It therefore appears likely that CEP noise measured before compression and the additional jitter arising in the HFC share the same origin, which is intensity fluctuation.

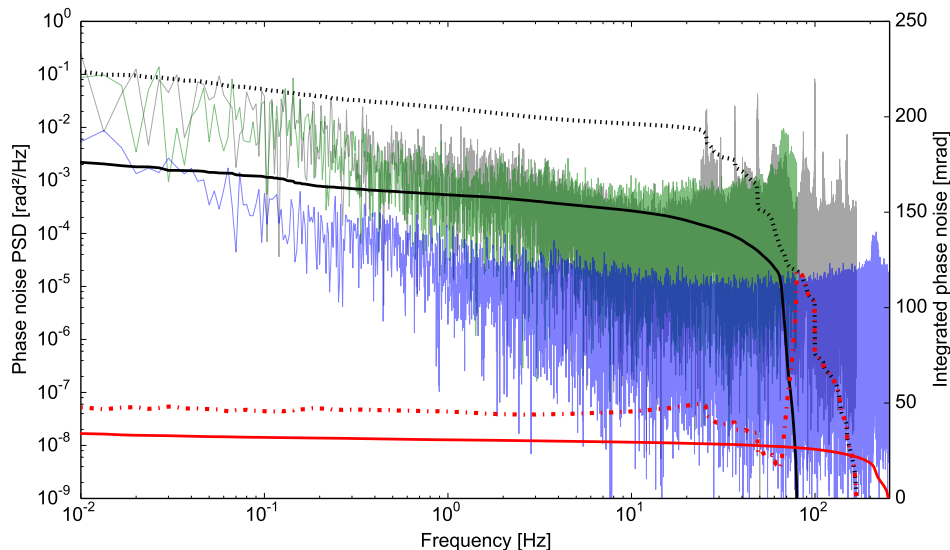


**Figure 4.13:** Fourier analysis of CEP noise in pressure gradient HFC, showing PSD/IPN measured at IF2 after the HFC (grey/black dotted trace), IF1 before the HFC (green/black trace) and nonlinear contribution of the fibre as extracted from ISI (blue/red trace). The red dotted trace shows the arithmetic subtraction of the IPN traces from IF1 and IF2 .

The CEP noise emerging in the HFC appears to be moderately overestimated in the f-to-2f measurement as compared to the ISI measurement (dotted and solid red lines in Figure 4.13, respectively, differing by about 15 mrad). Interferometer drift, which might be expected to play a role in an arrangement such as this, is not a likely explanation because the discrepancy appears already at high frequency. Rather, this can be traced back to the fact that IF2 records spectral interference fringes on the short-wavelength edge of the spectrum (485–515 nm), where the spectral intensity is low and exhibits large fluctuations. Impairing the accuracy of the phase retrieval, this results in an increased CEP detection noise floor. In contrast, the ISI method relies on fringes recorded close to the central region of the spectrum in the wavelength range of 760–800 nm. The signal recorded there is stronger and more stable, allowing a robust, artefact-free retrieval of the phase.

Next, the HFC assembly was configured for static pressure operation. In the hope to exclude CEP drift, the amplifier feed-back loop was closed for this experiment. The vacuum pump was turned off and the chamber was statically filled with helium. With the same input pulse energy of 6 mJ, the pressure was adjusted such that the output spectrum corresponded approximately to the same bandwidth-limited pulse duration as in the PG measurement. The output energy had decreased significantly to 1.6 mJ, indicative of the onset of filamentation effects in helium before the fibre entrance facet. As can be seen in Figure 4.14, this also resulted in increased CEP noise. The in-loop data recorded by IF1 showed a standard deviation of 177 mrad over the measurement duration of 4 minutes. After compression, CEP noise at IF2 amounted to

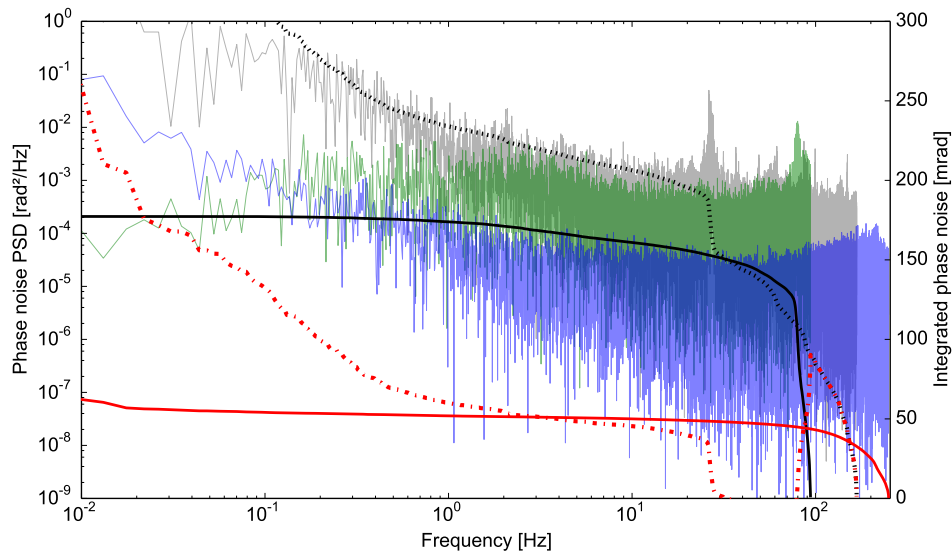


**Figure 4.14:** Fourier analysis of CEP noise in static pressure HFC, showing PSD/IPN measured at IF2 after the HFC (grey/black dotted trace), IF1 before the HFC (green/black trace) and nonlinear contribution of the fibre as extracted from ISI (blue/red trace). The red dotted trace shows the arithmetic subtraction of the IPN traces from IF1 and IF2 .

489 mrad. The ISI measurement indicated an accumulated phase fluctuation of 66 mrad. The upward slope of the IPN in the case of IF2 suggests that more effects played a role than just nonlinear amplitude-to-phase coupling in the waveguide. Rather, the large discrepancy in the form of a sub-hertz drift might have been caused by beam pointing issues before the  $f$ -to- $2f$ . A similar but much smaller tendency was seen in the ISI data as well. The short-term noise at IF2 yields in the order of 300 mrad (5 s, 1674 shots OOL), which would be closer to the value to be expected from adding the readings of IF1 and ISI. Doubtlessly, however, the CEP noise in the case of the SP geometry was higher than that obtained with a pressure gradient, at least when attempting to achieve similar output spectra. The conditions were less than optimal for the static pressure compressor, especially in terms of the input energy, but this shows that comparable output pulse energy to the PG case is not within reach with the original scheme. Several methods have been proposed to alleviate coupling instabilities in static pressure HFCs seeded with multi-mJ pulses, such as using pulses with circular polarisation [Ghi05, Che09, Che11]. These would surely benefit the CEP stability of such schemes as well. It is notable that, although the PG set-up involves additional vacuum pumps connected to the fibre enclosure, it delivers considerably lower CEP noise than the SP type. As a result indicated by both ISI and the  $f$ -to- $2f$  devices, this underlines the importance of avoiding ionisation in HFC schemes, and the potential for further energy scaling in this mode of operation.

#### 4.4.5 XUV generation with different loop configurations

The experiments described above confirmed the assumption that even power-scalable means of temporal pulse compression leave the CEP of ultrashort pulses intact. For the first time, the isolated contribution of the compressor itself was quantified. It thus appears that sub-hertz drifts, such as occurred during measurement performed in the SP configuration (see Figure 4.14), pose a greater threat to the availability of constant-waveform pulses. Aggravated with decreasing pulse duration, CEP drifts directly determine the spectral and temporal fidelity of the extreme ultraviolet (XUV) emission in high-harmonic generation (HHG) [Nis03]. Consequently, such experiments should benefit from a feed-back correction loop that does merely account for the CEP noise of the amplifier, but instead encompasses the temporal compression stage, too. Although this type of feed-back has been tried before [Oke13], the author is unaware of a comparison of the schemes. During the third and last experiment campaign in Milan, the opportunity arose to put this conjecture to a simple test in a realistic HHG set-up. In the following, the performance of the CEP correction loop is benchmarked on the actual application, i. e., generation of XUV radiation in the form of isolated attosecond pulses (IAP).

The driver laser consisted of the system depicted in Figure 4.11, including the 6 mJ two-stage CPA, and the hollow-fibre compressor. The  $f$ -to- $2f$  interferometers were left in place, and either could be used to close a loop on the CEP actuator in the stretcher. The calcite plate was removed along with the beam splitter after the fibre. The HFC was used in PG configuration as described earlier, yielding pulses with an energy slightly above 2 mJ and a bandwidth-limited duration

of  $< 4$  fs. The compressed output was used to drive the XUV/attosecond beam-line of the Nisoli group at Politecnico di Milano, intended for IAP generation. In order to complement the few-cycle pulse duration, a polarisation gating set-up was placed immediately before the pulses were focused into the vacuum chamber [San06]. A pair of fused silica wedges was available for setting the driver pulse CEP, the wedge insertion remotely controllable via PC. The HHG process took place in a 5 mm-long gas cell containing argon at a backing pressure of  $1.4 \cdot 10^{-3}$  mbar. The IR driver pulses were subsequently filtered by an aluminium foil of 100 nm thickness, whereas the generated XUV radiation was imaged into a grating spectrometer with multi-channel plate detectors by a set of toroidal mirrors. The integration time of the XUV spectrometer was set to 1 second. Two sets of measurements were taken, with each consisting of two runs of the same scenario with inverted IL/OOL roles of the two  $f$ -to- $2f$  interferometers. First, the CEP of the IR driver pulse was locked to a constant value. It was then scanned by step-wise insertion of the wedges. At  $10 \mu\text{m}$  per step, the acquisition of a 150-step coarse scan was completed within 2.5 minutes. The resulting spectra are shown in the upper row of Figure 4.15, spanning from the 13<sup>th</sup> to the 27<sup>th</sup> harmonic order. They exhibited the characteristic change from discrete harmonic peaks to a smooth continuum with a periodicity in the CEP of  $\pi$ .

Both the pre- and post-HFC lock seem to preserve the CEP well enough to produce smooth spectra. However, the CEP jitter induced during compression results in notable variation of the XUV spectra from one CEP step to the next, visible as sharp horizontal lines in the plots. The most notable difference between the two plots is that these lines are almost absent in Figure 4.15b, where the loop was closed using IF2. It therefore seems that even the comparably slow loop action does improve the stability of the generated XUV emission. In the second set, the CEP was locked as before, and adjusted such that the HHG process yielded a smooth spectral continuum indicative of an IAP. The spectra were then logged for about 30 minutes, the outcome plotted in the lower row of Figure 4.15. As before, closing the CEP correction loop after the HFC apparently enhances the spectral stability of the generated XUV light. Even though the pronounced broadening of the spectrum after approximately 15 minutes might have been due to external effects such as a gas pressure change, there is visibly higher noise on the left-hand plot, where the CEP was locked before the HFC. This is also mirrored in the CEP values recorded by the interferometers. When using the signal of IF1 for locking, the residual IPN of the 30 minute dataset amounts to approximately 200 mrad before the fibre and 300 mrad thereafter. When disregarding slow drift, the values agree nicely with those given in Section 4.4.4 for the time-scale of minutes. On the other hand, employing IL2 for the lock led to a higher CEP noise before the fibre ( $\sigma = 289$  mrad), but a significantly more stable CEP after it ( $\sigma = 240$  mrad). The reduced noise in the XUV spectra can thus be traced back to the suppressed CEP noise on the driving pulse train, due to a CEP lock that also cancels low-frequency noise induced in the HFC. Moreover, the IPN of 240 mrad obtained when locking the CEP on the post-HFC detection underlines the conclusions drawn from the ISI measurements. These yielded an intensity-dependent contribution by the HFC of 40 mrad at a frequency which the slow loop employed here cannot correct for. With a baseline CEP noise of 190 to 200 mrad after the amplifier as measured with IF1 in the first run, the result of

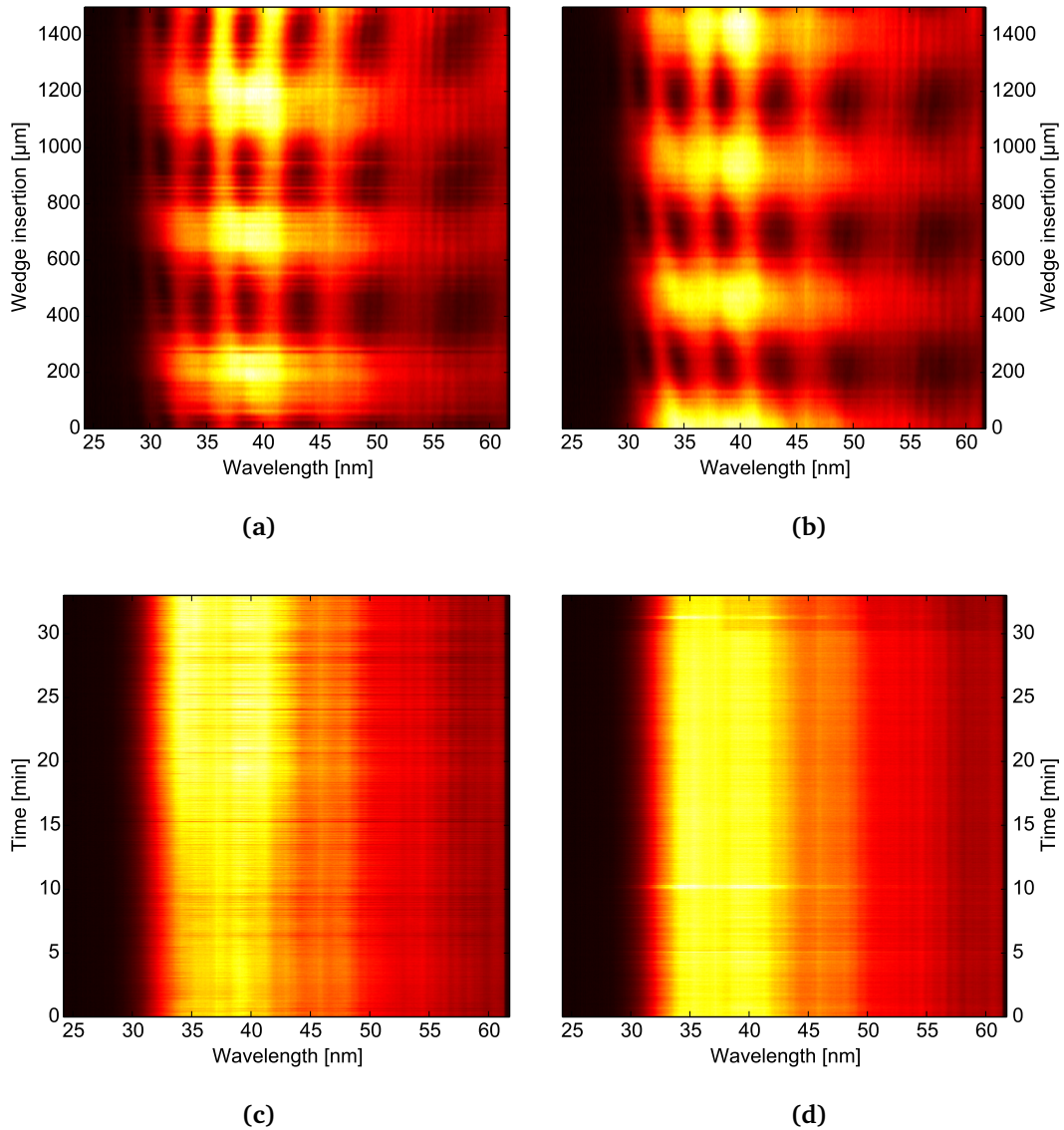


**Figure 4.15:** Comparison of spectra from HHG in argon obtained with CEP loop closed on IF1 (left column, **a**) & **c**) before the HFC, and IF2 (right column, **b**) & **d**) after the HFC. Signal strength is encoded in brightness. The upper row shows HHG spectra obtained during stepwise insertion of the fused silica wedges, scanning the driver pulse CEP. In the lower row, the CEP was locked to a value that resulted in a smooth XUV continuum. The HHG emission spectrum was then monitored for about 30 minutes. IR pulse energy  $< 2$  mJ; duration  $< 4$  fs; Ar backing pressure  $1.4 \cdot 10^{-3}$  mbar.

an in-loop measurement at IF2 approaches the sum of baseline and HFC contribution, as slow drift up the the 10 Hz-range is corrected.

The results portrayed in this section show that pulse compression, even of multi-millijoule pulses, is compatible with CEP stability. The detailed comparison of two different schemes of pulse compression in gas-filled hollow fibres in terms of their CEP noise properties shows that there exist ways to further scale up the energy of few-cycle pulses without compromising CEP stability. The insight gained by the novel ISI method, however, clearly marks the limits to this rationale. Noise added in compression is strongly correlated to that of the input pulses, meaning that energy fluctuations directly transfer to CEP noise. Energy stability, both of the pulses themselves as of their coupling into the compression device, is therefore crucial for any source intended for CEP-sensitive experiments. Although far from exhaustive, the last experiment showed that even noise induced in compression schemes can be compensated to a certain extent. Especially for long-term experiments, placing the CEP detection of a correction loop as late as possible in the driving laser chain should result in elevated CEP performance of the entire system.

## 4.5 Summary

Attosecond science requires ultrafast driver lasers with pulse energy on the millijoule level and beyond. Although several emerging technologies are poised to make such pulses available at far higher repetition rate than currently possible, sources based on any of them will face very similar challenges in terms of CEP stabilisation as the chirped-pulse amplifier systems treated in this chapter.

The experiments presented have shown that cavity-external frequency stabilisation of the seed oscillator enables day-long CEP-stable operation of millijoule-class amplifiers. Two systems with different pulse energy were demonstrated to maintain a constant CEP for more than 24 hours without discontinuities, as proven by out-of-loop measurements. It was then argued that CEP noise induced in amplification is of markedly different origin from that seen in oscillators. Consequently, it needs to be compensated separately in order to maintain the favourably low CEP noise of the seed oscillator. Enabled by a fast CEP measurement, an extension of the cavity-external shifting technique was shown to provide CEP actuation at a bandwidth potentially in excess of 100 kHz. The combination of fast measurement and correction shed new light on the limitations of CEP stability for high-energy pulses. The outcome was a millijoule-level pulse train whose residual CEP noise approached that of the seed oscillator. To the best of the author's knowledge, the presented system was the first-ever laser source with a CEP noise below 100 mrad RMS measured on a single-pulse basis. The last section treated the impact of high-energy pulse compression in hollow fibres on the CEP. To this end, a novel means to measure nonlinear phase changes was employed, its results corroborated with conventional

f-to-2f interferometry. The experiment showed that a hollow fibre compressor in pressure-gradient mode not only accommodates higher pulse energy, but also adds less CEP noise than a fibre under static pressure. Finally, the resulting pulses were used for high harmonic generation. The acquired spectra demonstrate that enclosing the compressor within the feed-back CEP correction loop results in a more stable XUV radiation. Considering the low bandwidth of a few tens of hertz available in this case, much is to be expected from including the compressor in a fast feed-back loop such as the one presented in Section 4.3.

In conclusion, the investigation into the CEP properties of millijoule-class laser systems has resulted in new insights into the origins of CEP noise and new ways of compensating it. Although having been achieved with conventional chirped-pulse amplification, the results are applicable directly to other technologies. In fact, the lessons learned in this chapter perfectly complement the higher repetition rates to be expected from such sources. With power and energy scaling invariably leading to bulkier mechanical dimensions of CEP-relevant building blocks, feed-back stabilisation of amplification-related CEP noise is likely to gain importance.

## Chapter 5

### Conclusion

As attosecond science comes of age, ultrashort XUV pulses gradually become a routine tool in the exploration of the fastest processes in nature. CEP control as the enabling technology must therefore overcome its current limitations in terms of short-term stability, long-term robustness, and scalability towards higher average power. The aim of this work was the investigation of techniques and methods fit to meet this threefold challenge at all levels in the laser chain.

An alternative approach to CEP control in nanojoule oscillators, based on cavity-external frequency shifting, was shown to circumvent the stability-versus-robustness dilemma that plagues the conventional feed-back method. To this end, the technique was adapted for few-cycle pulses, which enabled the use of interferometers with low phase drift over time. Record-low CEP error ( $<50$  mrad out-of-loop, 50 MHz-500 kHz) and more than 24 hours of operation free from phase discontinuities were demonstrated. A modified version of the technique was introduced that requires practically no intervention in a free-running laser. In conjunction with a sealed-cavity seed oscillator, it opens up the possibility for constant-waveform operation of amplifiers over several days without user interaction.

In recent years, diode-pumped ultrafast lasers have become increasingly realistic alternatives to the established Ti:sa platform, the last issue left unsolved being CEP stabilisation. Two systems were investigated, one based on thin-disk oscillator technology, the other on fibre amplification and subsequent enhancement in a passive resonator. Compression of the thin-disk laser output on the microjoule level was demonstrated to yield pulses down to 16 fs duration at close to two order of magnitude higher output power and energy than the Ti:sa oscillators employed before. CEP control was attempted using the cavity-external technique, but met limited success due to the large frequency excursions of the system. The experiment still provided valuable insight that resulted in the first CEP-stable thin-disk oscillator. The fibre-based system was used to evaluate the CEP properties of fibre amplifiers with different levels of nonlinear propagation. CEP control of the system was achieved, but the results provide evidence that both amplification regimes tend to induce significant CEP noise. Amplified spontaneous emission is assumed to be the dominant cause at low seed levels, whereas pump diode noise is pronounced in linear amplifiers at elevated power levels. However, even with the resulting coarse CEP lock, intensity enhancement in a passive resonator was shown to benefit significantly.

The last chapter provided the tools to meet the three-fold challenge in the high-energy regime close to or above the millijoule level. Although the experiments drew on Ti:sapphire chirped-pulse technology, their results hold equal relevance to other technologies. An oscillator with cavity-external CEP control was used to seed multi-millijoule amplifiers at different repetition rates. In both cases, more than 24 hours of operation without CEP discontinuities were demonstrated and confirmed by out-of-loop measurements. The residual CEP noise, extracted from single-shot measurements of more than  $10^7$  shots, ranged from about 210 mrad (in-loop), to about 470 mrad (out-of-loop). Subtracting interferometer drift, all out-of-loop values were close to or below 300 mrad. These figures rival the best published values for millijoule pulse CEP stability, but still exceed the precision measured in the seed laser by about one order of magnitude. Under the hypothesis that CEP noise in the seed source and the amplifier are largely uncorrelated, seed pulses with low noise must be matched by low noise in the amplifier to achieve higher performance of the entire system. To this end, a 10-kHz amplifier was fitted with a CEP correction loop at the full repetition rate. It was based on a fast spectrometer that enabled the CEP measurement of every single amplifier shot, and an equally fast novel actuator based on the cavity-external CEP stabilisation of the seed source. A loop bandwidth in the kilohertz range was demonstrated. The combination resulted in the most CEP-stable pulse train ever characterised on a single-shot basis (98 mrad, 50 s,  $> 5 \cdot 10^5$  shots, in-loop), underlining the importance of a highly stable seed source and fast amplifier correction alike. The out-of-loop error was kept below 150 mrad for hours. In order for high-energy pulses to reach the few-cycle regime, temporal compression is indispensable. A method was introduced to characterise the CEP noise added during by spectral broadening in gas-filled hollow-core fibres. It allowed to trace the origin of nonlinear CEP noise to stochastic fluctuations in the pulse energy. A geometry that reduced the amount of pre-fibre ionisation correspondingly yielded superior CEP stability. A correction loop encompassing the compression stage was found to increase the CEP stability of the generated few-cycle pulses. Different loop configurations were applied to the generation of isolated attosecond pulses, confirming the assumption that active CEP correction should include as much of the experimental chain as possible.

In summary, the work presented in this thesis has extended CEP control technology in every respect. The results will benefit current and future sources of ultrafast IR pulses alike. It was demonstrated that simultaneously low-noise and long-term robust CEP operation is feasible not only for low-energy oscillators. Through careful analysis of the origins of CEP noise and corresponding correction methods, comparably high performance was maintained over six orders of magnitude in amplification to the millijoule level. The rise in repetition rate associated with power-scalable sub-picosecond lasers will open new avenues for feed-back correction to compensate the higher CEP noise associated with large optical components and high intensities. What technology the next generation of near-IR attosecond driver lasers will be based upon is an open question, but it will doubtlessly benefit from the insights presented herein.

Carrier-envelope phase control has helped us in opening a window into the microcosm. The results presented herein will allow our gaze to linger, and at the same time will render our vision more acute – whatever looking glass we should choose.

# Appendix A

## Noise Analysis in the Frequency Domain

The analysis of noise in the frequency domain is a powerful technique that is applied at several points in this work. This section introduces the basic concepts and terms used throughout the thesis. It was adapted from the Appendix in [Kok12] and [Car92, Ch. 10].

The measurements taken of an observable yield a time series of discrete values. As the carrier-envelope phase  $\Phi$  is the most common quantity of interest, let

$$\Phi(t_n), \quad n = 0, 1, \dots, N \quad (\text{A.1})$$

denote this set. The  $N$  samples are assumed to be taken at a constant time interval  $\Delta t$ , such that  $t_n = n\Delta t$ . The whole set spans a measurement time of  $N\Delta t$ . Its time and frequency domain representation are connected through the discrete Fourier transform

$$\Phi(t_n) \xrightarrow{DFT} \tilde{\Phi}(f_k) = \sum_{n=0}^{N-1} \Phi(t_n) \exp(-i2\pi f_k t_n) \quad (\text{A.2})$$

$$= \sum_{n=0}^{N-1} \Phi(t_n) \exp(-i2\pi kn/N) \quad (\text{A.3})$$

with  $f_k = k/(N\Delta t)$ . Apart from the constant term resulting from  $k = 0$ , the lowest frequency accessible to analysis is thus  $\Delta f = 1/(N\Delta t)$ . Because  $\Phi(t_n)$  is real-valued,  $\tilde{\Phi}(f_k)$  obeys the symmetry  $\tilde{\Phi}(f_k) = \tilde{\Phi}(f_k)^*$ . For the context of noise analysis, one is interested in the amplitude (rather than the phase) of the non-redundant frequency components. The so-called single-sided amplitude spectrum

$$M_{\Phi}^{\text{ss,RMS}}(f_k) = \begin{cases} |\tilde{\Phi}(f_0)|/N & \text{for } k = 0 \\ \sqrt{2} \cdot |\tilde{\Phi}(f_k)|/N & \text{for } k = 1, \dots, N/2 \end{cases} \quad (\text{A.4})$$

gives the amplitude of each frequency component in RMS units. Normalisation with  $\Delta f$  makes

the amplitude independent of the frequency resolution of the measurement,

$$S_{\Phi}^{\text{ss,RMS}}(f_k) = \left(1/\sqrt{\Delta f}\right) |M_{\Phi}^{\text{ss,RMS}}(f_k)| \quad (\text{A.5})$$

$$= \begin{cases} |\tilde{\Phi}(f_0)| / (N\sqrt{\Delta f}) & \text{for } k = 0 \\ \sqrt{2} \cdot |\tilde{\Phi}(f_k)| / (N\sqrt{\Delta f}) & \text{for } k = 1, \dots, N/2 \end{cases} \quad (\text{A.6})$$

yielding the single-sided power spectral density (PSD) of the time series  $\Phi(t_n)$ . Plancherel's theorem states that the integral over the squared modulus is equal for a function and its Fourier transform:

$$\sigma(f_m) = \sqrt{\sum_{k=m}^{N/2} (S_{\Phi}^{\text{ss,RMS}}(f_k))^2 \Delta f} \quad (\text{A.7})$$

thus represents the average noise contribution to be expected from all frequencies greater than  $f_m$ . In time domain, this is equivalent to the RMS error accumulated within a measurement duration of  $1/f_m$ . When measuring the phase noise of the CEO frequency or the noise on single-shot CEP values, Equation A.7 defines the integrated phase noise (IPN). It provides intuitive insight into the relative magnitude and location in frequency space of noise contributions to the overall measured noise. Furthermore, it provides a sanity check for the numerical evaluation, as the RMS error of the time series must equal the IPN of the calculated PSD:

$$\sigma_{\text{tot}} = \sqrt{\frac{1}{N} \sum_{n=0}^N (\Phi(t_n))^2} = \sqrt{\sum_{k=0}^{N/2} (S_{\Phi}^{\text{ss,RMS}}(f_k))^2 \Delta f} \quad (\text{A.8})$$

## Appendix B

### Numerical Analysis and Data Archiving

Most data analysis and plotting in this work were done using the WinPython 64-bit distribution of Python 2.7.5. Source code and data are available on the data archive server of the Laboratory of Attosecond Physics, Max-Planck-Institute of Quantum Optics, at the address `/afs/ipp-garching.mpg.de/mpq/lap/`. The subfolder corresponding to this thesis is `/publication_archive/Theses/2014/Luecking_Fabian/raw_data/`. The code is commented and mostly self-explanatory, with additional notes being listed below. For a list of the raw data and scripts used to generate the plots in the work, see the end of this section.

- Section 2.4: The evaluation of the mixer output sampled by the digital oscilloscope was done using `phasenoise.py`. It applies a frequency-domain correction for the anti-aliasing low-pass filter response (using measured data from the respective filters: `lp2500.txt`, `lp500.txt`, `lp5.txt`), then performs the voltage-to-phase calibration (using the frequency-dependent voltage response of the RF mixer), and calculates the phase noise PSD and IPN.
- Section 2.5: The DSO was used in memory segmentation mode, resulting in one 5 kSa trace for each consecutive trigger, with 18462 traces being saved in binary form. The scripts `pulsedff-shortterm2-a.py`, `pulsedff-shortterm2-b.py`, and `pulsedff-longterm.py` perform the necessary evaluation. The plots show one-dimensional histograms for each time bin without further processing. The phase calculation follows the algorithm presented in [Tak82]: Each trace is Fourier-transformed, and the mean frequency of the measured beat is detected and isolated from high-frequency and DC components by a 4<sup>th</sup> order super-Gaussian filter. The phase of the result of an inverse FFT yields the phase value for each time bin of a trace. Statistics over the entire dataset are then performed for the time bins of the traces in order to obtain the RMS phase jitter for each. In order to characterise the phase stability for long measurement time, the time-varying phase is considered for a fixed delay bin. Parallel extraction of the mean frequency each trace allows a decomposition of the phase drift to a) drift caused by in-loop CEO frequency changes and b) total phase error (CEO frequency change, interferometer noise and drift, external sources...). Finally, Fourier analysis can be performed on the time series data.

- Section 4.2: The long-term measurements presented in this section generate amounts of data that approach the limits of what can be processed on present-day desktop PCs without resorting to sophisticated memory management. The software controlling the APS800 interferometer offered only a plain text ASCII format for data logging, producing files weighing more than 2 GB. These were first stripped of unneeded information (such as control loop state and target phase in an OOL dataset) and then converted to a binary format using `men1o2bin.py`. The format was chosen similar to that used by default in the home-built software.

## Plot data sources

Figure 2.2b	<code>/2.2/output-angle.py</code>
Figure 2.6	<code>/2.4/output-angle.py</code> <code>/2.4/after_corr.txt</code> <code>/2.4/after_spec.txt</code> <code>/2.4/pc125.txt</code> <code>/2.4/pc125-target.txt</code>
Figure 2.8b	<code>/2.4/ff-phasenoise.py</code> <code>/2.4/no7-monolithic-62,50MHz-4s--5,0dBm.mat</code>
Figure 2.9	<code>/2.4/ff-phasenoise.py</code> <code>/2.4/mt3_monolithic-62,6MHz-20s--5dBm.mat</code> <code>/2.4/lt4_monolithic-59,00MHz-i35-o30-2000s--5,0dBm.mat</code>
Figure 2.10	<code>/2.4/ff-28hours.py</code> <code>/2.4/28h-envdrift_fullexp.txt</code>
Figure 2.11	<code>/2.4/ff-10hours.py</code> <code>/2.4/10h_fullexp.txt</code>
Figure 2.13	<code>/2.5/pulsedff-shortterm2-a.py</code> <code>/2.5/RefCurve_Beat_OOL_43.wfm</code> <code>/2.5/RefCurve_Beat_OOL_15</code> <code>/2.5/RefCurve_Beat_OOL_57.wfm</code>
Figure 2.14	<code>/2.5/pulsedff-shortterm2-b.py</code> <code>/2.5/RefCurve_Beat_OOL_1.wfm</code> <code>/2.5/RefCurve_Beat_OOL_14</code>
Figure 2.15	<code>/2.5/pulsedff-fourier-st.py</code> <code>/2.5/RefCurve_Beat_OOL_14</code>
Figure 2.16	<code>/2.5/pulsedff-fourier-1t.py</code> <code>/2.5/RefCurve_Beat_OOL_2</code>

---

Figure 2.17	/2.5/hameg_eval.py /2.5/hameg_capture2_2013-10-30-1800_2013-11-04-1043.txt
Figure 3.1	/3.2/hp-td-stage1.py /3.2/stage1-spectra.txt
Figure 3.2	/3.2/hp-td-stage2.py /3.2/lma35x60-lma15x20-sl8x3+s20x2_sf57x12 /3.2/lma35x60-lma15x20-sl8x3+s20x2_sf57x12_spectrum
Figure 3.4	/3.2/stabilisation.qti (Plotted using QtiPlot) /3.2/TRACE088.csv
Figure 3.5	/3.2/stabilisation.qti (Plotted using QtiPlot) /3.2/TRACE120.csv
Figure 3.7	/3.3/ec-oscstab.py /3.3/2013-08-27_tek0001CH1.mat /3.3/2013-08-27_tek0001CH4.mat
Figure 3.9	/3.3/ec-ampcomp.py /3.3/2013-08-12_tek0001CH2.mat
Figure 3.10	/3.3/tek00000.png /3.3/tek00001.png
Figure 4.2	/4.2/he-24-1.py /4.2/121124_overnight_femto_il_24h_oscfail_crop.dat /4.2/121124_menlo_ool_time-cep-fft-only_crop.dat
Figure 4.3	/4.2/he-24-10.py /4.2/CEP_log_2013-06-04_11-35-07.dat /4.2/CH10kHz_ool_menlo_13-06-03.bin
Figure 4.5	/4.3/he-fastamp-slow.py /4.3/50Sa-g32 /4.3/50Sa-g32-cl
Figure 4.6	/4.3/rfps.py /4.3/sigatek-75mhz.txt /4.3/sigatek-90mhz.txt
Figure 4.7	/4.3/khz-spectro-jumps.py /4.3/10Sa-g32-directalt-1.4v

Figure 4.8     /4.3/khz-spectro-jumps.py  
              /4.3/10Sa-g32-2pi-alt-higain  
              /4.3/10Sa-g32-2pi-alt-midgain  
              /4.3/10Sa-g32-2pi-alt-logain

Figure 4.9     /4.3/he-fastamp-fast.py  
              /4.3/50Sa-g32  
              /4.3/250Sa-g16-pi

Figure 4.10    /4.3/he-fastamp-hist.py  
              /4.3/250Sa-g16-pi  
              /4.3/CEP\_log\_2013-11-20\_10-53-22\_export.txt  
              /4.3/CEP\_log\_2013-11-21\_16-34-47\_export.txt

Figure 4.12    /4.4/he-hfc-slope.py  
              /4.4/Milano\_2013\_05\_Femto\_IFN\_Fastlite.doc  
              /4.4/p[1...5] - Pressure[...]

Figure 4.13    /4.4/he-hfc-pg.py  
              /4.4/calcite-aps-3.dat  
              /4.4/calcite-cepset-3\_CEP\_log\_2013-10-28\_20-03-16.txt  
              /4.4/calcite\_wizzler\_3.dat

Figure 4.14    /4.4/he-hfc-sp.py  
              /4.4/static-calcite-aps-3.dat  
              /4.4/static-calcite-cepset-3\_CEP\_log\_2013-10-30\_16-08-08.txt  
              /4.4/static\_calcite\_apson\_wizzler3.dat

Figure 4.15    /4.4/he-hhg-cepscan.py  
              /4.4/scan\_17753\_17902.dat (Panel a)  
              /4.4/scan\_11467\_11616.dat (Panel b)  
              /4.4/he-hhg-time.py  
              /4.4/scan\_13017\_15016.dat (Panel c)  
              /4.4/scan\_11617\_13016.dat (Panel d)

## List of Acronyms

<b>AOFS</b>	acousto-optic frequency shifter
<b>AO(PDF)</b>	acousto-optic (programmable dispersive filter)
<b>ASE</b>	amplified spontaneous emission
<b>CCD</b>	charge-coupled device
<b>CEO</b>	carrier-envelope offset
<b>CEP</b>	carrier-envelope phase
<b>CPA</b>	chirped pulse amplification
<b>CW</b>	continuous wave
<b>DFG</b>	difference frequency generation
<b>DM</b>	dispersive mirror
<b>DPSS</b>	diode-pumped solid state
<b>DSO</b>	digital sampling oscilloscope
<b>FF</b>	cavity-external (CEP stabilisation technique)
<b>FFT</b>	fast Fourier transform
<b>(FR)AC</b>	(fringe-resolved) autocorrelation
<b>FWHM</b>	full width at half the maximum
<b>GD(D)</b>	group delay (dispersion)
<b>GVD</b>	group velocity dispersion
<b>HFC</b>	hollow fibre compression
<b>HHG</b>	high-order harmonic generation
<b>IAP</b>	isolated attosecond pulse
<b>IL</b>	in-loop
<b>IPN</b>	integrated phase noise

---

<b>IR</b>	infrared
<b>KLM</b>	Kerr lens mode-locking
<b>MFD</b>	mode field diameter
<b>MOPA</b>	master oscillator, power amplifier
<b>OOL</b>	out-of-loop
<b>OPA</b>	optical parametric amplification
<b>PC</b>	personal computer
<b>PCF</b>	photonic crystal fibre
<b>PI(D)</b>	proportional-integral(-derivative)
<b>PLL</b>	phase-locked loop
<b>PPLN</b>	periodically poled lithium niobate
<b>PSD</b>	power spectral density
<b>RBW</b>	resolution bandwidth
<b>RMS</b>	root mean square
<b>RF</b>	radio frequency
<b>ROC</b>	radius of curvature
<b>SC</b>	supercontinuum
<b>SFG</b>	sum frequency generation
<b>SNR</b>	signal-to-noise ratio
<b>SPM</b>	self-phase modulation
<b>TD</b>	thin-disk
<b>Ti:sa</b>	titanium-doped sapphire
<b>VCO</b>	voltage-controlled oscillator
<b>XUV</b>	extreme ultra-violet
<b>Yb:YAG</b>	ytterbium-doped yttrium aluminium garnet

## List of Figures

1.1	Three-step model of high-order harmonic generation . . . . .	2
1.2	Overview of thesis structure . . . . .	4
1.3	Output of a mode-locked laser in time and frequency domain . . . . .	6
1.4	Self-referencing technique . . . . .	8
1.5	f-to-2f interferometers for CEO frequency and CEP detection . . . . .	9
1.6	Diagram of feed-back CEP stabilisation using a PLL . . . . .	11
2.1	Cavity-external CEP stabilisation . . . . .	16
2.2	Bragg grating angular chirp compensation . . . . .	20
2.3	Different varieties of the self-referencing scheme . . . . .	22
2.4	Self-oscillation with IL interferometer after AOFS . . . . .	23
2.5	RF tracking filter block diagram . . . . .	26
2.6	Spectral and temporal properties of the CEP-stabilised output pulse train . . . . .	28
2.7	RF signal chain for cavity-external CEP stabilisation . . . . .	30
2.8	Setup for CEP noise characterisation of FF-stabilised few-cycle pulses . . . . .	31
2.9	Fourier analysis of 20 and 2000 s phase noise measurements . . . . .	32
2.10	28-hour phase log showing slow drift with ambient conditions . . . . .	34
2.11	10-hour phase log without drifts after slow loop re-design . . . . .	34
2.12	Pulsed-mode FF stabilisation scheme . . . . .	36
2.13	Histograms of traced obtained in pulsed-mode FF operation . . . . .	38
2.14	Delay-induced CEP jitter in pulsed-mode FF CEP stabilisation . . . . .	38
2.15	Short-term CEP performance of pulsed-mode FF technique . . . . .	40
2.16	Long-term CEP performance of pulsed-mode FF technique . . . . .	40
2.17	5-day free-running CEO frequency recording of sealed-cavity oscillator . . . . .	41
3.1	Single-stage LMA fibre compression results . . . . .	48
3.2	Two-stage LMA fibre compression results . . . . .	49
3.3	Thin-disk laser CEO stabilisation set-up . . . . .	50
3.4	RF spectrogram of thin-disk laser CEO frequency . . . . .	51
3.5	Noisy OOL measurement of CEO-stabilised thin-disk laser . . . . .	51
3.6	Set-up drawing of enhancement cavity seeded by MOPA system . . . . .	53
3.7	MOPA CEO stability characterisation for different means of compression . . . . .	54
3.8	Experimental layout for fibre amplifier CEO noise comparison . . . . .	56
3.9	Phase difference of CEO signals before and after main fibre amplifiers . . . . .	56

---

3.10 Comparison of EC lock parameters with and without CEO lock . . . . .	57
4.1 General layout of millijoule CPA and subsequent CEP measurement . . . . .	60
4.2 24-hour CEP data of 2 mJ CPA . . . . .	63
4.3 24-hour CEP data of 10 kHz CPA . . . . .	65
4.4 Set-up for mJ pulse CEP detection & correction at 10 kHz repetition rate . . . . .	69
4.5 Every-single-shot characterisation of slow feed-back loop performance . . . . .	70
4.6 RF phase shifter voltage-to-phase characteristics . . . . .	72
4.7 Arbitrary CEP jumps from one shot to the next in kHz, mJ pulses . . . . .	72
4.8 Step response of fast amplifier feed-back CEP correction . . . . .	73
4.9 98 mrad residual CEP noise in a mJ-class amplifier . . . . .	74
4.10 CEP time domain comparison: open vs. fast loop (IL/OOL) . . . . .	75
4.11 Experimental layout of the ISI technique . . . . .	79
4.12 Characterisation of ISI technique . . . . .	81
4.13 Fourier analysis of CEP noise in pressure gradient HFC . . . . .	82
4.14 Fourier analysis of CEP noise in static pressure HFC . . . . .	83
4.15 Comparison of HHG spectra obtained with CEP loop closed before and after HFC	86

## Bibliography

- [Ado11] D. Adolph, A. M. Sayler, T. Rathje, K. Rühle, and G. G. Paulus. *Improved carrier-envelope phase locking of intense few-cycle laser pulses using above-threshold ionization*. Opt. Lett. **36** (18), pp. 3639–3641 (2011). (cited on pages 72 and 76)
- [Agr08] G. P. Agrawal. *Applications of Nonlinear Fiber Optics*. Academic Press (2008). (cited on page 50)
- [And11a] A. Anderson, F. Lücking, T. Prikoszovits, M. Hofer, Z. Cheng, C. Neacsu, M. Scharrer, S. Rammler, P. Russell, G. Tempea, and A. Assion. *Multi-mJ carrier envelope phase stabilized few-cycle pulses generated by a tabletop laser system*. Appl. Phys. B **103**, pp. 531–536 (2011). (cited on page 66)
- [And11b] A. Anderson, F. Lücking, T. Prikoszovitz, M. Hofer, Z. Cheng, T. Le, C. C. Neacsu, G. Tempea, and A. Assion. *Tabletop generation of carrier envelope phase stabilized multi-mJ few-cycle pulses*. In *CLEO:2011 - Laser Applications to Photonic Applications*, p. CWG6. Optical Society of America (2011).
- [Apo00] A. Apolonski, A. Poppe, G. Tempea, C. Spielmann, T. Udem, R. Holzwarth, T. W. Hänsch, and F. Krausz. *Controlling the phase evolution of few-cycle light pulses*. Phys. Rev. Lett. **85**, pp. 740–743 (2000). (cited on page 9)
- [Bal02] A. Baltuška, T. Fuji, and T. Kobayashi. *Controlling the carrier-envelope phase of ultrashort light pulses with optical parametric amplifiers*. Phys. Rev. Lett. **88**, p. 133901 (2002). (cited on page 11)
- [Bal14] T. Balčiūnas, T. Flöry, A. Baltuška, T. Stanislauskas, R. Antipenkov, A. Varanavičius, and G. Steinmeyer. *Direct carrier-envelope phase control of an amplified laser system*. Opt. Lett. **39** (6), pp. 1669–1672 (2014). (cited on page 58)
- [Bir97] T. A. Birks, J. C. Knight, and P. S. Russell. *Endlessly single-mode photonic crystal fiber*. Opt. Lett. **22** (13), pp. 961–963 (1997). (cited on page 44)
- [Boh98] A. de Bohan, P. Antoine, D. B. Milošević, and B. Piraux. *Phase-dependent harmonic emission with ultrashort laser pulses*. Phys. Rev. Lett. **81**, pp. 1837–1840 (1998). (cited on page 2)

- [Böh14] F. Böhle, M. Kretschmar, A. Jullien, M. Kovacs, M. Miranda, R. Romero, H. Crespo, P. Simon, R. Lopez-Martens, and T. Nagy. *Generation of 3-mJ, 4-fs CEP-stable pulses by long stretched flexible hollow fibers*. In *Research in Optical Sciences: Postdeadline Papers*, p. HW5C.2. Optical Society of America (2014). (cited on page 76)
- [Bor11] B. Borchers, S. Koke, A. Husakou, J. Herrmann, and G. Steinmeyer. *Carrier-envelope phase stabilization with sub-10 as residual timing jitter*. *Opt. Lett.* **36** (21), pp. 4146–4148 (2011). (cited on pages 18 and 33)
- [Bor13] B. Borchers, M. Mero, and G. Steinmeyer. *Acoustic frequency combs for unconditionally stable long-term carrier-envelope phase stabilization*. In *CLEO: 2013*, p. CTh4M.2. Optical Society of America (2013). (cited on page 35)
- [Bor14a] B. Borchers, A. Anderson, and G. Steinmeyer. *On the role of shot noise in carrier-envelope phase stabilization*. *Laser & Photonics Reviews* pp. n/a–n/a (2014). (cited on pages 33 and 66)
- [Bor14b] B. Borchers, F. Lücking, and G. Steinmeyer. *Acoustic frequency combs for carrier-envelope phase stabilization*. *Opt. Lett.* **39** (3), pp. 544–547 (2014). (cited on page 35)
- [Boy09] R. W. Boyd, S. G. Lukishova, and Y. R. Shen (editors). *Self-focusing: Past and Present*. Springer (2009). (cited on page 77)
- [Bro99] A. Brodeur and S. L. Chin. *Ultrafast white-light continuum generation and self-focusing in transparent condensed media*. *J. Opt. Soc. Am. B* **16** (4), pp. 637–650 (1999). (cited on page 10)
- [Can09] L. Canova, X. Chen, A. Trisorio, A. Jullien, A. Assion, G. Tempea, N. Forget, T. Oksenhendler, and R. Lopez-Martens. *Carrier-envelope phase stabilization and control using a transmission grating compressor and an AOPDF*. *Opt. Lett.* **34** (9), pp. 1333–1335 (2009). (cited on pages 71 and 72)
- [Car92] G. E. Carlson. *Signal and Linear Systems Analysis*. Houghton Mifflin (1992). (cited on page 91)
- [Car14] H. Carstens, N. Lilienfein, S. Holzberger, C. Jocher, T. Eidam, J. Limpert, A. Tünnermann, J. Weitenberg, D. C. Yost, A. Alghamdi, Z. Alahmed, A. Azzeer, A. Apolonski, E. Fill, F. Krausz, and I. Pupeza. *Megawatt-scale average-power ultrashort pulses in an enhancement cavity*. *Opt. Lett.* **39** (9), pp. 2595–2598 (2014). (cited on page 46)
- [Che09] X. Chen, A. Jullien, A. Malvache, L. Canova, A. Borot, A. Trisorio, C. G. Durfee, and R. Lopez-Martens. *Generation of 4.3 fs, 1 mJ laser pulses via compression of circularly polarized pulses in a gas-filled hollow-core fiber*. *Opt. Lett.* **34** (10), pp. 1588–1590 (2009). (cited on page 84)

- [Che11] X. Chen, A. Malvache, A. Ricci, A. Jullien, and R. Lopez-Martens. *Efficient hollow fiber compression scheme for generating multi-mJ, carrier-envelope phase stable, sub-5 fs pulses*. *Laser Physics* **21**, pp. 198–201 (2011). (cited on page 84)
- [Chi14] M. Chini, K. Zhao, and Z. Chang. *The generation, characterization and applications of broadband isolated attosecond pulses*. *Nature Photonics* **8** (3), pp. 178–186 (2014). (cited on page 45)
- [Cor93] P. B. Corkum. *Plasma perspective on strong field multiphoton ionization*. *Phys. Rev. Lett.* **71**, pp. 1994–1997 (1993). (cited on page 2)
- [Cor07] P. B. Corkum and F. Krausz. *Attosecond science*. *Nature Physics* **3** (6), p. 381–387 (2007). (cited on pages 2 and 3)
- [Cre08] H. M. Crespo, J. R. Birge, E. L. Falcão-Filho, M. Y. Sander, A. Benedick, and F. X. Kärtner. *Nonintrusive phase stabilization of sub-two-cycle pulses from a prismless octave-spanning Ti:sapphire laser*. *Opt. Lett.* **33** (8), pp. 833–835 (2008). (cited on page 22)
- [Cro11] V. Crozatier, N. Forget, and T. Oksenhendler. *Towards single shot carrier-envelope phase stabilization for multi kHz ultrafast amplifiers*. In *CLEO/Europe and EQEC 2011 Conference Digest*, pp. CF1–4. Optical Society of America (2011). (cited on page 68)
- [Die13] A. Diebold, F. Emaury, C. Schriber, M. Golling, C. J. Saraceno, T. Südmeyer, and U. Keller. *Sesam mode-locked Yb:CaGdAlO<sub>4</sub> thin disk laser with 62 fs pulse generation*. *Opt. Lett.* **38**, pp. 3842–3845 (2013). (cited on page 45)
- [Dre83] R. Drever, J. Hall, F. Kowalski, J. Hough, G. Ford, A. Munley, and H. Ward. *Laser phase and frequency stabilization using an optical resonator*. *Applied Physics B* **31** (2), pp. 97–105 (1983). (cited on page 53)
- [Eck78] J. N. Eckstein. *High resolution spectroscopy using multiple coherent interactions*. Ph.D. thesis, Department of Physics, Stanford University (1978). (cited on pages 1 and 7)
- [Eid08] T. Eidam, F. Röser, O. Schmidt, J. Limpert, and A. Tünnermann. *57 W, 27 fs pulses from a fiber laser system using nonlinear compression*. *Applied Physics B* **92** (1), pp. 9–12 (2008). (cited on page 52)
- [Eid10] T. Eidam, S. Hanf, E. Seise, T. V. Andersen, T. Gabler, C. Wirth, T. Schreiber, J. Limpert, and A. Tünnermann. *Femtosecond fiber CPA system emitting 830 W average output power*. *Opt. Lett.* **35** (2), pp. 94–96 (2010). (cited on page 44)
- [Ema13] F. Emaury, C. F. Duting, C. J. Saraceno, M. Trant, O. H. Heckl, Y. Y. Wang, C. Schriber, F. Jerome, T. Südmeyer, F. Benabid, and U. Keller. *Beam delivery and pulse compression to sub-50 fs of a modelocked thin-disk laser in a gas-filled Kagome-type HC-PCF fiber*. *Opt. Express* **21** (4), pp. 4986–4994 (2013). (cited on page 46)

- [Fat12] H. Fattahi, C. Y. Teisset, O. Pronin, A. Sugita, R. Graf, V. Pervak, X. Gu, T. Metzger, Z. Major, F. Krausz, and A. Apolonski. *Pump-seed synchronization for MHz repetition rate, high-power optical parametric chirped pulse amplification*. *Opt. Express* **20** (9), pp. 9833–9840 (2012). (cited on page 76)
- [Fen13] C. Feng, J.-F. Hergott, P.-M. Paul, X. Chen, O. Tcherbakoff, M. Comte, O. Gobert, M. Reduzzi, F. Calegari, C. Manzoni, M. Nisoli, and G. Sansone. *Complete analog control of the carrier-envelope-phase of a high-power laser amplifier*. *Opt. Express* **21** (21), pp. 25248–25256 (2013). (cited on page 72)
- [Fey60] R. P. Feynman. *There's plenty of room at the bottom*. *Engineering and Science*, February Issue, pp. 22–36 (1960). (cited on page 1)
- [FF10] E. L. Falcão-Filho, C.-J. Lai, K.-H. Hong, V.-M. Gkortsas, S.-W. Huang, L.-J. Chen, and F. X. Kärtner. *Scaling of high-order harmonic efficiencies with visible wavelength drivers: A route to efficient extreme ultraviolet sources*. *Applied Physics Letters* **97** (6), 061107 (2010). (cited on page 3)
- [For09] N. Forget, L. Canova, X. Chen, A. Jullien, and R. Lopez-Martens. *Closed-loop carrier-envelope phase stabilization with an acousto-optic programmable dispersive filter*. *Opt. Lett.* **34** (23), pp. 3647–3649 (2009). (cited on page 71)
- [For11] T. Fordell, M. Miranda, C. L. Arnold, and A. L'Huillier. *High-speed carrier-envelope phase drift detection of amplified laser pulses*. *Opt. Express* **19** (24), pp. 23652–23657 (2011). (cited on page 68)
- [Fuj05] T. Fuji, J. Rauschenberger, A. Apolonski, V. S. Yakovlev, G. Tempea, T. Udem, C. Gohle, T. W. Hänsch, W. Lehnert, M. Scherer, and F. Krausz. *Monolithic carrier-envelope phase-stabilization scheme*. *Opt. Lett.* **30** (3), pp. 332–334 (2005). (cited on page 22)
- [Gan11] T. Ganz, V. Pervak, A. Apolonski, and P. Baum. *16 fs, 350 nJ pulses at 5 MHz repetition rate delivered by chirped pulse compression in fibers*. *Opt. Lett.* **36** (7), pp. 1107–1109 (2011). (cited on pages 46 and 49)
- [Gar79] F. M. Gardner. *Phaselock Techniques*. Wiley (New York), 2<sup>nd</sup> edition (1979). (cited on pages 12 and 26)
- [Gen07] G. Genty, S. Coen, and J. M. Dudley. *Fiber supercontinuum sources (Invited)*. *J. Opt. Soc. Am. B* **24** (8), pp. 1771–1785 (2007). (cited on pages 9, 44, and 50)
- [Ghi05] S. Ghimire, B. Shan, C. Wang, and Z. Chang. *High-energy 6.2-fs pulses for attosecond pulse generation*. *Laser physics* **15** (6), p. 838–842 (2005). (cited on page 84)
- [Gie94] A. Giesen, H. Hügel, A. Voss, K. Wittig, U. Brauch, and H. Opower. *Scalable concept for diode-pumped high-power solid-state lasers*. *Appl. Phys. B* **58**, p. 363 (1994). (cited on page 44)

- [Gob11] O. Gobert, P. Paul, J. Hergott, O. Tcherbakoff, F. Lepetit, P. d'Oliveira, F. Viala, and M. Comte. *Carrier-envelope phase control using linear electro-optic effect*. *Opt. Express* **19** (6), pp. 5410–5418 (2011). (cited on page 71)
- [God13] T. Godin, B. Wetzell, T. Sylvestre, L. Larger, A. Kudlinski, A. Mussot, A. B. Salem, M. Zghal, G. Genty, F. Dias, and J. M. Dudley. *Real time noise and wavelength correlations in octave-spanning supercontinuum generation*. *Opt. Express* **21** (15), pp. 18452–18460 (2013). (cited on page 51)
- [Goh05a] C. Gohle, J. Rauschenberger, T. Fuji, T. Udem, A. Apolonski, F. Krausz, and T. W. Hänsch. *Carrier envelope phase noise in stabilized amplifier systems*. *Opt. Lett.* **30** (18), pp. 2487–2489 (2005). (cited on page 67)
- [Goh05b] C. Gohle, T. Udem, M. Herrmann, J. Rauschenberger, R. Holzwarth, H. A. Schuessler, F. Krausz, and T. W. Hänsch. *A frequency comb in the extreme ultraviolet*. *Nature* **436** (7048), pp. 234–237 (2005). (cited on page 46)
- [Gou04] E. Goulielmakis, M. Uiberacker, R. Kienberger, A. Baltuska, V. Yakovlev, A. Scrinzi, T. Westerwalbesloh, U. Kleineberg, U. Heinzmann, M. Drescher, and F. Krausz. *Direct measurement of light waves*. *Science* **305** (5688), pp. 1267–1269 (2004). (cited on page 2)
- [Gre09] C. Grebing, S. Koke, B. Manschwetus, and G. Steinmeyer. *Performance comparison of interferometer topologies for carrier-envelope phase detection*. *Appl. Phys. B* **95** (81), pp. 81–84 (2009). (cited on pages 9, 18, 22, 37, and 50)
- [Gri82] D. Grischkowsky and A. C. Balant. *Optical pulse compression based on enhanced frequency chirping*. *Applied Physics Letters* **41** (1), pp. 1–3 (1982). (cited on page 47)
- [Hal84] J. L. Hall and T. W. Hänsch. *External dye-laser frequency stabilizer*. *Opt. Lett.* **9** (11), pp. 502–504 (1984). (cited on page 15)
- [Hän06] T. W. Hänsch. *Nobel lecture: Passion for precision*. *Rev. Mod. Phys.* **78**, pp. 1297–1309 (2006). (cited on page 1)
- [Har64] L. E. Hargrove, R. L. Fork, and M. A. Pollack. *Locking of he–ne laser modes induced by synchronous intracavity modulation*. *Applied Physics Letters* **5** (1), pp. 4–5 (1964). (cited on pages 1 and 5)
- [Hel03] F. Helbing, G. Steinmeyer, and U. Keller. *Carrier-envelope offset phase-locking with attosecond timing jitter*. *Selected Topics in Quantum Electronics, IEEE Journal of* **9** (4), pp. 1030–1040 (2003). (cited on page 7)
- [Hen01] M. Hentschel, R. Kienberger, C. Spielmann, G. A. Reider, N. Milosevic, T. Brabec, P. Corkum, U. Heinzmann, M. Drescher, and F. Krausz. *Attosecond metrology*. *Nature* **414** (6863), pp. 509–513 (2001). (cited on page 2)

- [Her11] J.-F. Hergott, O. Tcherbakoff, P.-M. Paul, P. Demengeot, M. Perdrix, F. Lepetit, D. Garzella, D. Guillaumet, M. Comte, P. D. Oliveira, and O. Gobert. *Carrier-envelope phase stabilization of a 20 W, grating based, chirped-pulse amplified laser, using electro-optic effect in a LiNbO<sub>3</sub> crystal*. *Opt. Express* **19** (21), pp. 19935–19941 (2011). (cited on page 67)
- [Hit14] K. Hitachi, A. Ishizawa, T. Nishikawa, M. Asobe, and T. Sogawa. *Carrier-envelope offset locking with a 2f-to-3f self-referencing interferometer using a dual-pitch PPLN ridge waveguide*. *Opt. Express* **22** (2), pp. 1629–1635 (2014). (cited on page 22)
- [Jon00] D. J. Jones, S. A. Diddams, J. K. Ranka, A. Stentz, R. S. Windeler, J. L. Hall, and S. T. Cundiff. *Carrier-envelope phase control of femtosecond mode-locked lasers and direct optical frequency synthesis*. *Science* **288** (5466), pp. 635–639 (2000). (cited on page 12)
- [Jon01] R. J. Jones and J.-C. Diels. *Stabilization of femtosecond lasers for optical frequency metrology and direct optical to radio frequency synthesis*. *Phys. Rev. Lett.* **86** (15), pp. 3288–3291 (2001). (cited on page 15)
- [Jon05] R. J. Jones, K. D. Moll, M. J. Thorpe, and J. Ye. *Phase-coherent frequency combs in the vacuum ultraviolet via high-harmonic generation inside a femtosecond enhancement cavity*. *Phys. Rev. Lett.* **94**, p. 193201 (2005). (cited on page 46)
- [Kak01] M. Kakehata, H. Takada, Y. Kobayashi, K. Torizuka, Y. Fujihira, T. Homma, and H. Takahashi. *Single-shot measurement of carrier-envelope phase changes by spectral interferometry*. *Opt. Lett.* **26** (18), pp. 1436–1438 (2001). (cited on pages 9, 40, 61, and 68)
- [Kak04] M. Kakehata, H. Takada, Y. Kobayashi, K. Torizuka, H. Takamiya, K. Nishijima, T. Homma, H. Takahashi, K. Okubo, S. Nakamura, and Y. Koyamada. *Carrier-envelope-phase stabilized chirped-pulse amplification system scalable to higher pulse energies*. *Opt. Express* **12** (10), pp. 2070–2080 (2004). (cited on pages 36 and 67)
- [Kan83] T. Kane, R. Eckardt, and R. Byer. *Reduced thermal focusing and birefringence in zig-zag slab geometry crystalline lasers*. *Quantum Electronics, IEEE Journal of* **19** (9), pp. 1351–1354 (1983). (cited on page 44)
- [Kim10] E. B. Kim, J. H. Lee, W. K. Lee, T. T. Luu, and C. H. Nam. *Long-term maintenance of the carrier-envelope phase coherence of a femtosecond laser*. *Opt. Express* **18** (25), pp. 26365–26372 (2010). (cited on page 35)
- [Kle13] A. Klenke, S. Breitkopf, M. Kienel, T. Gottschall, T. Eidam, S. Hädrich, J. Rothhardt, J. Limpert, and A. Tünnermann. *530 W, 1.3 mJ, four-channel coherently combined femtosecond fiber chirped-pulse amplification system*. *Opt. Lett.* **38** (13), pp. 2283–2285 (2013). (cited on page 76)

- [Kli13] N. G. Kling, K. J. Betsch, M. Zohrabi, S. Zeng, F. Anis, U. Ablikim, B. Jochim, Z. Wang, M. Kübel, M. F. Kling, K. D. Carnes, B. D. Esry, and I. Ben-Itzhak. *Carrier-envelope phase control over pathway interference in strong-field dissociation of  $\text{H}_2^+$* . Phys. Rev. Lett. **111**, p. 163004 (2013). (cited on page 13)
- [Kok08] S. Koke, C. Grebing, B. Manschwetus, and G. Steinmeyer. *Fast  $f$ -to- $2f$  interferometer for a direct measurement of the carrier-envelope phase drift of ultrashort amplified laser pulses*. Opt. Lett. **33** (21), pp. 2545–2547 (2008). (cited on page 68)
- [Kok10] S. Koke, C. Grebing, H. Frei, A. Anderson, A. Assion, and G. Steinmeyer. *Direct frequency comb synthesis with arbitrary offset and shot-noise-limited phase noise*. Nature Photonics **4**, pp. 462–465 (2010). (cited on pages 15, 18, 24, 25, and 32)
- [Kok11] S. Koke, A. Anderson, H. Frei, A. Assion, and G. Steinmeyer. *Noise performance of a feed-forward scheme for carrier-envelope phase stabilization*. Applied Physics B: Lasers and Optics **104**, pp. 799–804 (2011). (cited on pages 18 and 39)
- [Kok12] S. Koke. *Fundamental Limitations in the Measurement and Stabilization of the Carrier-Envelope Phase of Ultrashort Laser Pulses*. Ph.D. thesis, Mathematisch-Naturwissenschaftliche Fakultät I, Humboldt-Universität Berlin (2012). (cited on pages 19, 25, and 91)
- [Kre11] M. Kremer, C. Hofrichter, B. Fischer, V. Sharma, N. Camus, T. Pfeifer, R. Moshhammer, and J. Ullrich. *Minimizing dispersive distortions in carrier-envelope phase sweeping with glass wedges*. Opt. Lett. **36** (8), pp. 1455–1457 (2011). (cited on page 71)
- [Krü11] M. Krüger, M. Schenk, and P. Hommelhoff. *Attosecond control of electrons emitted from a nanoscale metal tip*. Nature **475**, p. 81 (2011). (cited on page 12)
- [Küb13] M. Kübel, N. G. Kling, K. J. Betsch, N. Camus, A. Kaldun, U. Kleineberg, I. Ben-Itzhak, R. R. Jones, G. G. Paulus, T. Pfeifer, J. Ullrich, R. Moshhammer, M. F. Kling, and B. Bergues. *Nonsequential double ionization of  $\text{N}_2$  in a near-single-cycle laser pulse*. Phys. Rev. A **88**, p. 023418 (2013). (cited on page 62)
- [Lam08] G. Lambert, T. Hara, D. Garzella, T. Tanikawa, M. Labat, B. Carre, H. Kitamura, T. Shintake, M. Bougeard, S. Inoue, Y. Tanaka, P. Salieres, H. Merdji, O. Chubar, O. Gobert, K. Tahara, and M.-E. Couprie. *Injection of harmonics generated in gas in a free-electron laser providing intense and coherent extreme-ultraviolet light*. Nature Physics **4**, pp. 269–300 (2008). (cited on page 3)
- [Lee05] Y. S. Lee, J. Sung, C. Nam, T. Yu, and K.-H. Hong. *Novel method for carrier-envelope phase stabilization of femtosecond laser pulses*. Opt. Express **13** (8), pp. 2969–2976 (2005). (cited on page 12)
- [L’H93] A. L’Huillier and P. Balcou. *High-order harmonic generation in rare gases with a 1-ps 1053-nm laser*. Phys. Rev. Lett. **70**, pp. 774–777 (1993). (cited on page 45)

- [Li08] C. Li, H. Mashiko, H. Wang, E. Moon, S. Gilbertson, and Z. Chang. *Carrier-envelope phase stabilization by controlling compressor grating separation*. *Applied Physics Letters* **92** (19), 191114 (2008). (cited on page 67)
- [Li09] C. Li, E. Moon, H. Mashiko, H. Wang, C. M. Nakamura, J. Tackett, and Z. Chang. *Mechanism of phase-energy coupling in  $f$ -to- $2f$  interferometry*. *Appl. Opt.* **48** (7), pp. 1303–1307 (2009). (cited on page 74)
- [Lin04] F. Lindner, G. G. Paulus, H. Walther, A. Baltuška, E. Goulielmakis, M. Lezius, and F. Krausz. *Gouy phase shift for few-cycle laser pulses*. *Phys. Rev. Lett.* **92**, p. 113001 (2004). (cited on page 53)
- [Lüc11a] F. Lücking, A. Assion, A. Apolonski, and F. Krausz. *Long-term CEP-stable few-cycle pulses using the feed-forward method in an all-monolithic setup (Post-deadline)*. In *CLEO/Europe and EQEC 2011 Conference Digest*, p. PDB.2. Optical Society of America (2011).
- [Lüc11b] F. Lücking, A. Assion, A. Apolonskiy, F. Krausz, and G. Steinmeyer. *Long-term CEP-stable few-cycle pulses using the feed-forward method*. In *8th International Conference on Ultrafast Optics, Monterey, California, USA* (2011).
- [Lüc12a] F. Lücking, A. Assion, A. Apolonski, F. Krausz, and G. Steinmeyer. *Long-term carrier-envelope-phase-stable few-cycle pulses by use of the feed-forward method*. *Opt. Lett.* **37** (11), pp. 2076–2078 (2012). (cited on page 27)
- [Lüc12b] F. Lücking, O. Pronin, J. Brons, A. Assion, A. Apolonski, and F. Krausz. *Reliable carrier-envelope phase control for current and future attosecond experiments (Invited)*. In *Conference on Lasers and Electro-Optics 2012*, p. CW1D.3. Optical Society of America (2012).
- [Lüc13] F. Lücking, A. Apolonskiy, A. Assion, and F. Krausz. *24-hour constant waveform operation of a Ti:sapphire amplifier*. In *9th International Conference on Ultrafast Optics, Davos, Switzerland* (2013).
- [Lüc14a] F. Lücking, V. Crozatier, and A. Assion. *Arbitrary carrier-envelope phase control in a 10 kHz, mJ-class amplifier*. In *Conference on Lasers and Electro-Optics 2014*, p. STh3E.2. Optical Society of America (2014).
- [Lüc14b] F. Lücking, V. Crozatier, and A. Assion. *High-speed carrier-envelope phase control in a 10 kHz, mJ-class amplifier*. In *Ultrafast Phenomena 2014*, p. 09.Wed.P3.52. Optical Society of America (2014).
- [Lüc14c] F. Lücking, V. Crozatier, N. Forget, A. Assion, and F. Krausz. *Approaching the limits of carrier-envelope phase stability in a millijoule-class amplifier*. *Opt. Lett.* **39** (13), pp. 3884–3887 (2014). (cited on page 66)

- [Lüc14d] F. Lücking, A. Trabattoni, S. Anumula, G. Sansone, F. Calegari, M. Nisoli, T. Oksenhendler, and G. Tempea. *Direct measurement of nonlinear carrier-envelope phase changes in hollow fiber compression*. In *Conference on Lasers and Electro-Optics 2014*, p. SW1E.2. Optical Society of America (2014).
- [Lüc14e] F. Lücking, A. Trabattoni, S. Anumula, G. Sansone, F. Calegari, M. Nisoli, T. Oksenhendler, and G. Tempea. *In-situ measurement of intensity-dependent carrier-envelope phase changes in hollow fiber compression*. In *Ultrafast Phenomena 2014*, p. 08.Tue.P2.52. Optical Society of America (2014).
- [Lüc14f] F. Lücking, A. Trabattoni, S. Anumula, G. Sansone, F. Calegari, M. Nisoli, T. Oksenhendler, and G. Tempea. *In situ measurement of nonlinear carrier-envelope phase changes in hollow fiber compression*. *Opt. Lett.* **39** (8), pp. 2302–2305 (2014). (cited on page 77)
- [Mai60] T. H. Maiman. *Stimulated optical radiation in ruby*. *Nature* **187**, pp. 493–494 (1960). (cited on page 1)
- [McD67] O. P. McDuff and S. E. Harris. *Nonlinear theory of the internally loss-modulated laser*. *IEEE Journal of Quantum Electronics* **3**, p. 101 (1967). (cited on page 7)
- [Mer01] G. Merziger, G. Mühlbach, and D. W. und Thomas Wirth (editors). *Formeln und Hilfen zur höheren Mathematik*. Binomi Verlag (Springer) (2001). (cited on page 67)
- [Mol06] K. D. Moll, R. J. Jones, and J. Ye. *Output coupling methods for cavity-based high-harmonic generation*. *Opt. Express* **14** (18), pp. 8189–8197 (2006). (cited on page 47)
- [Moo14] R. O. Moore. *Trade-off between linewidth and slip rate in a mode-locked laser model*. *Opt. Lett.* **39** (10), pp. 3042–3045 (2014). (cited on page 12)
- [Mor99] U. Morgner, F. X. Kärtner, S. H. Cho, Y. Chen, H. A. Haus, J. G. Fujimoto, E. P. Ippen, V. Scheuer, G. Angelow, and T. Tschudi. *Sub-two-cycle pulses from a kerr-lens mode-locked ti:sapphire laser*. *Opt. Lett.* **24** (6), pp. 411–413 (1999). (cited on page 5)
- [Mou10] A. Moulet, S. Grabielle, C. Cornaggia, N. Forget, and T. Oksenhendler. *Single-shot, high-dynamic-range measurement of sub-15 fs pulses by self-referenced spectral interferometry*. *Opt. Lett.* **35** (22), pp. 3856–3858 (2010). (cited on page 68)
- [Müc05] O. Mücke, R. Ell, A. Winter, J.-W. Kim, J. Birge, L. Matos, and F. Kärtner. *Self-referenced 200 MHz octave-spanning Ti:sapphire laser with 50 attosecond carrier-envelope phase jitter*. *Opt. Express* **13** (13), pp. 5163–5169 (2005). (cited on page 22)
- [Neu08] J. Neuhaus. *Passively mode-locked Yb:YAG thin-disk laser with active multipass geometry*. Ph.D. thesis, Center for Applied Photonics, University of Konstanz (2008). (cited on page 45)

- [Nis96] M. Nisoli, S. De Silvestri, and O. Svelto. *Generation of high energy 10 fs pulses by a new pulse compression technique*. Applied Physics Letters **68** (20), pp. 2793–2795 (1996). (cited on page 76)
- [Nis97] M. Nisoli, S. D. Silvestri, O. Svelto, R. Szipöcs, K. Ferencz, C. Spielmann, S. Sartania, and F. Krausz. *Compression of high-energy laser pulses below 5 fs*. Opt. Lett. **22** (8), pp. 522–524 (1997). (cited on page 76)
- [Nis03] M. Nisoli, G. Sansone, S. Stagira, S. De Silvestri, C. Vozzi, M. Pascolini, L. Poletto, P. Villorresi, and G. Tondello. *Effects of carrier-envelope phase differences of few-optical-cycle light pulses in single-shot high-order-harmonic spectra*. Phys. Rev. Lett. **91**, p. 213905 (2003). (cited on pages 2 and 84)
- [Oke13] W. A. Okell, T. Witting, D. Fabris, D. Austin, M. Bocoum, F. Frank, A. Ricci, A. Jullien, D. Walke, J. P. Marangos, R. Lopez-Martens, and J. W. G. Tisch. *Carrier-envelope phase stability of hollow fibers used for high-energy few-cycle pulse generation*. Opt. Lett. **38** (19), pp. 3918–3921 (2013). (cited on pages 76 and 84)
- [Oks10] T. Oksenhendler, S. Coudreau, N. Forget, V. Crozatier, S. Grabielle, R. Herzog, O. Gobert, and D. Kaplan. *Self-referenced spectral interferometry*. Applied Physics B **99** (1-2), pp. 7–12 (2010). (cited on page 68)
- [Par11] I.-Y. Park, S. Kim, J. Choi, D.-H. Lee, Y.-J. Kim, M. F. Kling, M. I. Stockman, and S.-W. Kim. *Plasmonic generation of ultrashort extreme-ultraviolet light pulses*. Nature Photonics **5**, pp. 677–681 (2011). (cited on page 12)
- [Pau01] G. G. Paulus, F. Grasbon, H. Walther, P. Villorresi, M. Nisoli, S. Stagira, E. Priori, and S. De Silvestri. *Absolute-phase phenomena in photoionization with few-cycle laser pulses*. Nature **414** (6860), p. 182–184 (2001). (cited on page 68)
- [Pau03] G. G. Paulus, F. Lindner, H. Walther, A. Baltuška, E. Goulielmakis, M. Lezius, and F. Krausz. *Measurement of the phase of few-cycle laser pulses*. Phys. Rev. Lett. **91**, p. 253004 (2003). (cited on pages 10 and 68)
- [PC14] T. Paasch-Colberg, A. Schiffrin, N. Karpowicz, S. Kruchinin, O. Sağlam, S. Keiber, O. Razskazovskaya, S. Mühlbrandt, A. Alnaser, M. Kübel, V. Apalkov, D. Gerster, J. Reichert, T. Wittmann, J. V. Barth, M. I. Stockman, R. Ernstorfer, V. S. Yakovlev, R. Kienberger, and F. Krausz. *Solid-state light-phase detector*. Nature Photonics (2014). (cited on page 10)
- [Pek11] S. Pekarek, T. Südmeyer, S. Lecomte, S. Kundermann, J. M. Dudley, and U. Keller. *Self-referenceable frequency comb from a gigahertz diode-pumped solid-state laser*. Opt. Express **19** (17), pp. 16491–16497 (2011). (cited on page 50)
- [Pop01] A. Poppe, R. Holzwarth, A. Apolonski, G. Tempea, C. Spielmann, T. Hänsch, and F. Krausz. *Few-cycle optical waveform synthesis*. Appl. Phys. B **72**, pp. 373–376 (2001). (cited on page 12)

- [Pro11a] O. Pronin, J. Brons, C. Grasse, V. Pervak, G. Boehm, M.-C. Amann, V. L. Kalashnikov, A. Apolonski, and F. Krausz. *High-power 200 fs Kerr-lens mode-locked Yb:YAG thin-disk oscillator*. *Opt. Lett.* **36**, pp. 4746–4748 (2011). (cited on page 47)
- [Pro11b] O. Pronin, V. Pervak, E. Fill, J. Rauschenberger, F. Krausz, and A. Apolonski. *Ultrabroadband efficient intracavity XUV output coupler*. *Opt. Express* **19** (11), pp. 10232–10240 (2011). (cited on page 47)
- [Pro12a] O. Pronin. *Towards a compact thin-disk-based femtosecond XUV source*. Ph.D. thesis, Fakultät für Experimentalphysik, Ludwig-Maximilians-Universität München (2012). (cited on pages 45 and 48)
- [Pro12b] O. Pronin, J. Brons, C. Grasse, V. Pervak, G. Boehm, M.-C. Amann, A. Apolonski, V. L. Kalashnikov, and F. Krausz. *High-power Kerr-lens mode-locked Yb:YAG thin-disk oscillator in the positive dispersion regime*. *Opt. Lett.* **37** (17), pp. 3543–3545 (2012). (cited on page 47)
- [Pro13] O. Pronin, M. Seidel, J. Brons, F. Lücking, V. Pervak, A. Apolonski, T. Udem, and F. Krausz. *Carrier-envelope phase stabilized thin-disk oscillator*. In *Advanced Solid-State Lasers Congress*, p. AF3A.5. Optical Society of America (2013).
- [Pro14] O. Pronin, M. Seidel, F. Lücking, J. Brons, V. Pervak, A. Apolonski, T. Udem, and F. Krausz. *Next-generation source of waveform-controlled light* (2014). Manuscript in preparation. (cited on pages 52 and 55)
- [Pup13] I. Pupeza, S. Holzberger, T. Eidam, H. Carstens, D. Esser, J. Weitenberg, P. Rußbüldt, J. Rauschenberger, J. Limpert, T. Udem, A. Tünnermann, T. W. Hänsch, A. Apolonski, F. Krausz, and E. Fill. *Compact high-repetition-rate source of coherent 100 eV radiation*. *Nature Photonics* **7** (8), pp. 608–612 (2013). (cited on pages 46 and 52)
- [Rau06] J. Rauschenberger, T. Fuji, M. Hentschel, A.-J. Verhoef, T. Udem, C. Gohle, T. W. Hänsch, and F. Krausz. *Carrier-envelope phase-stabilized amplifier system*. *Laser Physics Letters* **3** (1), pp. 37–42 (2006). (cited on page 67)
- [Rau09] S. Rausch, T. Binhammer, A. Harth, E. Schulz, M. Siegel, and U. Morgner. *Few-cycle oscillator pulse train with constant carrier-envelope phase and 65 as jitter*. *Opt. Express* **17** (22), pp. 20282–20290 (2009). (cited on pages 12 and 22)
- [Rei97] G. A. Reider. *Photonik – eine Einführung in die Grundlagen*. Springer (Wien/New York) (1997). (cited on pages 16 and 20)
- [Ric12] A. Ricci, A. Jullien, N. Forget, V. Crozatier, P. Tournois, and R. Lopez-Martens. *Grism compressor for carrier-envelope phase-stable millijoule-energy chirped pulse amplifier lasers featuring bulk material stretcher*. *Opt. Lett.* **37** (7), pp. 1196–1198 (2012). (cited on page 67)

- [Rus09] P. Russbuehdt, T. Mans, G. Rotarius, J. Weitenberg, H. D. Hoffmann, and R. Poprawe. *400W Yb:YAG innoslab fs-amplifier*. *Opt. Express* **17** (15), pp. 12230–12245 (2009). (cited on page 44)
- [San06] G. Sansone, E. Benedetti, F. Calegari, C. Vozzi, L. Avaldi, R. Flammini, L. Poletto, P. Villoresi, C. Altucci, R. Velotta, S. Stagira, S. De Silvestri, and M. Nisoli. *Isolated single-cycle attosecond pulses*. *Science* **314** (5798), pp. 443–446 (2006). (cited on page 85)
- [Sar14] C. J. Saraceno, F. Emaury, C. Schriber, M. Hoffmann, M. Golling, T. Südmeyer, and U. Keller. *Ultrafast thin-disk laser with 80  $\mu$ J pulse energy and 242 W of average power*. *Opt. Lett.* **39** (1), pp. 9–12 (2014). (cited on page 44)
- [Saw14] S. Sawai, A. Hosaka, H. Kawauchi, K. Hirose, and F. Kannari. *Demonstration of a Ti:sapphire mode-locked laser pumped directly with a green diode laser*. *Applied Physics Express* **7** (2), p. 022702 (2014). (cited on page 44)
- [Say11] A. M. Saylor, T. Rathje, W. Müller, K. Rühle, R. Kienberger, and G. G. Paulus. *Precise, real-time, every-single-shot, carrier-envelope phase measurement of ultrashort laser pulses*. *Opt. Lett.* **36** (1), pp. 1–3 (2011). (cited on page 68)
- [Sch04] M. Schätzel, F. Lindner, G. Paulus, H. Walther, E. Goulielmakis, A. Baltuška, M. Lezius, and F. Krausz. *Long-term stabilization of the carrier-envelope phase of few-cycle laser pulses*. *Applied Physics B* **79** (8), pp. 1021–1025 (2004). (cited on page 62)
- [Sch10] M. Schultze, M. Fieß, N. Karpowicz, J. Gagnon, M. Korbman, M. Hofstetter, S. Neppl, A. L. Cavalieri, Y. Komninos, T. Mercouris, C. A. Nicolaides, R. Pazourek, S. Nagele, J. Feist, J. Burgdörfer, A. M. Azzeer, R. Ernstorfer, R. Kienberger, U. Kleineberg, E. Goulielmakis, F. Krausz, and V. S. Yakovlev. *Delay in photoemission*. *Science* **328** (5986), pp. 1658–1662 (2010). (cited on pages 2 and 3)
- [Sch12] A. Schwarz, M. Ueffing, Y. Deng, X. Gu, H. Fattahi, T. Metzger, M. Ossiander, F. Krausz, and R. Kienberger. *Active stabilization for optically synchronized optical parametric chirped pulse amplification*. *Opt. Express* **20** (5), pp. 5557–5565 (2012). (cited on page 76)
- [Sch13] A. Schiffrin, T. Paasch-Colberg, N. Karpowicz, V. Apalkov, D. Gerster, S. Mühlbrandt, M. Korbman, J. Reichert, M. Schultze, S. Holzner, J. V. Barth, R. Kienberger, R. Ernstorfer, V. S. Yakovlev, M. I. Stockman, and F. Krausz. *Optical-field-induced current in dielectrics*. *Nature* **493**, pp. 70–74 (2013). (cited on pages 2 and 72)
- [Sei13] M. Seidel, O. Pronin, J. Brons, E. Fedulova, F. Lücking, I. Angelov, V. Pervak, A. Apolonski, and F. Krausz. *Approaching the few-cycle pulse regime with thin-disk oscillators*. In *Advanced Solid-State Lasers Congress*, p. ATu4A.7. Optical Society of America (2013).
- [Ser12] E. Seres, J. Seres, and C. Spielmann. *Extreme ultraviolet light source based on intracavity high harmonic generation in a mode locked ti:sapphire oscillator with 9.4 mhz repetition rate*. *Opt. Express* **20** (6), pp. 6185–6190 (2012). (cited on page 45)

- [Sie86] A. E. Siegman. *Lasers*. University Science Books (Mill Valley) (1986). (cited on pages 6, 47, 67, and 76)
- [Spe91] D. E. Spence, P. N. Kean, and W. Sibbett. *60-fsec pulse generation from a self-mode-locked Ti:sapphire laser*. *Opt. Lett.* **16** (1), pp. 42–44 (1991). (cited on page 5)
- [Ste13] G. Steinmeyer, B. Borchers, and F. Lücking. *Carrier-envelope phase stabilization*. In K. Yamanouchi and K. Midorikawa (editors), *Progress in Ultrafast Intense Laser Science*, volume 104 of *Springer Series in Chemical Physics*, pp. 89–110. Springer Berlin Heidelberg (2013). (cited on page 66)
- [Sti94] A. Stingl, R. Szipöcs, C. Spielmann, and F. Krausz. *Generation of 11-fs pulses from a Ti:sapphire laser without the use of prisms*. *Opt. Lett.* **19** (3), pp. 204–206 (1994). (cited on page 28)
- [Str85] D. Strickland and G. Mourou. *Compression of amplified chirped optical pulses*. *Optics Communications* **56** (3), pp. 219 – 221 (1985). (cited on pages 43 and 60)
- [Sud05] A. Suda, M. Hatayama, K. Nagasaka, and K. Midorikawa. *Generation of sub-10-fs, 5-mJ-optical pulses using a hollow fiber with a pressure gradient*. *Appl. Phys. Lett.* **86** (11), 111116 (2005). (cited on page 76)
- [Tak82] M. Takeda, H. Ina, and S. Kobayashi. *Fourier-transform method of fringe-pattern analysis for computer-based topography and interferometry*. *J. Opt. Soc. Am.* **72** (1), pp. 156–160 (1982). (cited on pages 10, 37, and 93)
- [Tei05] C. Teisset, N. Ishii, T. Fuji, T. Metzger, S. Köhler, R. Holzwarth, A. Baltuška, A. Zheltikov, and F. Krausz. *Soliton-based pump-seed synchronization for few-cycle OPCPA*. *Opt. Express* **13** (17), pp. 6550–6557 (2005). (cited on page 46)
- [Tel99] H. Telle, G. Steinmeyer, A. Dunlop, J. Stenger, D. Sutter, and U. Keller. *Carrier-envelope offset phase control: A novel concept for absolute optical frequency measurement and ultrashort pulse generation*. *Applied Physics B: Lasers and Optics* **69**, pp. 327–332 (1999). (cited on pages 1 and 8)
- [Tsa10] V. Tsatourian, H. Margolis, G. Marra, D. Reid, and P. Gill. *Common-path self-referencing interferometer for carrier-envelope offset frequency stabilization with enhanced noise immunity*. *Opt. Lett.* **35** (8), pp. 1209–1211 (2010). (cited on page 22)
- [Ude99] T. Udem, J. Reichert, R. Holzwarth, and T. W. Hänsch. *Absolute optical frequency measurement of the cesium D1 line with a mode-locked laser*. *Phys. Rev. Lett.* **82**, pp. 3568–3571 (1999). (cited on page 12)
- [Uib07] M. Uiberacker, T. Uphues, M. Schultze, A. J. Verhoef, V. Yakovlev, M. F. Kling, J. Rauschenberger, N. M. Kabachnik, H. Schröder, M. Lezius, K. L. Kompa, H.-G. Müller, M. J. J. Vrakking, S. Hendel, U. Kleineberg, U. Heinzmann, M. Drescher,

- and F. Krausz. *Attosecond real-time observation of electron tunnelling in atoms*. *Nature* **446** (7136), pp. 627–632 (2007). (cited on page 2)
- [Ver11] A. Vernaleken, J. Weitenberg, T. Sartorius, P. Russbueldt, W. Schneider, S. L. Stebbings, M. F. Kling, P. Hommelhoff, H.-D. Hoffmann, R. Poprawe, F. Krausz, T. W. Hänsch, and T. Udem. *Single-pass high-harmonic generation at 20.8 MHz repetition rate*. *Opt. Lett.* **36** (17), pp. 3428–3430 (2011). (cited on page 46)
- [Ver12] A. Vernaleken, B. Schmidt, M. Wolferstetter, T. W. Hänsch, R. Holzwarth, and P. Hommelhoff. *Carrier-envelope frequency stabilization of a Ti:sapphire oscillator using different pump lasers*. *Opt. Express* **20** (16), pp. 18387–18396 (2012). (cited on pages 39 and 67)
- [Ver14] A. Vernaleken, B. Schmidt, T. Hänsch, R. Holzwarth, and P. Hommelhoff. *Carrier-envelope frequency stabilization of a Ti:sapphire oscillator using different pump lasers: part II*. *Applied Physics B* pp. 1–7 (2014). (cited on pages 39 and 67)
- [Wan09] H. Wang, M. Chini, E. Moon, H. Mashiko, C. Li, and Z. Chang. *Coupling between energy and phase in hollow-core fiber based f-to-2f interferometers*. *Opt. Express* **17** (14), pp. 12082–12089 (2009). (cited on pages 76 and 80)
- [Web03] M. J. Weber. *Handbook of Optical Materials*. CRC Press (Boca Raton/London/New York) (2003). (cited on pages 19, 44, and 78)
- [Wei11] J. Weitenberg, P. Rußbüldt, T. Eidam, and I. Pupeza. *Transverse mode tailoring in a quasi-imaging high-finesse femtosecond enhancement cavity*. *Opt. Express* **19** (10), pp. 9551–9561 (2011). (cited on page 47)
- [Wir11] A. Wirth, M. T. Hassan, I. Grguraš, J. Gagnon, A. Moulet, T. T. Luu, S. Pabst, R. Santra, Z. A. Alahmed, A. M. Azzeer, V. S. Yakovlev, V. Pervak, F. Krausz, and E. Goulielmakis. *Synthesized light transients*. *Science* **334** (6053), pp. 195–200 (2011). (cited on page 76)
- [Wit09] T. Wittmann, B. Horvath, W. Helml, M. G. Schätzel, X. Gu, A. L. Cavalieri, G. G. Paulus, and R. Kienberger. *Single-shot carrier-envelope phase measurement of few-cycle laser pulses*. *Nature Physics* **5** (5), pp. 357–362 (2009). (cited on pages 13 and 62)
- [Wit12] S. Witte and K. S. E. Eikema. *Ultrafast optical parametric chirped-pulse amplification*. *IEEE Journal of Selected Topics in Quantum Electronics* **18** (1), pp. 296–307 (2012). (cited on pages 46 and 76)
- [Xu96] L. Xu, C. Spielmann, A. Poppe, T. Brabec, F. Krausz, and T. W. Hänsch. *Route to phase control of ultrashort light pulses*. *Opt. Lett.* **21** (24), pp. 2008–2010 (1996). (cited on pages 1, 8, and 27)

- 
- [You13] M. D. Young, S. Backus, C. Durfee, and J. Squier. *Multiphoton imaging with a direct-diode pumped femtosecond Ti:sapphire laser*. *Journal of Microscopy* **249** (2), pp. 83–86 (2013). (cited on page 44)
- [Yun09] C. Yun, S. Chen, H. Wang, M. Chini, and Z. Chang. *Temperature feedback control for long-term carrier-envelope phase locking*. *Appl. Opt.* **48** (27), pp. 5127–5130 (2009). (cited on page 27)
- [Zew88] A. H. Zewail. *Laser femtochemistry*. *Science* **242** (4886), pp. 1645–1653 (1988). (cited on page 1)



## Acknowledgements

This work was made possible by a bunch of lucky coincidences and the support of countless people, some of which I would like to mention here.

Foremost, I am indebted to Ferenc Krausz for accepting me as part of his group, even though my time in Garching was limited. I greatly appreciate the patience he has had with me and with the chaos that arose from the division of my work between Femtolasers and the LMU/MPQ. I have learned a lot at either of the two, and no-one else could have granted me this chance.

In between Vienna and Garching, there was always one among the following three persons that I could turn to when seeking help, advice, or an opinion. I thank Andreas Assion for the trust he put in me when granting me the freedom to pursue my ideas, be it in Vienna or Garching, and for the support to put these ideas into reality. I would like to thank Sasha Apolonskiy for welcoming me into his group at the LMU with open arms and making me feel part of a truly amazing team. Special thanks go to Günter Steinmeyer, whose ideas grew into the starting point of this thesis. I am grateful for all the knowledge and wisdom he has shared with me, and for the support he gave me in many crucial moments during my work.

Many thanks go to everyone at Femtolasers. In particular, I would like to thank Harald Frei and the oscillator wizards for getting me started with Ti:sa oscillators and for their patience and endurance with CEP4; Manfred Riemer and the electronics lab for experimental RF components and for mid-night test runs; Martin Hofer and the amplifier team for lending me their expertise and risking their mental health during 24-hour CEP measurements; Tuan Le and Gabriel Tempea for their knowledge and willingness to share it; and Thomas Ganz and the entire R&D team for inspiration and discussions.

The time I spent with the Laboratory of Attosecond Physics in Garching was wonderful experience. As a creature of the “realm of necessary evil” (as Reinhard Kienberger once paraphrased the field of laser development), I could not have hoped to come closer to ground-breaking fundamental research. I am thankful to everyone at the LAP for making the place what it is. I would like to thank Oleg Pronin for all our discussions, and for reminding me how good team-work in the lab can feel like; Ioachim Pupeza for initiating the enhancement cavity CEP project and for sounding like Tom Waits when in the mood; Simon Holzberger for his admirable perseverance in the lab, and for being the greatest spaceship pilot I know; Stefan Lahme for cussing the sky blue not only on rainy days; Henning Carstens for caring for the coffee when I left; and Siegfried Herbst for the Privateigentum.

This work was part of the Marie Curie Initial Training Network “ATTOFEL” which provided a great environment for scientific exchange and gave me numerous opportunities for discussion and co-operation. My sincere thanks to the organisers of ATTOFEL, Marc Vrakking and Thomas Schultz, as well as to all the other PhD fellows. Some of the experiments that shaped this work were the result of co-operations with groups both within ATTOFEL and outside it, and I am grateful to everyone who made those happen. I would like to thank Bastian Borchers of the Max-Born-Institut Berlin as my frequency-domain counterpart with respect to FF CEP stabilisation; Vincent Crozatier of Fastlite for the fruitful co-operation and his insight into noise analysis; Francesca Calegari and Andrea Trabattoni of Politecnico di Milano for the chance to actually generate attosecond pulses for real; and the team of Jens Limpert at the Friedrich-Schiller-Universität Jena for their fibre expertise.

The last years have taught me much, but I am equally grateful for all the people I was lucky enough to meet. Thanks to everyone who made Munich and Vienna feel like home. In particular, I am grateful to Friedrich Kirchner for his friendship and for teaching me most of what I know about getting up a mountain and down again. I thank Alexandria Anderson for having been a great colleague, and for remaining a likewise friend.

I am indebted to my partner Lilla Hajdu for her love and support. Thank you for making sure my head remained where it belonged.

The debt I can least hope to repay I owe to my parents, Bärbel and Rüdiger Lücking. Thank you for everything.